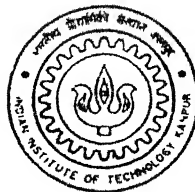# Numerical Investigation of Supersonic Mixed-Compression Inlet using Euler Equations

by
Vaibhav Jain

DEPARTMENT OF AEROSPACE ENGINEERING
INDIAN INSTITUTE OF TECHNOLOGY KANPUR
April, 2000

Numerical Investigation of Supersonic Mixed-Compression Inlet using Euler Equations.

A Thesis Submitted
in Partial Fulfillment of the Requirements
for the Degree of
Master of Technology

by

Vaibhav Jain

to the
Department of Aerospace Engineering
Indian Institute of Technology, Kanpur

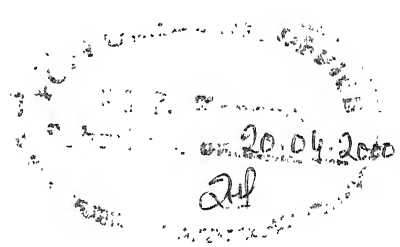**April 2000**

Certificate

This is to certify that the work contained in the thesis entitled "*Numerical Investigation of Supersonic Mixed-Compression Inlet using Euler Equations.*", by *Vaibhav Jain*, has been carried out under our supervision and that this work has not been submitted elsewhere for a degree.

April 2000

(Dr. R. K. Sullerey)   (Dr. Sanjay Mittal)
Department of Aerospace Engineering,
Indian Institute of Technology,
Kanpur.

Contents

Acknowledgments

There are many persons responsible for helping me become what I am today, and I would like to take a few moments to thank them.

Dr. Sanjay Mittal whose insight, support and encouragement has provided me with much of the computational knowledge I now possess. I am also thankful to him for providing me the computational codes and for helping me in implementing them. I will always be grateful to him for the energy he has invested in me.

I would like to express my gratitude towards Dr. R. K. Sullerey for his guidance and support to me during the course of the project.

I would like to thank all the members of the CFD Laboratory, Aerospace Engg., who have been great help to me in times.

I would also like to thank all of my friends in Hall-IV who always kept me fresh with frequent gulla.

To my family, words seem insufficient to describe the amount of strength they have brought to my life. May I show my appreciation by never disappointing them.

List of Figures

Abstract

Numerical simulation of a two-dimensional mixed compression supersonic inlet by solving time-dependent compressible Euler equations is presented. It is demonstrated that the stabilized finite-element method can be utilized to simulate and analyze supersonic inlets. An implicit treatment of the impermeable wall boundary condition is also presented. Two benchmark problems, one involving *Mach* 1.4 flow on parabolic arc bump and other a *Mach* 3 flow over a compression corner, have been computed to establish confidence in the formulation and its implementation. The inlet experimentally studied by Anderson and Wong at the design Mach number 3.0 is successfully simulated. The computations are capable of simulating the *start-up* problems associated with the mixed compression supersonic inlets. The present numerical experiments shows that the flow is unstarted (choked) for original configuration. However, an overspeed to Mach number 3.1 can start the inlet flow. To start the inlet at design Mach number 3.0, a minimum of 7% increase in the throat area is found necessary. The effect of engine-face to inlet pressure ratio on the total pressure recovery and flow distortion is studied.

Chapter 1

Introduction

1.1   Why Mixed Compression Two-Dimensional Inlet ?

The performance and efficiency of any turbojet engine depends strongly upon the engine's inlet. This is because the inlet determines the amount of air entering the engine as well as the pressure and velocity of the air at the engine's compressor face. The inlet must ensure that a sufficient amount of air enters the engine under all operating conditions without disrupting the low-drag/high-lift aerodynamics of the airframe. Also, because the compressor requires air at low subsonic speeds, supersonic air entering the inlet must be decelerated, but with maximum pressure recovery and minimum flow distortion.

Compression in the supersonic range is by means of one or several oblique shocks and by a weak normal shock which brings the flow to subsonic speed. Up to Mach 2.5, this compression process is concluded on the entry of the flow into the inlet, with the final normal shock, leading to subsonic speed, lying immediately behind the inlet lip. As the compression takes place outside the intake duct, it is termed "External Compression".

At flight Mach numbers beyond 2.5 the sole use of external compression leads to relatively large inlet diameters with high drag. For this reason the aircrafts flying at such Mach numbers only a part of the deceleration process is due to external compression while the rest is achieved as internal compression into the annular duct of the inlet. This form of compression is called "Mixed Compression".

However advantageous an axisymmetric inlet may be for optimum pressure recovery, it turns out to be equally unfavorable when the flow is not symmetrical to the axis of cone but is at an angle to it. In contrast, the two dimensional intake is considerably less sensitive to oblique flow, even if the pressure recovery which can be attained is less as discussed by Klous [1].

1.2   Types of Flows

There are three different types of flows through inlets: subcritical, critical and supercritical. A flow is said to be "Subcritical" if a bow shock forms outside of the inlet causing most of the flow approaching the inlet to be spilled away. Clearly this is highly undesirable because the engine will not receive sufficient mass of air. A flow is said to be "Supercritical" if it is supersonic everywhere inside of the inlet. This is also undesirable because the flow at the engine's compressor face must be subsonic. A flow is said to be "Critical" if a normal shock forms inside the inlet so that the flow downstream of the normal shock is subsonic. To minimize losses across the terminal shock, it should form just downstream of the inlet's throat, where Mach number is only slightly above unity.

Critical flow with the normal shock stabilized near the throat is the type of flow sought in inlets. Although such a flow is desirable, it is difficult to maintain. This is because small perturbations in the flow-field can move the normal shock upstream of the throat. Once the normal shock moves upstream of the throat, it will continue to move upstream until the flow is subsonic throughout the inlet with a bow shock formed outside of the inlet, i.e., the flow becomes subcritical. This is known as the "Unstart Condition".

A typical two-dimensional mixed compression supersonic geometry consists of two parts: supersonic diffuser ahead of the throat and subsonic diffuser behind the throat. The mixed compression inlet is characterized by multiple reflected oblique shocks in the supersonic diffuser and a normal shock immediately downstream of the throat. The flow-field is complicated due to multiple shock reflections. There are two basic inlet characteristics that greatly influence the inlet performance. The first is the total pressure recovery, and second is the flow distortion entering the engine compressor.

1.3 Literature Review

A two-dimensional inlet though can be found frequently used in practice. However, the studies of mixed compression inlets are mostly confined to the axisymmetric type. Smeltzer and Sorensen [2, 3] did experiments on an axisymmetric inlets. They showed as the Mach number increases the boundary layer dominates the flow through the throat. A review of the data-base available for shock-wave/boundary-layer interactions in supersonic inlets has been presented by Hamed [4]. An exhaustive study is also done on the effect of quantity and location of bleed on an axisymmetric mixed compression inlet has been conducted by several authors [5, 6, 7].

In 1970, Anderson and Wong [8] studied a two dimensional supersonic mixed compression inlet at design Mach number 3.0. At the design Mach number, a total pressure recovery of 0.90 was obtained with 14% boundary-layer bleed based on the captured mass flow. Apart from the viscous calculations they also did inviscid analysis which, showed the total pressure recovery of 0.95 in the supersonic diffuser region.

Numerical computations on supersonic inlets have been carried out by several authors. In 1972, inviscid analysis was presented by Reyhner and Hickcox [9]. Numerical predictions were made on supersonic diffusers only. Bush [10, 11] investigated external compression type inlets that are frequently used for Mach number lower than 2.5. Knight [12, 13] studied two- and three-dimensional flows in supersonic diffusers with simple geometries. His computation were limited by the numerical stability constraint and were also time consuming. Buggeln [14] and Anderson and Towne [15] solved a reduced form of the three-dimensional Navier-Stokes equations by neglecting the diffusion in the primary flow direction in a supersonic inlet. Their solution ends just upstream of the throat because of a subsonic flow occurring in the core of the flow-field (i.e. the inlet is unstarted).

Liang and Chan [16, 17] in 1992 studied mixed compression inlets. They used an inviscid solution as initial condition for viscous calculations. The work done by them is quite exhaustive. Even though there are some discrepancies in the inlet geometry their work has been extremely useful in carrying out the present study.

Work has also been done by several researchers on air intakes for scramjet applications using, both, Euler [18] and Navier-Stokes equations [19, 20, 21].

To summarize, numerical studies are mainly on simulating either supersonic diffuser or external-type supersonic inlets. Also most of the studies are concerned with

the axisymmetric inlets. Numerical studies done on the mixed compression two-dimensional supersonic inlet have been limited perhaps because of the numerical difficulties associated with the start-up problem.

The governing equations for the flow are the compressible Euler equations in the conservation law form. They are solved using a stabilized finite element formulation based on conservation variables. The SUPG (streamline-upwind/Petrov-Galerkin) stabilization technique is employed to stabilize the computations against spurious numerical oscillations due to advection dominated flows [22, 23, 24, 25, 26]. A shock-capturing term is added to the formulation to provide stability to the computations in the presence of discontinuities and large gradients in the flow.

In any numerical formulation of the compressible Euler equations, the implementation of the impermeable wall boundary condition requires special attention. Traditionally, an explicit implementation of this boundary condition has been used at the solid surfaces through flux-vector manipulation at the surface. Because this explicit treatment of the boundary adversely affects the stability properties of an implicit method, Le Beau [27] developed an implicit implementation of such case. In this formulation, the normal and tangential components of the momentum are kept track of, rather than the cartesian components. The normal component of the momentum can then be set to zero as a Dirichlet boundary condition. Movement between the normal-tangential components frame and the Cartesian components frame is accomplished by using a local transformation rule, dependent on the geometry of the boundary.

1.4   Description of Problem

Though a lot of work has been done on supersonic inlets but start-up in two-dimensional mixed compression supersonic flow is still not fully understood. In fact, design conditions cannot be achieved without momentarily overspeeding the inlet air or varying the diffuser geometry. This difficulty is due to shocks that arise during the deceleration process and it need not be related to boundary layer behavior. Therefore let us neglect boundary layer effects, while we examine the starting behavior of mixed compression inlet that is isentropic except for the losses that occur across the shocks. This simplified analysis contains the essential features of the phenomena and it approximates the real flow from which the wall boundary layer fluid has been carefully removed by suction through porous walls as discussed by Peterson [28].

1.5 Organization of the Thesis

The rest of the thesis is organized as follows.

- In Chapter 2, the mathematical formulation i.e. the governing equations, the finite element formulation, appropriate boundary conditions are introduced and the applicability of the Euler equations is discussed.

- Chapter 3, discusses the benchmark problems validated for present computation, gives the preliminary results and discusses them on the working of the proposed approach.

- Chapter 4, gives the conclusions and the scope for future work in the area.

Chapter 2

Mathematical Formulation

2.1 The Governing Equations

Let $\Omega \subset \mathbb{R}^{n_{sd}}$ and $(0, T)$ be the spatial and temporal domains respectively, where n_{sd} is the number of space dimensions, and let Γ denote the boundary of Ω. The spatial and temporal coordinates are denoted by $\mathbf{x}$ and t. The Euler equations governing the fluid flow, in conservation form, are

$$\frac{\partial \rho}{\partial t} + \nabla \cdot (\rho \mathbf{u}) = 0 \qquad \text{on } \Omega \ for \ (0, T), \tag{1}$$

$$\frac{\partial (\rho \mathbf{u})}{\partial t} + \nabla \cdot (\rho \mathbf{u} \mathbf{u}) + \nabla p = 0 \qquad \text{on } \Omega \ for \ (0, T), \tag{2}$$

$$\frac{\partial (\rho e)}{\partial t} + \nabla \cdot (\rho e \mathbf{u}) + \nabla \cdot (p \mathbf{u}) = 0 \qquad \text{on } \Omega \ for \ (0, T). \tag{3}$$

Here ρ, $\mathbf{u}$, p and e are the density, velocity, pressure and the total energy per unit mass respectively.

Pressure is related to the other variables via the equation of state. For ideal gases, the equation of state assumes the special form

$$p = (\gamma - 1)\rho i, \tag{4}$$

where γ is the ratio of specific heats and i is the internal energy per unit mass that is related to the total energy per unit mass and velocity as

$$i = e - \frac{1}{2} \| \mathbf{u} \|^2. \tag{5}$$

11

The temperature(θ) is related to the internal energy by the following relation

$$\theta = \frac{\gamma - 1}{R} i, \tag{6}$$

where R is the ideal gas constant.

The compressible Euler equations (1), (2), and (3) can be written in the conservation variables

$$\frac{\partial \mathbf{U}}{\partial t} + \frac{\partial \mathbf{F}_i}{\partial x_i} = \mathbf{0} \qquad \text{on } \Omega \text{ } for \text{ } (0, T), \tag{7}$$

where $\mathbf{U} = (\rho, \rho u_1, \rho u_2, \rho e)$, is the vector of conservation variables, and $\mathbf{F}_i$ is, the Euler vector defined as

$$\mathbf{F}_i = \begin{pmatrix} u_i \rho \\ u_i \rho u_1 + \delta_{i1} p \\ u_i \rho u_2 + \delta_{i2} p \\ u_i (\rho e + p) \end{pmatrix}. \tag{8}$$

Here u_i are the components of the velocity. In the quasi-linear form, equation (7) is written as

$$\frac{\partial \mathbf{U}}{\partial t} + \mathbf{A}_i \frac{\partial \mathbf{U}}{\partial x_i} = \mathbf{0} \qquad \text{on } \Omega \text{ } for \text{ } (0, T), \tag{9}$$

where

$$\mathbf{A}_i = \frac{\partial \mathbf{F}_i}{\partial \mathbf{U}}, \tag{10}$$

is the Euler Jacobian Matrix.

Corresponding to equation (9), the following boundary and initial conditions are chosen

$$\mathbf{U} = \mathbf{g} \qquad \text{on } \Gamma_g \text{ } for \text{ } (0, T), \tag{11}$$

$$\mathbf{U}(\mathbf{x}, 0) = \mathbf{U_0} \qquad \text{on } \Omega_0. \tag{12}$$

2.2   Finite Element Formulation

Consider a finite element discretization of Ω into subdomains Ω^e, $e = 1, 2, ..., n_{el}$, where n_{el} is the number of elements. Based on this discretization, we define the finite element trial function space $\mathcal{S}^h$ and weighting function space $\mathcal{V}^h$. These function

spaces are selected, by taking the Dirichlet boundary conditions into account, as subsets of $[\mathbf{H}^{1h}(\Omega)]^{n_{dof}}$, where $\mathbf{H}^{1h}(\Omega)$ is the finite-dimensional function space over Ω and n_{dof} is the number of degrees of freedom.

$$\mathcal{S}^h = \{\mathbf{U}^h | \mathbf{U}^h \in [\mathbf{H}^{1h}(\Omega)]^{n_{dof}}, \mathbf{U}^h|_{\Omega^e} \in [P^1(\Omega^e)]^{n_{dof}}, \mathbf{U}^h \cdot \mathbf{e}_k \doteq g_k \ on \ \Gamma_{g_k}\}, \quad (13)$$

$$\mathcal{V}^h = \{\mathbf{W}^h | \mathbf{W}^h \in [\mathbf{H}^{1h}(\Omega)]^{n_{dof}}, \mathbf{W}^h|_{\Omega^e} \in [P^1(\Omega^e)]^{n_{dof}}, \mathbf{W}^h \cdot \mathbf{e}_k \doteq 0 \ on \ \Gamma_{g_k}\}, \quad (14)$$

where $[P^1(\Omega^e)]$ represents the first order polynomial in Ω^e, and $k = 1, ..., n_{dof}$. The stabilized finite element formulation of Eq. (9) is written as follows: find $\mathbf{U}^h \in \mathcal{S}^h$ such that $\forall \mathbf{W}^h \in \mathcal{V}^h$,

$$\int_\Omega \mathbf{W}^h \cdot \left(\frac{\partial \mathbf{U}^h}{\partial t} + \mathbf{A}_i^h \frac{\partial \mathbf{U}^h}{\partial x_i}\right) d\Omega + \sum_{e=1}^{n_{el}} \int_{\Omega^e} \tau (\mathbf{A}_k^h)^T \left(\frac{\partial \mathbf{W}^h}{\partial x_k}\right) \cdot \left[\frac{\partial \mathbf{U}^h}{\partial t} + \mathbf{A}_i^h \frac{\partial \mathbf{U}^h}{\partial x_i}\right] d\Omega$$

$$+ \sum_{e=1}^{n_{el}} \int_{\Omega^e} \delta \left(\frac{\partial \mathbf{W}^h}{\partial x_i}\right) \cdot \left(\frac{\partial \mathbf{U}^h}{\partial x_i}\right) d\Omega = \mathbf{0} \quad (15)$$

In the variational formulation given by Eq. (15), the first two terms and the right-hand-side constitute the Galerkin formulation of the problem. The first series of element-level integrals in Eq. (15) are the SUPG stabilization terms added to the variational formulation to stabilize the computations against node-to-node oscillations in the advection-dominated range. The second series of element level integrals in the formulation are the shock capturing terms that stabilize the computations in the presence of sharp gradients. The stabilization coefficients δ and τ are the ones that are used by Mittal [25, 29] and quite similar to those employed by Aliabadi and Tezduyar [30]. They are defined as

$$\tau = max\left[0, \tau_a - \tau_\delta\right], \quad (16)$$

$$\tau_a = \frac{h}{2\left(c + \parallel \mathbf{u} \parallel\right)} \quad (17)$$

$$\tau_\delta = \frac{\delta}{2(c + \parallel \mathbf{u} \parallel)^2}\mathbf{I}, \quad (18)$$

13

$$\delta = \left[\frac{\left\| \frac{\partial \mathbf{U}}{\partial t} + \mathbf{A}_i \frac{\partial \mathbf{U}}{\partial x_i} \right\|_{\mathbf{A}_0^{-1}}}{\left\| J_{1i} \frac{\partial \mathbf{U}}{\partial x_i} \right\|_{\mathbf{A}_0^{-1}} + \left\| J_{2i} \frac{\partial \mathbf{U}}{\partial x_i} \right\|_{\mathbf{A}_0^{-1}}} \right]^{\frac{1}{2}}, \tag{19}$$

where c is the wave speed, h is the element length, J_{jk} are the components of Jacobian transformation matrix from physical to the local coordinates and $\mathbf{A}_0^{-1}$ is the inverse of Reimannian metric tensor related to the transformation between the conservation and entropy variables [31]. Matrix τ_δ is subtracted from τ_a to account for the shock-capturing term as shown in Eq. (16).

The time discretization of the variational formulation given by Eq. (15) is done via the generalized trapezoidal rule. For unsteady computations, we employ a second-order accurate-in-time procedure.

2.3 The Impermeable Wall Boundary Condition

In the case of Navier-Stokes equations, the implementation of the solid wall boundary condition is straight forward because the momentum equations contain a viscous term which requires that all components of the velocity on a surface must be zero(assuming the surface is stationary). For the Euler equations however, the Reynolds number is infinite, allowing the tangential flow at a solid surface. This boundary condition then mandates that the mass flux of the fluid normal to a stationary surface be zero. Mathematically, this is written

$$\mathbf{u} \cdot \mathbf{n} = 0 \tag{20}$$

where $\mathbf{u}$ is the velocity vector of a node on the surface and the $\mathbf{n}$ is the unit vector normal to the surface.

Typical implementation of this boundary condition in the past has involved manipulation of the velocity vectors such that the advection normal to the surface is zero after each iteration. This has been accomplished by simply killing the normal component of the velocity at the surface, or by rotation of the velocity vector tangent to the surface in an effort to maintain the kinetic energy at each point. But these methods are the the explicit treatment of the boundary condition. Thus even when using an implicit method the stability of the algorithm will be influenced by this

explicit treatment of boundary condition. Herein is a description of the method used for handling the impermeable wall in this research.

2.3.1 Implementation of Impermeable Wall Boundary Condition

The success of this implementation is due to the treatment of the solid surface as a Dirichlet boundary which, by definition of the trial space, allows us to dictate that the normal component of the velocity on a stationary surface must be zero.

In the finite element, the quantity $\mathbf{U}$ is determined within each element by the nodal values $\mathbf{U}^B$ and a set of shape or interpolation functions $\mathbf{R}^B$ such that

$$\mathbf{U} = \sum_{B=1}^{p} \mathbf{R}^B \mathbf{U}^B,\qquad(21)$$

where p is the number of nodes in the element. In the case of a general two-dimensional quadrilateral element, the previous summation can be written out as

$$\mathbf{U} = \begin{pmatrix} \mathbf{U}_1^1 \\ \mathbf{U}_2^1 \\ \mathbf{U}_3^1 \\ \mathbf{U}_4^1 \end{pmatrix} \mathbf{R}^1 + \begin{pmatrix} \mathbf{U}_1^2 \\ \mathbf{U}_2^2 \\ \mathbf{U}_3^2 \\ \mathbf{U}_4^2 \end{pmatrix} \mathbf{R}^2 + \begin{pmatrix} \mathbf{U}_1^3 \\ \mathbf{U}_2^3 \\ \mathbf{U}_3^3 \\ \mathbf{U}_4^3 \end{pmatrix} \mathbf{R}^3 + \begin{pmatrix} \mathbf{U}_1^4 \\ \mathbf{U}_2^4 \\ \mathbf{U}_3^4 \\ \mathbf{U}_4^4 \end{pmatrix} \mathbf{R}^4 \qquad(22)$$

where $\mathbf{U}_1 = \rho$, $\mathbf{U}_2 = \rho\mathbf{u}_1$, $\mathbf{U}_3 = \rho\mathbf{u}_2$, $\mathbf{U}_4 = \rho e$ and the superscripts associates the nodal vector of unknowns to its shape function.

Equation (22) uses a nodal vector of unknowns based on a cartesian coordinate system. Such a system does not directly allow enforcement of the requirement that the normal component of the velocity on a surface be zero because it is a geometric combination of the $\mathbf{x}_1$ and $\mathbf{x}_2$ components of the velocity at the surface node. Therefore a new nodal vector of unknowns for surface nodes is defined where the second and third components of this vector represent components of the velocity in the tangential (τ) and normal ($\mathbf{n}$) directions respectively. This new vector is defined as,

$$\mathbf{d} = \begin{pmatrix} \rho \\ \rho\mathbf{u}_\tau \\ \rho\mathbf{u}_\mathbf{n} \\ \rho e \end{pmatrix}\qquad(23)$$

Having the vector of unknowns in a local coordinate system allows the third degree of freedom to be designated as a Dirichlet boundary, and to assign it the appropriate value.

Although introduction of a local coordinate system permits the direct enforcement of a no penetration condition, there may be many such coordinate systems depending on the shape and the resolution of the surface. It then becomes obvious that it will not be possible to obtain a solution over a spatial domain where, conceivably, each node may use uniform system so that the proper governing equations can be used. Thus each of these τ-n systems must be rotated to one uniform system so that proper governing equations can be used. Triangular element is used in our computation but, here for explaining, general quadrilateral element is used. For example, in considering a typical quadrilateral boundary element such as the one shown in Figure 1, the equation (22) would be modified for boundary nodes 3 and 4, such that

$$
U = \begin{pmatrix} U_1^1 \\ U_2^1 \\ U_3^1 \\ U_4^1 \end{pmatrix} R^1 + \begin{pmatrix} U_1^2 \\ U_2^2 \\ U_3^2 \\ U_4^2 \end{pmatrix} R^2 + T^3 \begin{pmatrix} d_1^3 \\ d_2^3 \\ d_3^3 \\ d_4^3 \end{pmatrix} R^3 + T^4 \begin{pmatrix} d_1^4 \\ d_2^4 \\ d_3^4 \\ d_4^4 \end{pmatrix} R^4 \quad (24)
$$

where T_3 and T_4 are rotation matrices which rotate the normal and tangential components for nodes 3 and 4, to the cartesian system. Such nodal rotation matrices would be defined as

$$
T^B = \begin{pmatrix} 1 & 0 & 0 & 0 \\ 0 & cos\theta_B & -sin\theta_B & 0 \\ 0 & sin\theta_B & cos\theta_B & 0 \\ 0 & 0 & 0 & 1 \end{pmatrix}, \quad (25)
$$

where θ_B is the angle measured from the x_1 axis to the τ base vector for the surface node B. In general, this can be written for all elements as

$$
U = \sum_{B=1}^{p} R^B T^B d^B \quad (26)
$$

where the τ and n components of d for those nodes not on an solid surface would correspond to the cartesian components, and the rotation matrices would simply be the identity matrix. This same type of rotation must also take place on the trial functions;

$$W = \sum_{A=1}^{p} R^A T^A c^A \qquad (27)$$

Due to this transformation we replace,

$$m^e \leftarrow T^{e^T} m^e T^e \qquad (28)$$

$$c^e \leftarrow T^{e^T} c^e T^e \qquad (29)$$

$$r^e \leftarrow T^{e^T} r^e \qquad (30)$$

where m is mass matrix, c is general advection diffusion matrix and r is residual matrix.

2.4   Boundary and Initial Conditions

The computational domain is defined by the left boundary (a-f) slightly ahead of ramp and the right boundary on the outlet (c-d), as shown in Figure 2.

2.4.1   On body Surface

For inviscid flow over an impermeable wall, normal component of velocity V_n is set to zero.

2.4.2   Inflow and Outflow Boundary Conditions

For a supersonic inflow, the inflow boundary conditions are fixed at free stream values. But for a subsonic outflow, initially no back pressure condition is imposed but, once the inlet is started a back pressure $p = p_b$ is imposed.

2.5   Numerical Procedure

Numerical solutions are obtained in the following sequences. First starting with uniform flow at Mach 3, an inviscid supersonic flow is calculated. This supersonic flow acts as a initial condition for the flow with back pressure condition imposed at the outlet. Computations are carried out for various values of the back pressure.

Chapter 3

Results and Discussion

3.1 Benchmark Problems

Before the method is applied to the computation of flows in supersonic inlets it is validated via a couple of benchmark problems.

3.1.1 Flow past a Compression Corner

The Euler code is validated first on Mach 3 flow past a 10° compression corner. This problem involves supersonic flow past a flat plate followed by a compression corner where oblique shock is formed as shown in Figure 3. The change in the values of the various parameters like pressure, temperature, Mach number and density after the shock are shown in Figure 4. The results compares quite well to analytic results calculated from tables and charts in book by Anderson [32]

$M_1 = 3.0$

Deflection Angle, $\theta = 10^o$

Numerical Results	*Analytical Results*
Shock Angle $= 27.5^o$	Shock Angle $= 27^o$
$M_2 = 2.48$	$M_2 = 2.4835$
$P_2/P_1 = 2.12$	$P_2/P_1 = 2.124$
$T_2/T_1 = 1.25$	$T_2/T_1 = 1.260$
$\rho_2/\rho_1 = 1.7$	$\rho_2/\rho_1 = 1.705$

3.1.2 Flow past a Parabolic Arc Bump

We consider the problem of a thin parabolic shaped bump placed on the floor of a wind tunnel. The parabolic arc bounding the bump in this plane is described by the following expression;

$x_2 = b [1 - (2x_1)^2],$

where b is the ratio of the maximum arc thickness to the length. The bump is centered at the bottom of the tunnel and the domain extends L units in front and behind the arc and H units above the arc, where L and H are normalized by arc length. Figure 5 shows the configuration of the problem. The boundary conditions consist of Dirichlet-type for ρ, u_1, u_2 and e on the left hand side of the domain and for satisfying the no penetration condition along the upper and lower boundaries.

The free stream Mach number is set to 1.4. The dimensions of the domain for this problem are 1.0 each for L and H, while 'b' is set to 4%. The schematic mesh is shown in Figure 6(a). The structured mesh is formed in the region near the surface where oblique shock is formed. Unstructured mesh is generated in the remaining domain. The mesh on which computation is done is shown in Figure 6(b) which consists of 9552 nodes and 18702 elements. The problem, which is similar to that analyzed by Le Beau [27], creates an interesting shock interaction behind the bump. The shock from the leading edge of the bump is reflected down off the ceiling of the tunnel and crosses, then combines, with the shock formed at the trailing edge of the bump. The shock reflected off the ceiling of the tunnel is also seen to decrease in strength because of the expansion waves propagating from the curvature of the arc. Figure 7 compares pressure contours of our computation and of Le Beau [27] computation while, Figure 8 compares the density profile along the length at upper boundary.

3.2 Inlet Geometry

A two dimensional supersonic mixed compression inlet experimentally studied by Anderson and Wong [8] is employed here. The inlet length is 119.02 in. At the design condition, the initial compression ramp is fixed at 7° angle and the capture height and width are both fixed at 14 in. The second ramp starts from station x = 28.0 in to station x = 54.1 in. With an inclination angle of 14°. The cowl surface starts at station x = 30.4 in. The lip cowl angle is fixed 12° so that the reflected shock angle is small and thereby the lateral boundary can be located close to the inlet to

minimize the computation cost. The geometric throat is located at x = 58.8 in. In subsonic diffuser angle is fixed at 8°. Since the free stream Mach number is 3.0 and no information may propagate upstream, the size of the domain ahead of inlet may be kept small without affecting the solution downstream. The inflow boundary is fixed at x = -5.0 in . Here lateral boundary is kept at y = 68.0 in. Figure 2 shows the complete geometry. The details of the coordinates of the throat and the subsonic diffuser of the geometry can be found in the paper of Anderson and Wong [8]

3.3   Grid Generation

The grid system used is a combination of Structured and Unstructured meshes. Structured grid is used in the region near the surface of ramp and cowl. The grid is fine where the shocks are expected.

The unstructured grid is used in the remaining domain using Delaunay triangulation. It is ensured that there is no sudden change in grid size. The structured grid is extended ahead of the ramp and cowl surfaces to achieve this. Figure 9(a) shows the grid on the full domain of inlet. The number of nodes are 54,102 and number of elements are 1,02,952. The number of nodes and elements varies as the throat area is increased. In our study various meshes have been utilized. The number of nodes varies from 50,000 to 80,000 while number of elements varied from 95,000 to 1,50,000. Figure 9(b) shows the grid near the throat region. Figure 9(c) shows the grid near the cowl tip.

3.4   Modified Inlet and Effect of Throat Area Increase

The critical throat design is one of the major difficulty faced in the current study. To compare results with the experimental data of Wong [8], the supersonic inlet is simulated at the design condition of inlet Mach number 3.0. At inlet Mach number 3.0 it was observed that either the throat area or the Mach number is not enough to swallow the oblique shock formed near throat. It is seen that in the supersonic diffuser region, the oblique shock that is nearest to the throat moves upstream and its strength increases. It becomes normal shock and moves upstream of the throat

during the iteration process. As shown in Mach contours in Figure 10 and in pressure contours in Figure 11, a complex oblique shock pattern is formed near the throat. The oblique shock formed near the throat is unable to pass through the throat.It moves upstream with time and eventually forms a normal shock upstream of throat. Since a normal shock in the converging part of diffuser is unstable, it is expelled out. In this case no condition on pressure is imposed at the exit of the inlet. The flow phenomenon is commonly referred to as "Unstart". Figure 12(a) shows the behavior of pressure on the ramp surface with time. It can be observed how the shock nearest to the throat moves upstream and forms normal shock which is expelled out at later time. Figure 12(b) shows the behavior of pressure on the cowl surface with time. Since no pressure condition is imposed at the exit of the inlet, it acts like a converging diverging nozzle and the flow remains supersonic at exit. Figure 13(a) and 13(b) shows the behavior of Mach number on ramp and cowl surfaces, respectively, with time for the unstarted inlet.

Anderson and Towne [15] used a space marching scheme to simulate this problem. The marching process was terminated just upstream of the throat because of the subsonic flow upstream of the throat. To obtain the started inlet flows, inlet is modified at the throat. Compared to the throat area in the original configuration the area of the modified one is increased by 5.5%. Even with this increase the inlet is unstarted so the throat area is increased further by 7%. For the increased throat area an oblique shock pattern is formed at the throat. Once the steady oblique shock pattern is formed, the flow is established and the inlet starts.

The started flow with 7% throat area increase has throat Mach number of 1.22 comparable to the analytical results as depicted by Anderson and Wong, shown in Figure 14, Anderson observed the Mach number at the throat to be 1.2. Except at throat elsewhere the Mach number and the pressure recovery matches well with the analytical results depicted by Anderson and Wong. The difference at the throat may be due to increase in the throat area in our case. Figure 15 shows the Mach contours of the started inlet with time. In the established flow, the complex oblique shock pattern in the inlet due to reflection and interaction of various oblique shocks can be observed. Also it can be observed that due to multiple oblique shock interactions the flow becomes subsonic near the throat on the surfaces of ramp and cowl. Although there are weak normal shocks close to the throat, near the ramp and cowl walls, these do not unstart the inlet. Figure 15 shows two such subsonic regions one upstream of the throat on the cowl surface and other almost on the throat on the ramp surface. It

21

is these locally formed normal shocks that get stronger and form one strong normal shock upstream of the throat and unstart the inlet in the original configuration. Figure 16 shows the pressure contours of the started inlet with time. The subsonic zone near the cowl surface downstream of the throat can be clearly observed in this figure. Figure 17(a) shows the behavior of pressure of the inlet along ramp surface with time. The decrease in the pressure can be observed near the throat. This is because of the expansion waves propagating from the curvature of the throat. Also apparent is the sudden pressure rise caused due to locally formed normal shock. Figure 17(b) shows the behavior of pressure of the inlet along cowl surface with time. Two sudden pressure rise region can be observed showing formation of normal shocks on the cowl surface. It can be observed that these locally formed normal shocks are not strong enough to effect the flow as a whole i.e., these normal shocks formed are not strong enough to form one strong normal shock upstream of the throat which unstarts the inlet. Figure 18(a) and 18(b) shows the behavior of Mach number with time on the ramp and cowl surfaces, respectively. In Figure 18(a), Mach number increase due to expansion fan formed near the throat on the ramp surface can be observed. Compression can be observed at exit of the inlet which again may be because of the curvature of the geometry in that region. To validate the results obtain for the started flow a comparison is made with the experimental results of Wong [8] and with the computational results of Liang [17] in the supersonic diffuser. Figure 19(a) compares the pressure of the started inlet in supersonic diffuser along the ramp surface. It can be observed that the flow ahead of throat is almost similar. However, there is difference at the throat. The computational results of Liang [17] match well with ours. This implies that they also observed these locally subsonic regions which are not present in the experimental results. Figure 19(b) compares the pressure in supersonic diffuser along cowl surface.

To further study the effect of throat area increase, computations are carried out for area increase of 5.5%, 7.0%, 8.0% and 20.0%. To accommodate this area increase the second ramp is modified and now second ramp is from x = 28.0 in to x = 52.1 in. Figure 20 shows the modified inlet. Figure 21(a) and 21(b) shows the behavior of pressure along the ramp and cowl surfaces, respectively, with the increase in the throat area from original configuration to 20%. It can be seen that the subsonic zone on ramp and cowl surfaces becomes weaker as the throat area is increased. However, as the throat area gets larger the Mach number at the throat increases thereby reducing pressure recovery. When the pressure condition will be imposed at exit of the inlet,

the critical normal shock formed at the throat will be of higher strength and thus will lead to more shock losses and will thereby reduce pressure recovery. Figure 22(a) and 22(b) shows the behavior of Mach number along the ramp and cowl surfaces, respectively, with the increase in the throat area. It can be observed that the Mach number at the throat increases as the area of the throat increases. This difference is not much for 7% & 8% increase in throat area. But, for the 20% increase in throat area case the difference is clearly visible.

3.5　Effect of Overspeeding

Start-up problem can be solved with either the throat area increase or by increasing the free stream Mach number. Since the inlet cannot be started at Mach number 3.0 for the original configuration, a study was carried out to bring the effect of inflow Mach number. The free stream Mach number is made 3.05. This indicates a 1.7% deviation on inflow Mach number between the numerical simulation and experimental measurement. Based on the isentropic flow relation the 1.7% deviation seems to be consistent with the 4% throat area increase. As expected the inlet is unstarted. The overspeed study was extended to Mach number 3.1. The inlet started at Mach number 3.1. This corresponds to a 3.3% deviation on inflow Mach number of 3.0. This 3.3% deviation in the Mach number is consistent with the 7% throat area increase required for the inlet to start at M = 3.0. Figure 23(a) and 23(b) shows pressure along the ramp and cowl surfaces, respectively, with varying free stream Mach number. The normal shock can be seen formed upstream of the throat at Mach numbers 3.0 and 3.05 which unstarts the inlet. Figure 24(a) and 24(b) shows the behavior of Mach number along the ramp and cowl surfaces, respectively, with varying free stream Mach numbers. It can be seen that due to increase in the Mach number at the inlet the oblique shocks formed are stronger and thus more losses occurs in supersonic diffuser. However these losses are minor compared to the losses across normal shock.

The effect of decreasing the free stream Mach number from started inlet free stream Mach number is also studied. The Mach number 3.1 of the started inlet is reduce to 3.05 in the hope that the inlet will remain started. But, as the Mach number is reduced the oblique shocks which are downstream of the throat become stronger and form a normal shock upstream of the throat. Figure 25 shows the Mach contours for this case. The Mach number of the started inlet is reduced from 3.1 to 3.05 at

T = 7510. It can be seen that the started inlet with oblique shock pattern at Mach number 3.1, unstarts at Mach number 3.05. Figure 26 shows the pressure contours for the present case.

3.6 Effect of Back Pressure

Till now the study was focussed on the start-up problem. Now effect of the pressure imposed at exit of the inlet is studied.

Two parameters are used to define the performance of an inlet: Total pressure recovery and inlet distortion. Total pressure recovery is defined as the area-weighted total pressure at engine face divided by free stream total pressure.

$$Total\ Pressure\ Recovery = \frac{P_{t02}}{P_{01}}, \tag{1}$$

where P_{t02} is the area-weighted total pressure at the engine face.

$$P_{t02} = \frac{\int P_{02} dA}{\int dA} \tag{2}$$

Inlet distortion is defined as the difference between the maximum and minimum total pressures divided by the area-weighted total pressure at engine face.

$$Inlet\ Distortion = \frac{P_{max02} - P_{min02}}{P_{t02}} \tag{3}$$

where P_{max02} and P_{min02} is the maximum and minimum total pressure at the engine face respectively.

In addition to these two parameters used to define the performance of inlet, one more parameter *Inlet Stability Margin* is used to define the stable range in which the inlet can operate.

Once the start-up problem of the intake is resolved, the next step is to make sure that the Mach number at the exit of the intake, i.e., at the engine face is less than 0.4. The inlet is started either with overspeeding or with increase in throat area. The present study of effect of pressure condition imposed at the exit of the inlet i.e. effect

of the back pressure is done on the inlet with increased throat area from original configuration. The inlet started at greater then 7% increase in throat area. So the study of effect of back pressure was done on two configurations of inlet, one with 7% increase in throat area while other with 8% increase in throat area. An optimal inlet operating point demands the flow to have a highest total pressure recovery and lowest flow distortion level.

Now with the pressure condition imposed at the exit of the inlet, the normal shock is formed at exit. With the increase in the pressure at the exit the normal shock moves upstream. To obtain the objective of maximum pressure recovery, normal shock should form at the location where the losses due to normal shock are minimal. Losses due to the normal shocks are minimum when the normal shock is formed at the minimum Mach number location i.e. when the normal shock is formed nearest to the throat. In the present case the Mach number at the throat is 1.22.

The inlet with 7% increase in throat area is first started with no pressure condition imposed at exit of the inlet. Once the inlet is started the pressure is imposed at exit of the inlet. Initially when no pressure condition is applied at the exit there is no normal shock present, the pressure recovery is around 93% but the flow is supersonic at the engine face which is undesirable. Now as the back pressure is applied, $Pb/Pi=5.0$, a normal shock is formed at the engine face. The normal shock formed at this back pressure is quite strong since the Mach number at the exit is almost 3.0 so the pressure losses increase drastically and thus pressure recovery reduces to 36%. Figure 27 shows the Mach contours of the movement of the normal shock in subsonic diffuser. In Figure 27, it can be seen that when no pressure condition is imposed at the exit, there is no normal shock. As the pressure is imposed at the exit normal shock is formed which moves upstream with the increase in pressure at the exit. Also it can be observed that the shock pattern upstream of normal shock remains unaffected with rise in exit pressure. Figure 28 shows the pressure contours of the movement of the normal shock in subsonic diffuser. As the normal shock moves upstream the strength of normal shock reduces, because the Mach number upstream of the normal shock keeps reducing, thereby increasing the pressure recovery from 36% at $Pb/Pi=5.0$ to 92.35% at $Pb/Pi=33.07$. Distortion index lies within the acceptable range of 4-5%. In the case of 7% increase in throat area the $Pb/Pi=33.07$ is nearest to the desirable critical condition.

Inlet stability margin, the margin required for stable functioning of inlet. This margin is calculated by measuring distance of normal shock from throat w.r.t. inlet

length. If the normal shock is formed exactly on the throat then this margin will become zero. Though in such case the pressure recovery will be maximum but slight disturbance may cause the shock to move upstream and thus unstart the inlet. In the present study with 7% increase in throat area, the normal shock is nearest to throat at Pb/Pi=33.07, the inlet length margin is 0.9% while with Pb/Pi=33.0 though the pressure recovery is 92.14% slightly less than the recovery at Pb/Pi=33.07 but the inlet length stability margin is 2.0% to sustain a stable operation without unstarting the inlet.

Figure 29(a) and 29(b) shows the behavior of pressure with the variation of pressure at exit of the inlet along the ramp and cowl surfaces, respectively. It can be observed that upto Pb/Pi = 10.0, the normal shock is almost at the exit. The sensitivity of the back pressure can be observed as with slight increase in back pressure from Pb/Pi = 33.07 to Pb/Pi = 33.09 the inlet unstarts. Figure 30(a) and 30(b) shows the behavior of Mach number with the variation of back pressure along the ramp and cowl surfaces, respectively. It can be observed that as the pressure condition is imposed at exit of the inlet the Mach number at engine face becomes less than 0.4. It can be observed that as the normal shock moves upstream the strength of the normal shock reduces and thus increases pressure recovery as shown in Figure 31(a). Figure 31(b) shows the effect of the back pressure on the distortion index. Figure 31(c) shows the effect of the back pressure on the mass flow. It can be seen that the pressure recovery is almost linear with the increasing pressure at the exit of the inlet which may be useful in engineering application while the distortion index lies in the acceptable range of 4-5% and also the mass flow which is almost constant for supercritical and critical case but falls down once the normal shock is formed upstream throat.

A similar study was done with 8% increase in throat area. It was found that the behavior of normal shock in 8% increase in throat area case is almost similar to 7% increase in throat area case. Figure 32 shows the Mach contours of the flow with the variation of back pressure. Figure 33 shows the pressure contours of the flow. In this case the pressure at exit required to bring normal shock near the ideal critical condition is more. This is due to the increased mass flow across the throat. Now the Pb/Pi = 34.0 is nearest to the critical condition without unstarting the inlet. The normal shocks are located at x=0.5 for Pb/Pi=34.0. The pressure recovery is 94.73%, inlet stability margin is 1.2% and distortion index is 2.52%. As the back pressure is increased further to 34.5 the normal shock moves upstream and the critical

condition becomes subcritical condition and unstarts the inlet. Decreasing the back pressure, the normal shock wave moves downstream and its strength increases thereby decreasing the pressure recovery. For Pb/Pi= 25.0 the pressure recovery is 70.1% only. Figure 34(a) and 34(b) shows the effect on pressure with the variation in back pressure along the ramp and cowl surfaces, respectively. Figure 35(a) and 35(b) shows the effect on Mach number with the variation in back pressure along the ramp and cowl surfaces, respectively. Figure 36(a) shows the pressure recovery for different back pressures. Here again the pressure recovery is linear, versus back pressure.

Figure 36(b) shows the behavior of the distortion index with varying back pressure. The distortion index lies in the range of 4-5%. Mass flow which is constant through out falls once the shock moves from critical to subcritical condition as shown in Figure 36(c).

The comparison is made between the 7% increase in throat area case and 8% increase in throat area case. To compare, Pb/Pi = 25.0 is taken for both the cases. It is observed that the position of shock at this back pressure is almost similar, with 8% increase in throat area case having the normal shock slightly downstream. Normal shock with back pressure nearest to critical is also compared which is, 33.05 in the case of 7% increase in throat area and 34.0 in the case of 8% increase in throat area. Figure 37(a) and 37(b) shows the comparison of the behavior of pressure with back pressure for both the cases along the ramp and cowl surfaces, respectively. For both the cases the flow upstream of the throat is almost similar. Figure 38(a) and 38(b) shows the comparison of the behavior of Mach number with back pressure for both the cases along the ramp and cowl surfaces, respectively. Figure 39(a) shows an interesting result that the pressure recovery in the case of 8% throat area increase is more than the 7% case at nearest to critical condition. Figure 39(b) compares distortion index for two cases. Figure 39(c) compares mass flow for various back pressure values and throat areas. The trend is almost similar with slightly higher mass flow for 8% case.

3.7   Shock behavior in Supersonic Diffuser

The study was done with a modified inlet of 7% increase in throat area compared to the original configuration. The back pressure for critical operation of the inlet is 33.07. For Pb/Pi = 33.09 normal shock moves upstream of the throat and the intake's operation becomes subcritical. This is not a stable operation because a

shock cannot attain a stable position within the supersonic diffuser. The shock which is now upstream of the throat where the upstream Mach number is slightly higher. A greater stagnation pressure loss will occur across the shock, lowering the downstream stagnation pressure and the throat mass flow. Since the flow is supersonic upstream of the shock the conditions over there remain unaffected. The mass flow through the shock remains constant and there results an accumulation of mass and rise in pressure behind the shock. As the static pressure ratio across the shock increases, its propagation speed relative to the fluid increases and the shock moves further upstream. This further increases the stagnation pressure loss, of course, so that the mass flow imbalance increases and the shock continues to move upstream and out of the inlet. The final position of the shock is far enough outside the inlet area to allow correct "spilling" of air as explained in Peterson [28]

Figure 40 shows the Mach contours of the expelled flow. Figure 41 shows the presssure contours of the expelled flow. The shock is expelled from supersonic diffuser thereby unstarting the inlet, the flow now becomes subsonic everywhere. Figure 42(a) and 42(b) shows the behavior of pressure at the ramp and cowl surfaces, respectively for the expelled flow. It can be observed how the shock is expelled out. Figure 43(a) and 43(b) shows behavior of Mach number at the ramp and cowl surfaces,respectively for expelled flow. Figure 44 shows the decrease in mass flow with the shock movement.

This subcritical state may sometime exhibit a marked instability of flow in the form of an oscillation of the shock system, colloquially known as "Buzz". The phenomenon was first observed by Oswatitsch (1944) for external compression supersonic inlet. The buzz consists of a rapid oscillation of the inlet shock and flow pattern. The resultant internal disturbance is very detrimental to engine performance as explained by Seddon [33]. The buzz phenomena has been of considerable interest and has been studied extensively for external compression supersonic inlets. The present case is an effort to simulate buzz. The present computation indicate that although inviscid flow model can predict "start-up" problem of the intakes, "Buzz" can be simulated only via viscous flow models for mixed compression intakes.

Chapter 4

Summary and Conclusions

In this chapter a brief summary of the thesis is presented. Following the summary, conclusions are drawn and recommendations for future work are suggested.

4.1   Summary

This thesis presented the finite element computations of inviscid flows in mixed compression two-dimensional supersonic inlets using compressible Euler equations. This thesis also presented proper implementation of the impermeable wall boundary condition. This implementation maintained the no penetration condition by substituting a local coordinate system for the regular Cartesian system at surface nodes. The local coordinate system, consisting of normal and tangential components, allows direct enforcement of the zero normal velocity by use of a Dirichlet boundary condition.

The formulation has been tested on two benchmark problems involving *Mach* 3 flow on a 10° compression corner and supersonic flow of Mach number 1.4 on parabolic arc bump. The results are in good agreement with those from other researchers. The computations for the supersonic inlets are capable of simulating the start-up dynamics. If the diffuser throat is not large enough to allow the start-up normal shock to pass through the inlet it *unstarts*. Our computations result in the same observation. One would like to establish a uniform flow in the inlet with the minimum loss of stagnation pressure. The efficiency of the inlet depends on various parameters and their effect has been investigated in this work.

4.2 Conclusions

There are several conclusions which can be drawn from this work.

- The implicit treatment of the no penetration boundary condition has many merits, which makes it virtually essential in formulations that ignore the viscous terms of the Navier-Stokes equations.

- At M = 3.0, the mixed compression inlet studied by Anderson and Wong [8] was found to be unstarted in the present numerical simulation. The discrepancy may be attributed to the three-dimensional effect that is not taken into in the two-dimensional computation. The inlet cannot be started at design condition without overspeeding or without varying the throat area. Atleast 7% increase in throat area or Mach number 3.1 is required to startup the inlet with original configuration.

- The complex oblique shock pattern at throat forms normal shock at the surface of ramp and cowl, respectively, in the throat region. These normal shock though make the flow subsonic locally but are not strong enough to unstart the inlet.

- As the back pressure is imposed at the engine face, a normal shock is formed which moves upstream with the increasing back pressure. The change in back pressure does not affect the flow ahead of the throat as information does not propagate upstream in supersonic flows. The sensitivity of the flow to back pressure can be observed for the case with 7% increase in throat area. With Pb/Pi=33.07 the normal shock is downstream of the throat and the inlet is started while for Pb/Pi=33.09 the inlet is unstarted.

- It can be observed, that although it may be possible to start the inlet with less increase in throat area as with 7% increase in throat area and the pressure ratio required for the critical condition is less. but a higher pressure ratio may be needed for a better pressure recovery. So we may conclude that the 8% increase in throat area is desirable than 7% increase in throat area.

- It can be seen that the normal shock is unstable in supersonic diffuser and gets expelled.

4.3   Scope for Future Work

The following work which is done using compressible Euler equations do not consider the viscous effects. It has been demonstrated that the finite element method can be used as an effective tool in the design and analysis of mixed compression two-dimensional supersonic inlets.

- The boundary layer development in the inlet can be strongly influenced by the adverse pressure gradient caused by shock waves and geometric contours. Study of boundary layer i.e. viscous effects can be done by using compressible Navier-Stokes equations.

- With the adverse pressure gradient the boundary layer grows thicker and may separate from the walls when subjected to shock impingement. The proper use of Bleed and Vortex Generators to avoid boundary layer separation can be the next step.

- Buzz, the phenomenon of shock oscillation of supersonic intakes in subcritical operation below some value of the flow ratio. This flow instability retains, in addition to its considerable intrinsic interest, a basic practical importance related to its onset and the nature of its development as intake flow ratio is reduced. So the study of the "Buzz" phenomena can be one of the major future work.

Bibliography

[1] Klous Huenecke. *Modern Combat Aircraft Design*, Airlife England.

[2] D. B. Smeltzer. and N. E. Sorensen. investigation of a Nearly Isentropic Mixed-Compression Axisymmetric Inlet System at Mach Number 0.6 to 3.2, NASA TN D-4557, Jan. 1968.

[3] D. B. Smeltzer. and N. E. Sorensen. Study of a Family of Supersonic Inlet Systems, *Journal of Aircraft*, Vol. 6, No. 3, 1969 pp. 184-188.

[4] A. Hamed and J.S. Shang. Survey of validation data base for shockwave boundary-layer interactions in supersonic inlets. *Journal of Propulsion and Power*, 7(4):617–625, July-August 1991.

[5] R. W. Cubbison., E. T. Meleason, and D. F. Johnson. Effect of Porous Bleed in a High Performance Axisymmetric, Mixed-Compression Inlet at Mach 2.5, NASA TM X-1692, June 1968.

[6] M. K. Fukuda, W. G. Hingst, and E. Reshotko. Control of Shock Wave-Boundary Layer Interaction by Bleed in Supersonic Mixed-Compression Inlets, NASA CR-2595, 1975.

[7] A. Fujimoto, N. Niwa, and K. Sawada. Numerical investigation of supersonic inlet with realistic bleed and bypass systems. *Journal of Propulsion and Power*, 8(4):857–861, July-August 1992.

[8] W. E. Anderson and N. D. Wong. Experimental Investigation of a Large-Scale, Two Dimensional, Mixed Compression Inlet System-Performance at Design Conditions, M = 3.0, NASA TM X-2016, May 1970.

[9] T. A. Reyhner and T. E. Hickcox. Combined Viscous Inviscid Analysis of Supersonic Inlet Flow Fields, *Journal of Aircraft*, Vol. 9, No. 8, 1972, pp. 589-595.

[10] R. H. Bush. External Compression Inlet Predictions Using an Implicit, Upwind, Multiple Zone Approach, AIAA paper 85-1521 July 1985.

[11] R. H. Bush. Two-Dimensional Numerical Analysis for Inlets at Subsonic Through Hypersonic Speeds, *Journal of Propulsion*, Vol. 4, No. 6, 1988, pp. 549-556.

[12] D. D. Knight. Improved Calculation of High Speed Inlet Flows Part 2; Results, *AIAA Journal*, Vol. 19, No. 2, 1981, pp. 172-179.

[13] D. D. Knight. Calculation of Simulated 3-D High Speed Inlet Using the Navier-Stokes Equations, AIAA paper 83-1165, June 1983.

[14] R. Buggeln, H. McDonald, J. Kreskovsky, and R. Levy. Computation of Three-Dimensional Viscous Supersonic Flow in Inlets, AIAA paper 80-0194, Jan 1980.

[15] B. Anderson, and C. Towne. Numerical Simulation of Supersonic Inlets Using a Three-Dimensional Viscous Flow Analysis, AIAA paper 80-0384, Jan 1980.

[16] S. M. Liang, and J. J. Chan. An Improved Upwind Scheme for the Euler Equations, *Journal of Computational Physics*, Vol. 84, No. 2, 1989, pp. 461-473.

[17] S. M. Liang, and J. J. Chan. Numerical Investigation of Supersonic Mixed-Compression Inlet Using an Implicit Upwind Scheme, *Journal of Propulsion*, Vol. 8, No. 1, 1992, pp. 158-167.

[18] Y.C. Hsia and B.J. Gross J.P. Ortwerth. Inviscid analysis of a dual mode scramjet inlet. *Journal of Propulsion and Power*, 7(6):1030–1035, Nov-Dec 1991.

[19] Y.C. Hsia and E.W. Daso V.A. Padhye. Full Navier-Stokes analysis of a three-dimensional scramjet inlet. *Journal of Propulsion and Power*, 8(5):1071–1078, Sept-Oct 1992.

[20] Y.C. Hsia. Full Navier-Stokes analysis of an axisymmetric scramjet inlet. *Journal of Propulsion and Power*, 9(6):827–833, Nov-Dec 1993.

[21] J.J. Korte, D.J. Singh, A. Kumar, and A.A. Auslender. Numerical study of the performance of swept, curved, compression surface scramjet inlets. *Journal of Propulsion and Power*, 10(6):841–847, Nov-Dec 1994.

[22] T.E. Tezduyar and T.J.R. Hughes. Development of time-accurate finite element techniques for first-order hyperbolic systems with particular emphasis on the compressible Euler equations. report prepared under NASA-Ames University Consortium Interchange, No. NCA2-OR745-104, 1982.

[23] T.E. Tezduyar and T.J.R. Hughes. Finite element formulations for convection dominated flows with particular emphasis on the compressible Euler equations. In *Proceedings of AIAA 21st Aerospace Sciences Meeting*, AIAA Paper 83-0125, Reno, Nevada, 1983.

[24] T.J.R Hughes and T.E. Tezduyar. Finite element methods for first-order hyperbolic systems with particular emphasis on the compressible Euler equations. *Computer Methods in Applied Mechanics and Engineering*, 45:217–284, 1984.

[25] S. Mittal. Finite element computation of unsteady viscous compressible flows. *Computer Methods in Applied Mechanics and Engineering*, 157:151–175, 1998.

[26] S. Mittal. Finite element computation of unsteady viscous compressible flows past stationary airfoils. *Computational Mechanics*, 21:172–188, 1998.

[27] G. J. L. Beau. The Finite Element Computation of Compressible Flows. A Graduate thesis submitted to University of Minnesota, Dec. 1990

[28] P. G. Hill, and C. Peterson. *Mechanics and Theromodynamics of Propulsion.* Addison-Wesley Publishing Company, 1999.

[29] S. Mittal, V. Kumar, and A. Raghuvanshi. Unsteady incompressible flow past two cylinders in tandem and staggered arrangements. *International Journal for Numerical Methods in Fluids*, 25:1315–1344, 1997.

[30] S.K. Aliabadi and T.E. Tezduyar. Space-time finite element computation of compressible flows involving moving boundaries and interfaces. *Computer Methods in Applied Mechanics and Engineering*, 107:209–224, 1993.

[31] T.J.R. Hughes and M. Mallet. A new finite element formulation for computational fluid dynamics: IV. A discontinuity-capturing operator for multidimensional advective-diffusive systems. *Computer Methods in Applied Mechanics and Engineering*, 58:329–339, 1986.

[32] J. D. Anderson. *Modern Compressible Flow: With Historical Perspective.* McGraw-Hill Publishing Company, New York, 2nd edition, 1990.

[33] J. Seddon, and E. L. Goldsmith. *Intake Aerodynamics.* Blackwell Science ltd. 2nd edition,1999.
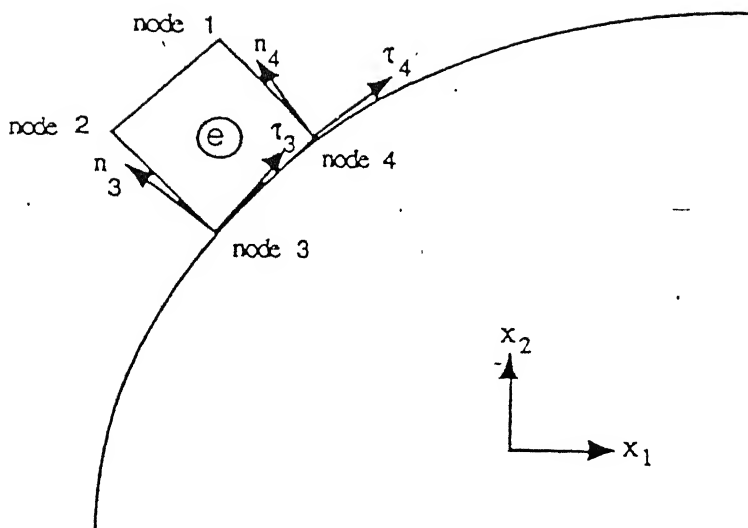
Element on surface with slip condition

Figure 1.   Typical Finite Element on Solid Surface.

Figure 2.   Geometry of the Inlet.

( )* : nondimensional scale

119.02" (1.00)*

30.4" (0.255)

58.8" (0.494)*

28" (0.235)*

14" (0.4176)*

14"

7°

(0.028)

Cowl

Ramp

throat

d

f

e

b

c

Y
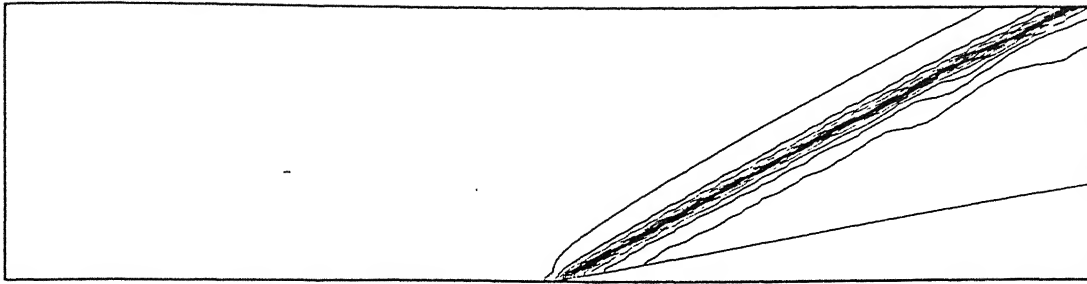
Figure 3.   Flow past a 10° Compression Corner.
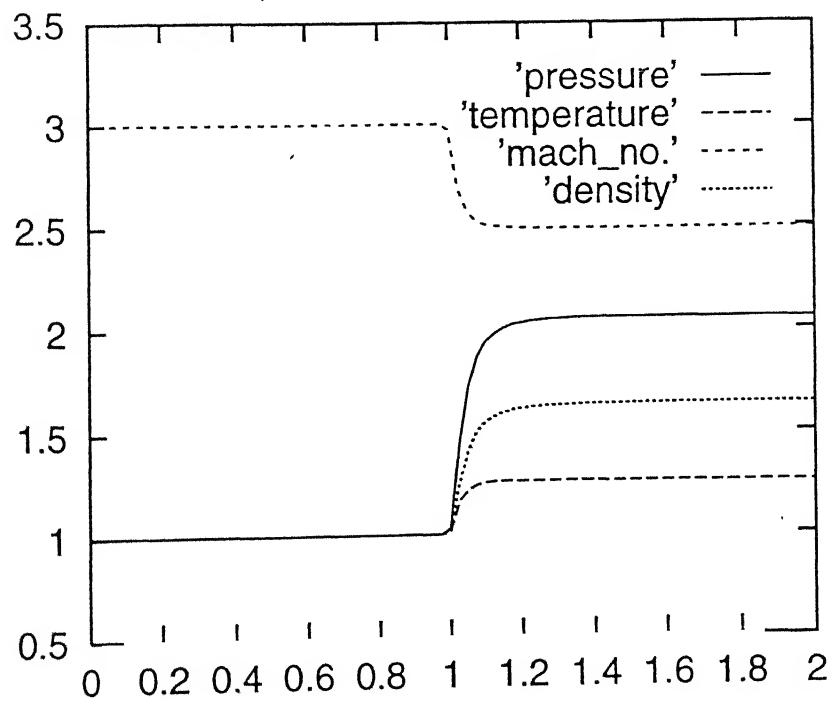
Figure 4.   Effect of Compression Corner on Various Parameters.
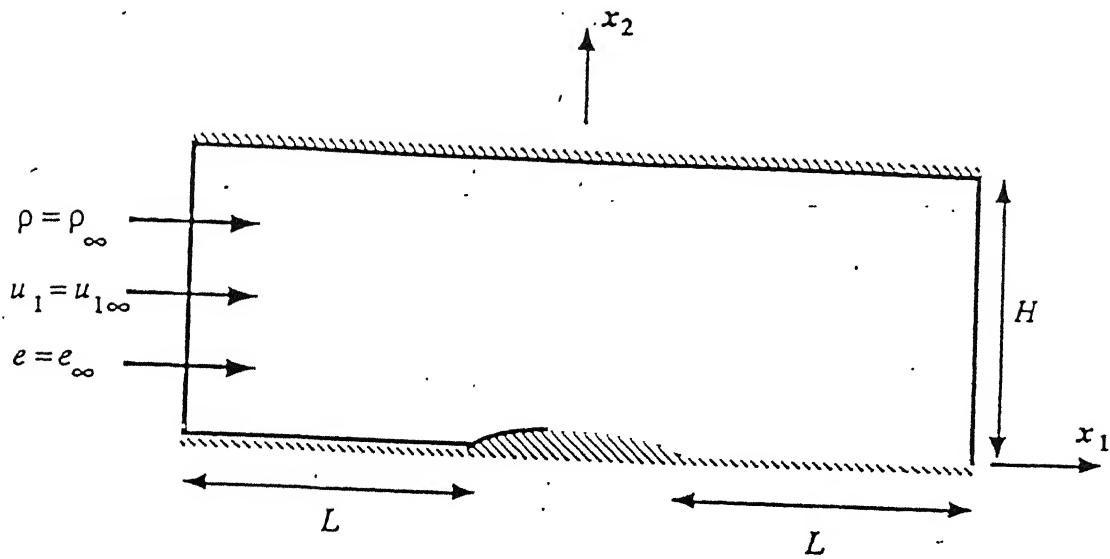
Figure 5. Flow past a Parabolic Arc Bump: Problem Statement.
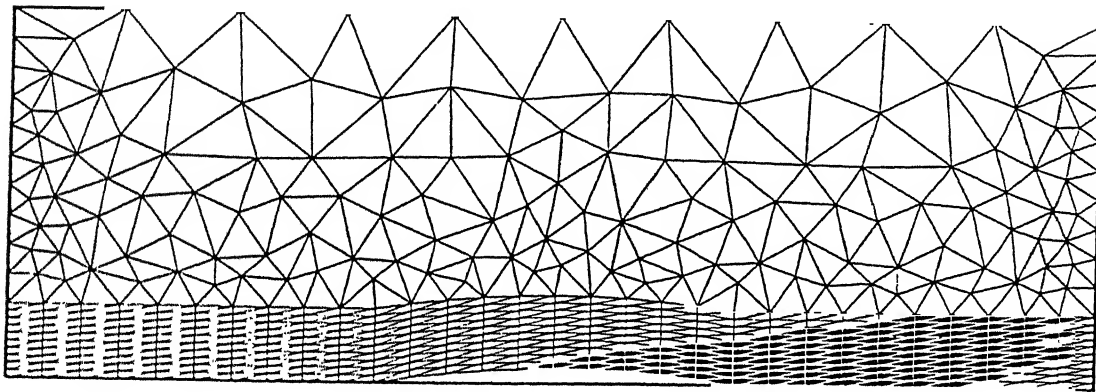
(a)
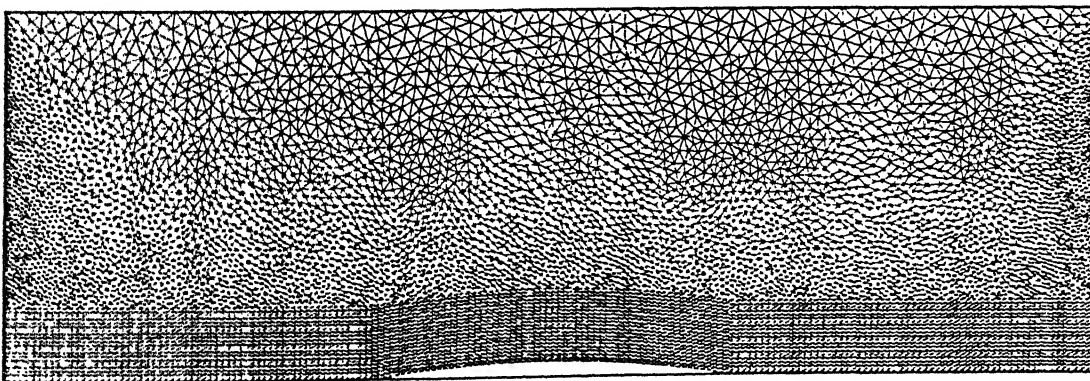
(b)

Figure 6. Finite Element Mesh For Flow past a Parabolic Arc Bump.
(a) Schematic Mesh, (b) Mesh used for Computation
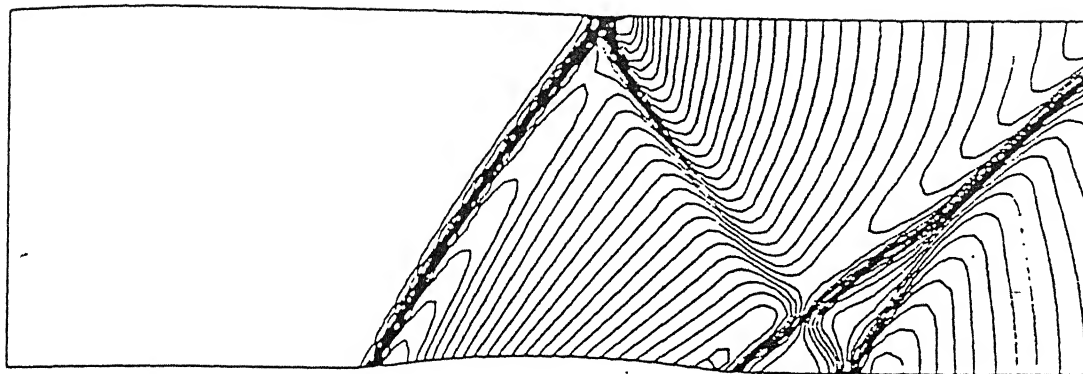
(a)
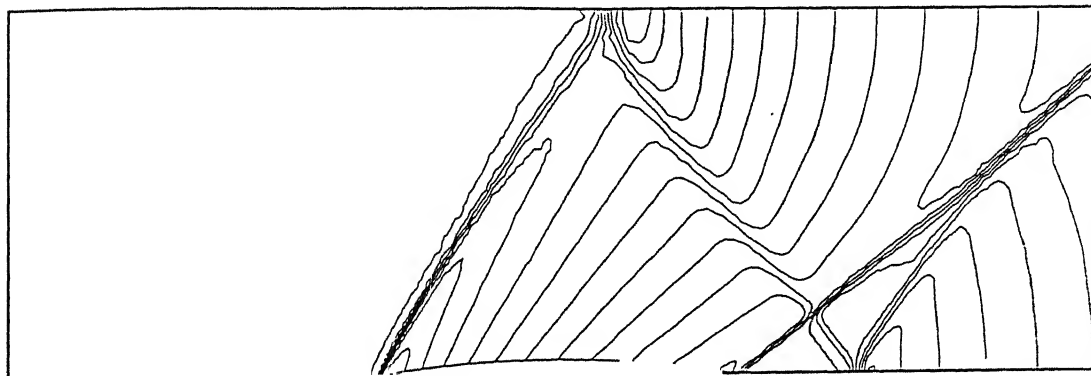
(b)

Figure 7.   Steady State Solution for free-stream Mach number of 1.4.

(a) Pressure Contours given by Beau [27],

(b) Pressure Contours from our calculations.
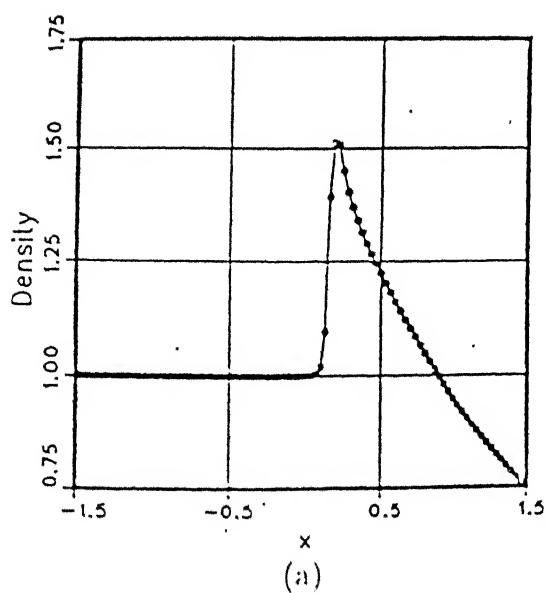
(a)
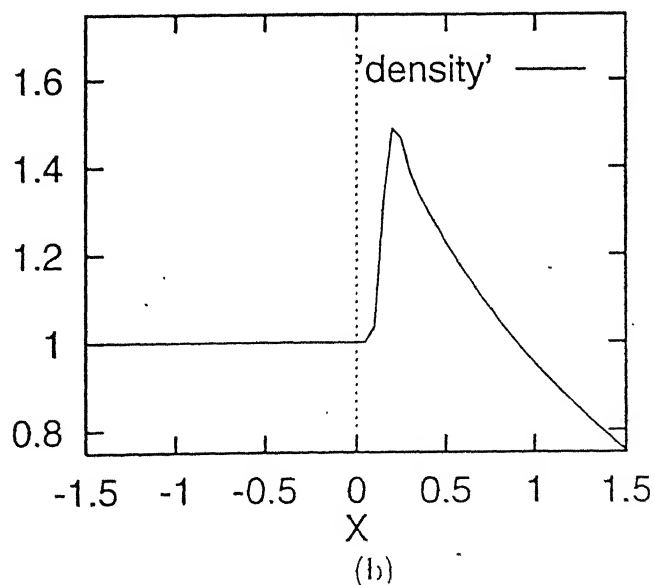
(b)

Figure 8.   Steady State Solution for free-stream Mach number of 1.4.

(a) Density given by Beau [27] at y = 1.0,

(b) Density at y = 1.0 from our calculations.
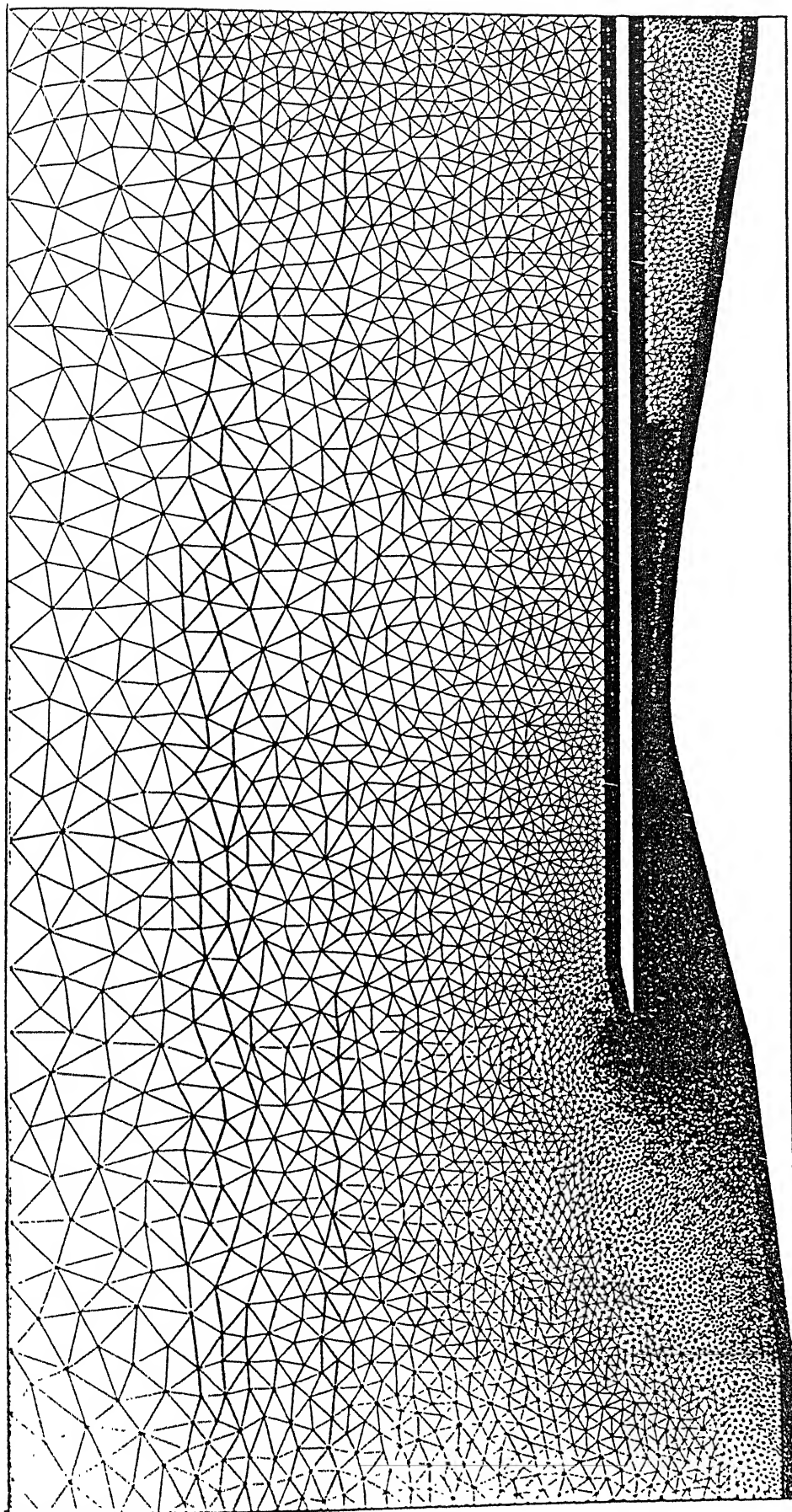
Figure 9.   Grid Generation on   (a) Complete Inlet,

(b) Near Throat,

(c) Near Cowl.

T=780

T=1130

T=1970

T=2470

T=3010

T=3370
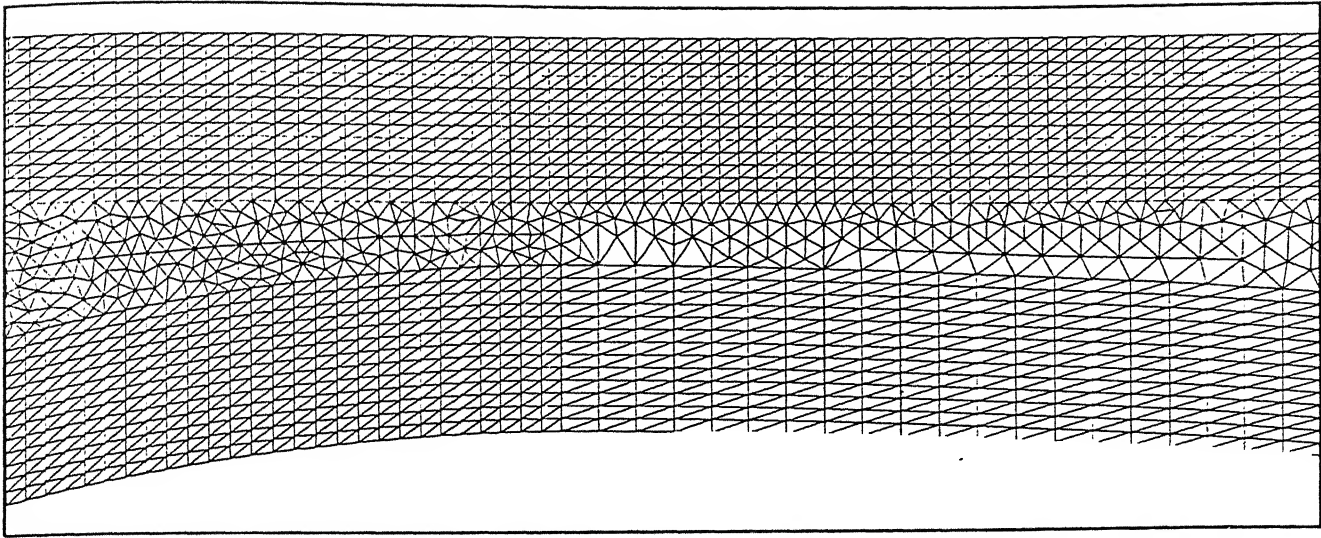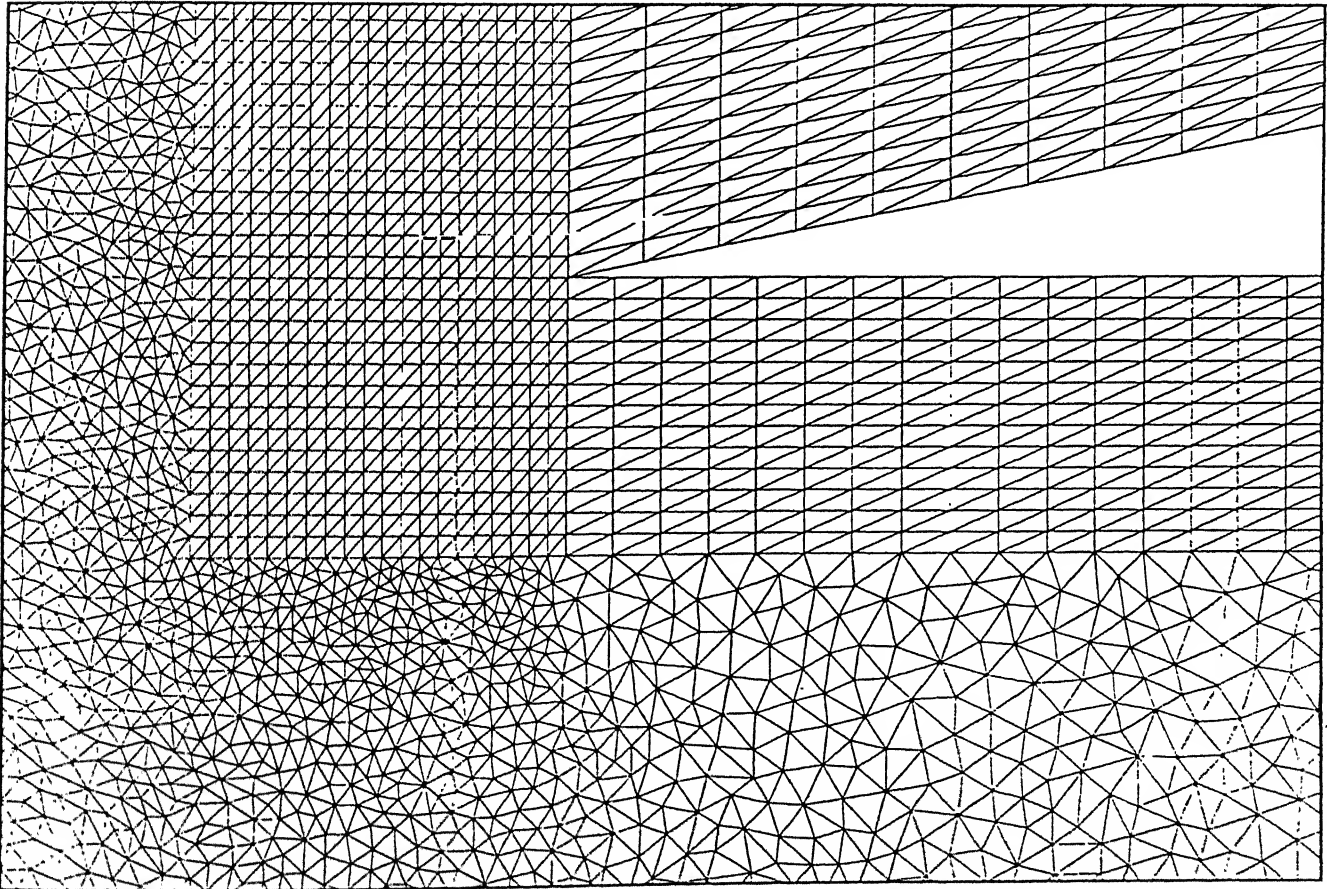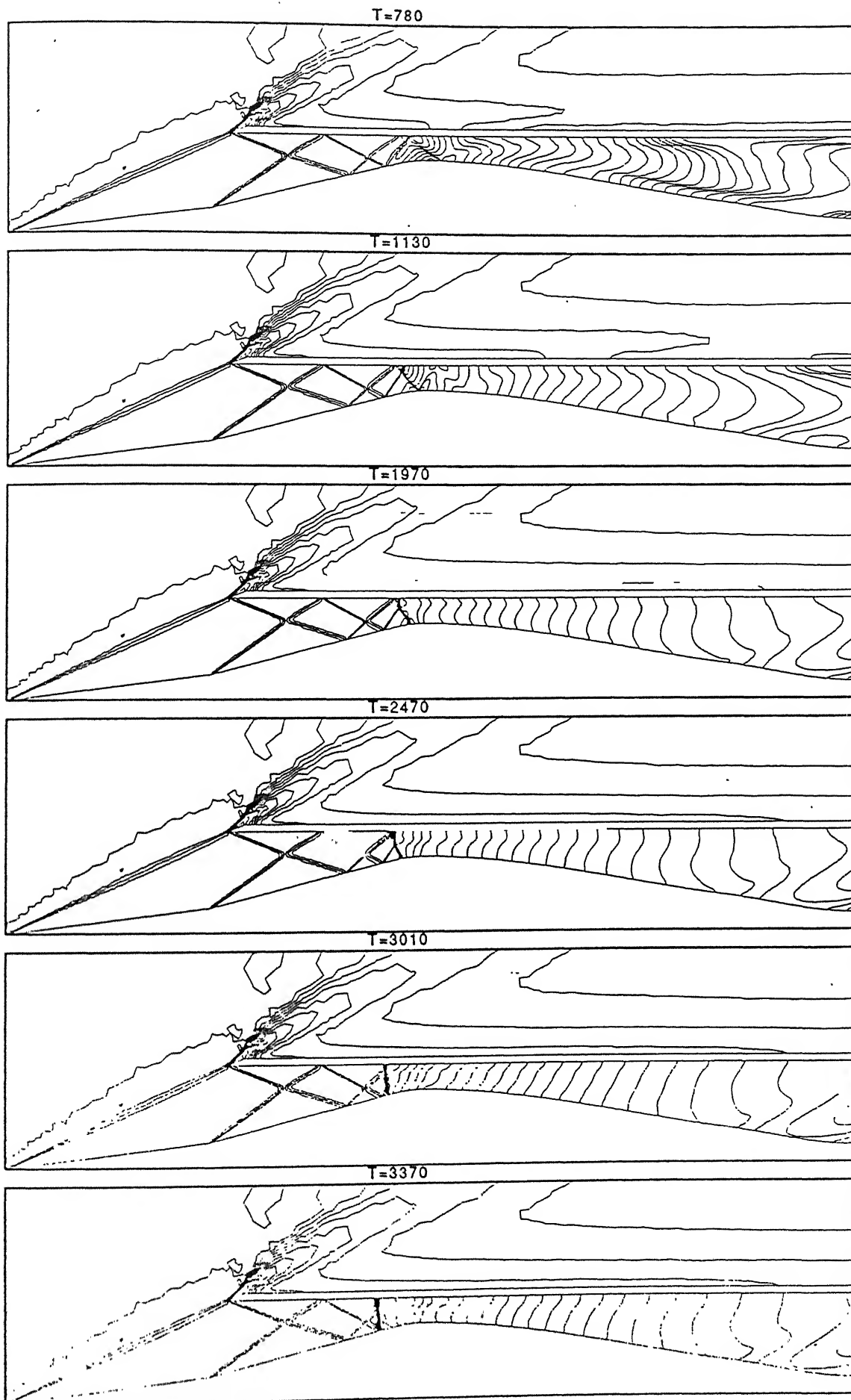
Figure 10.   Mach contours of the unstarted flow at M=3.0 with Time(T).

T=780

T=1130

T=1970

T=2470

T=3010

T=3370
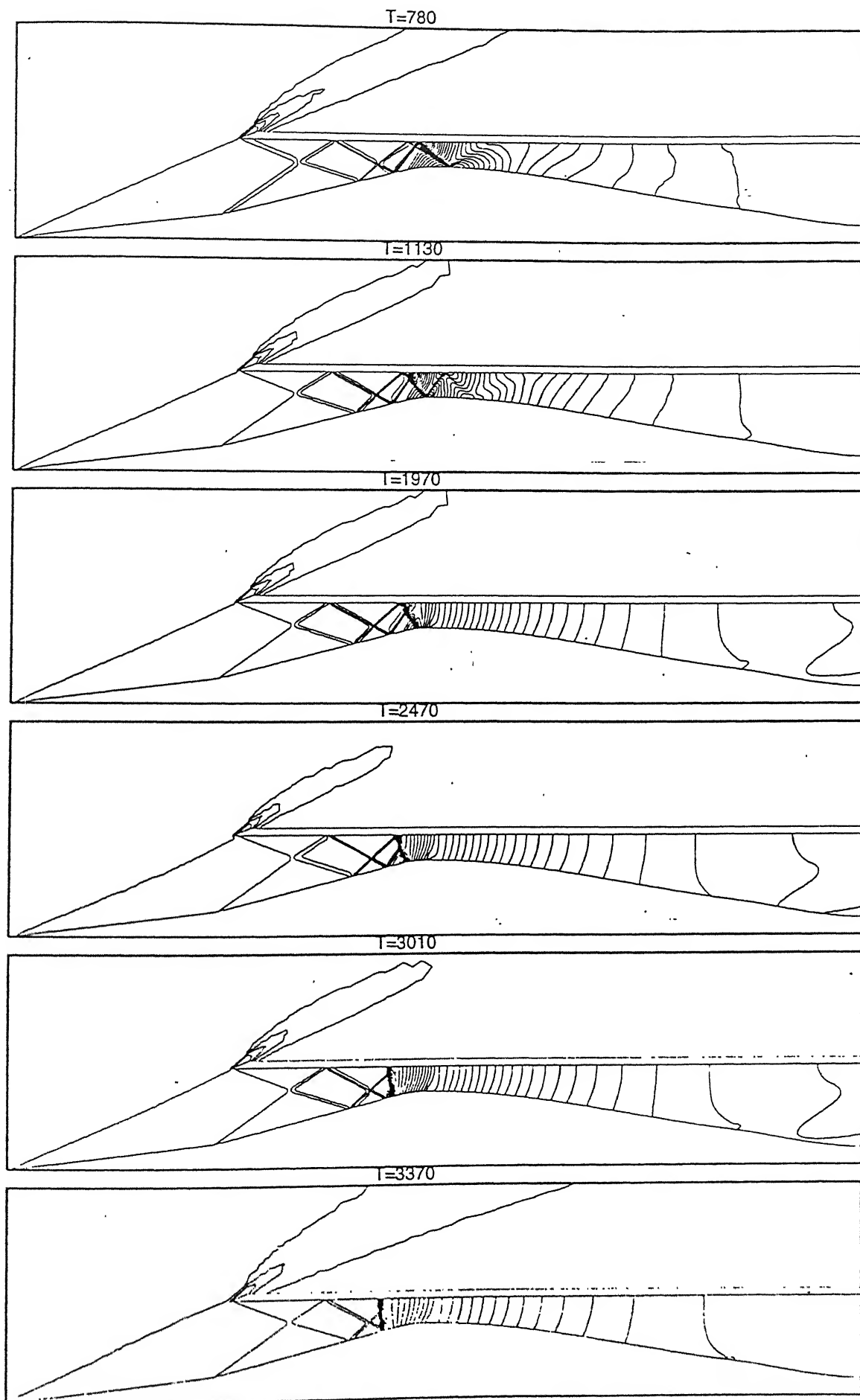
Figure 11. Pressure contours of the unstarted flow at M=3.0 with Time(T).
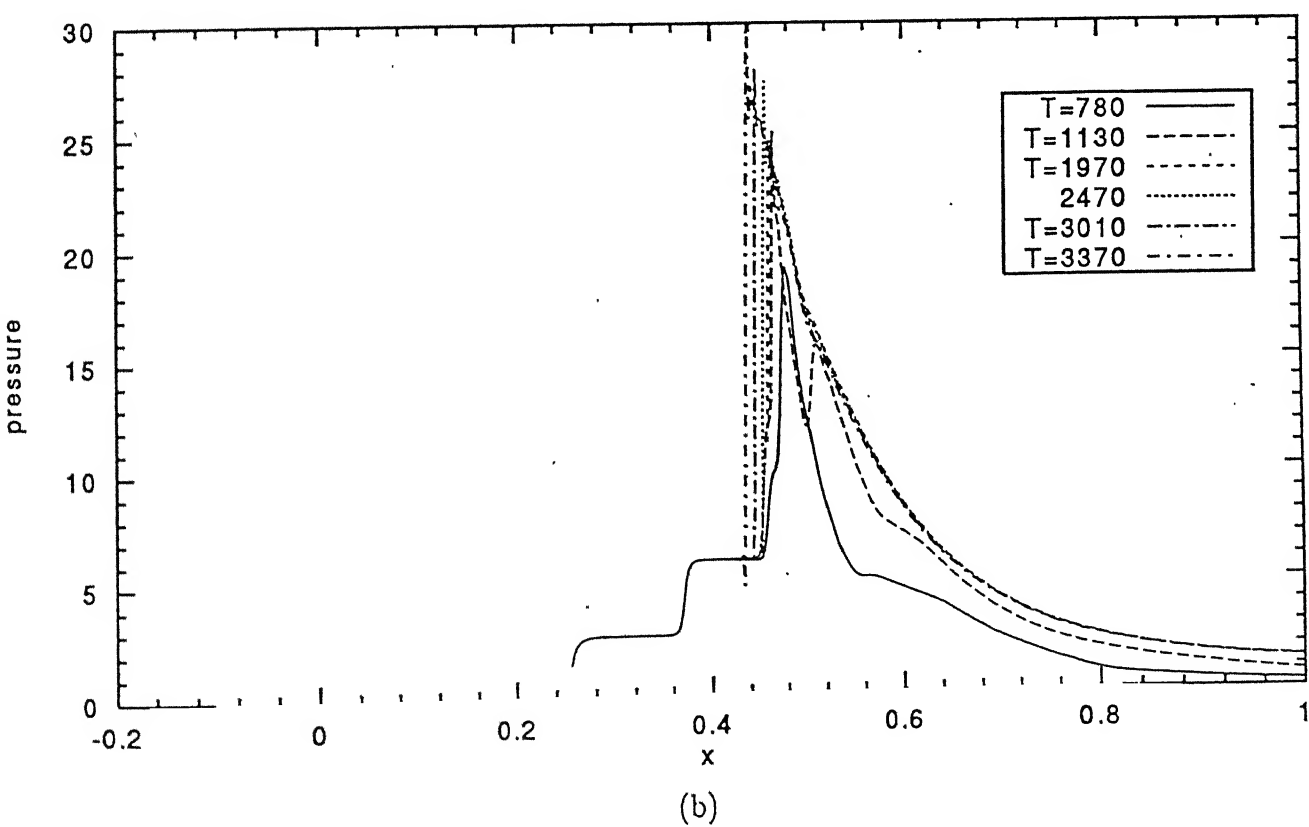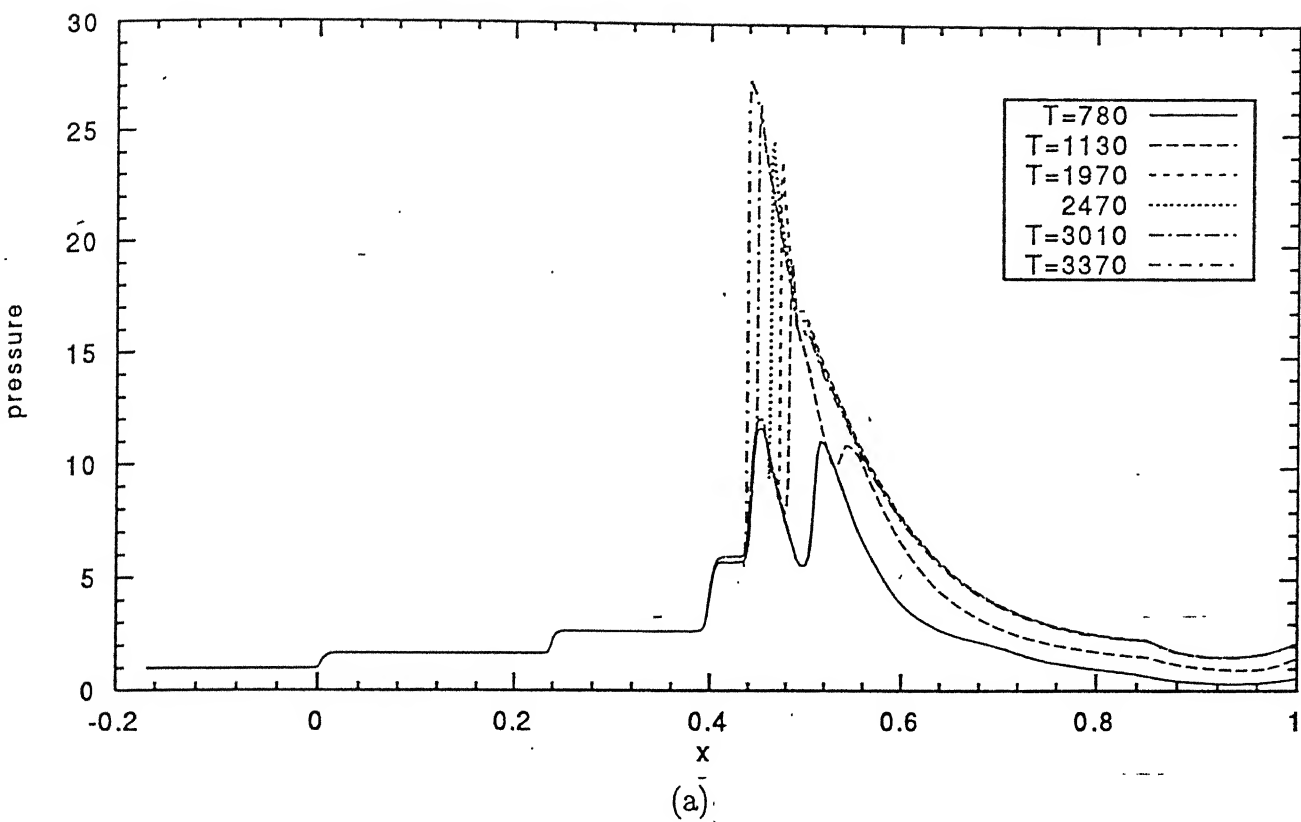
Figure 12.   Effect on Pressure with Time(T) for unstarted inlet along
(a) ramp surface, (b) cowl surface.
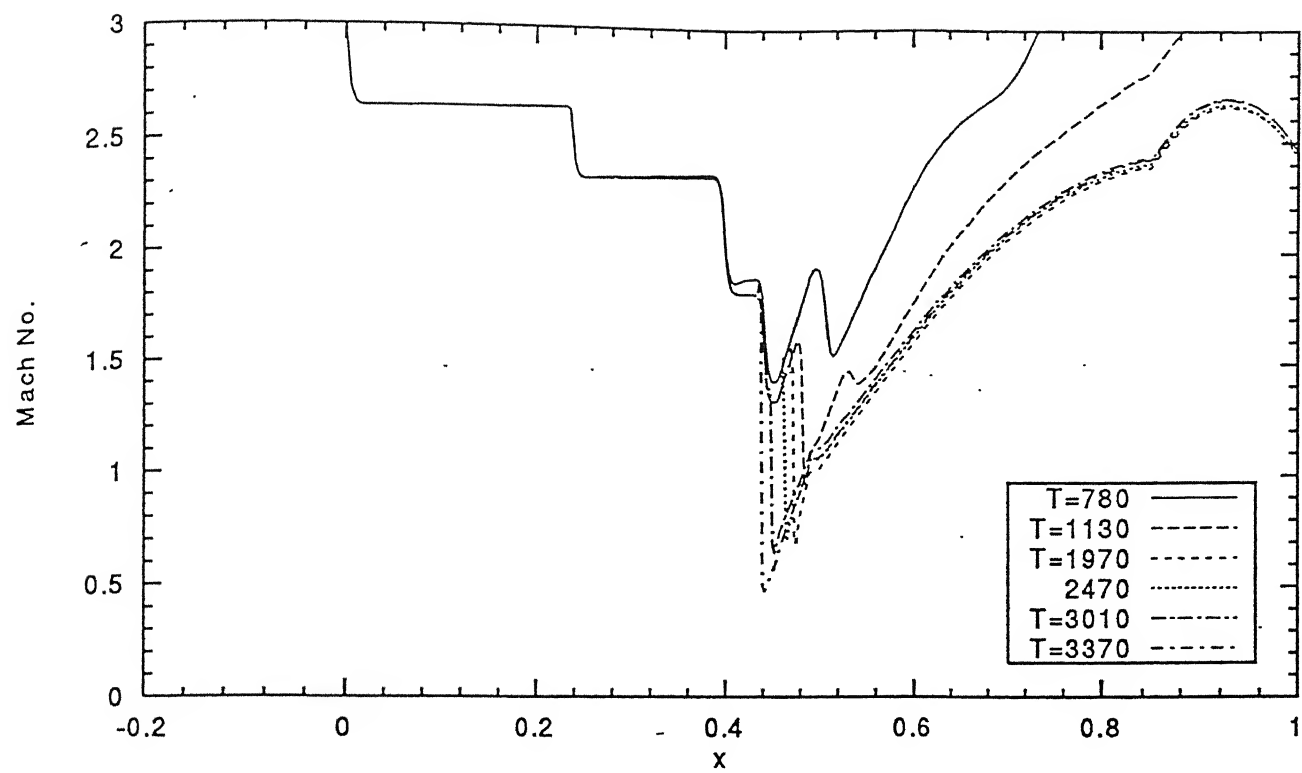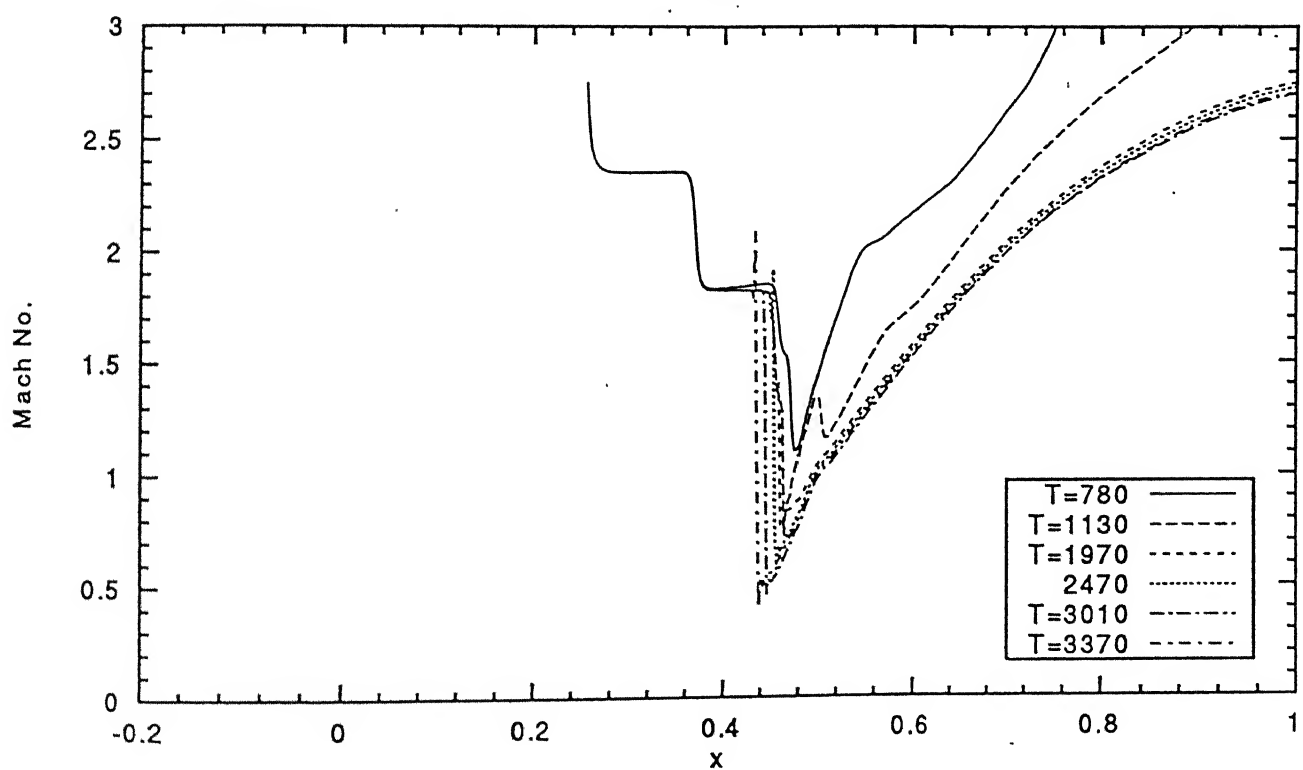
Figure 13.   Effect on Mach No. with Time(T) for unstarted inlet along
(a) ramp surface, (b) cowl surface.
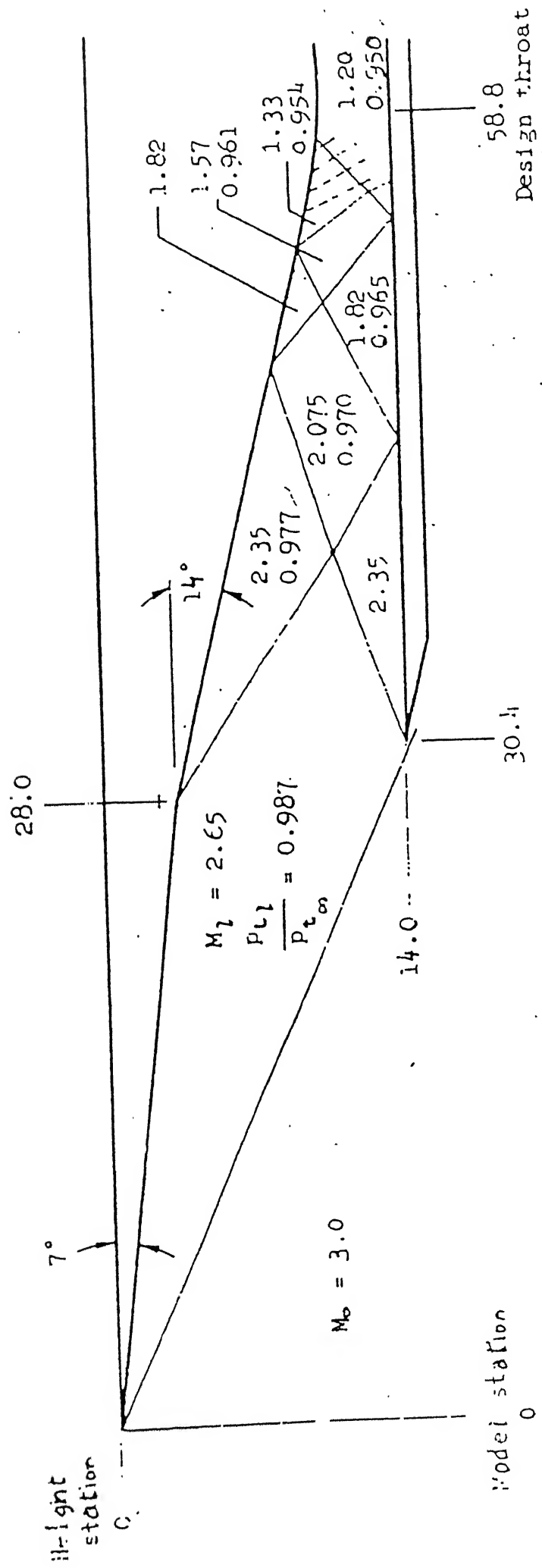
Figure 14.   Inviscid Shock Pattern in Supersonic Diffusor from Wong [8].

T=11.5

T=23.5

T=511.5

T=2470.5

T=12311.5
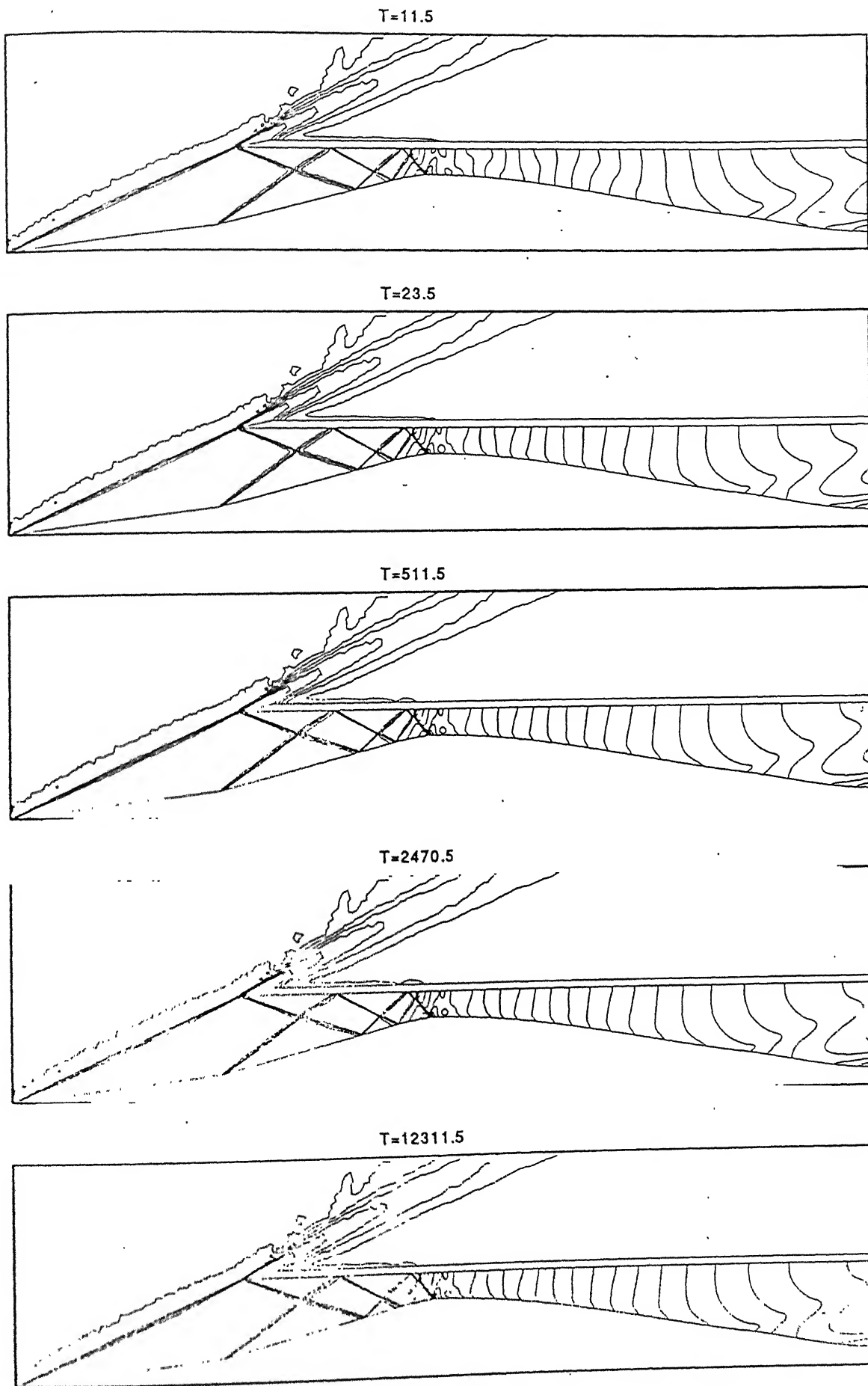
Figure 15.　　Mach Contours for the Started Inlet Flow at M=3.0 with Time(T).

T=11.5

T=23.5

T=511.5

T=2470.5

T=12311.5
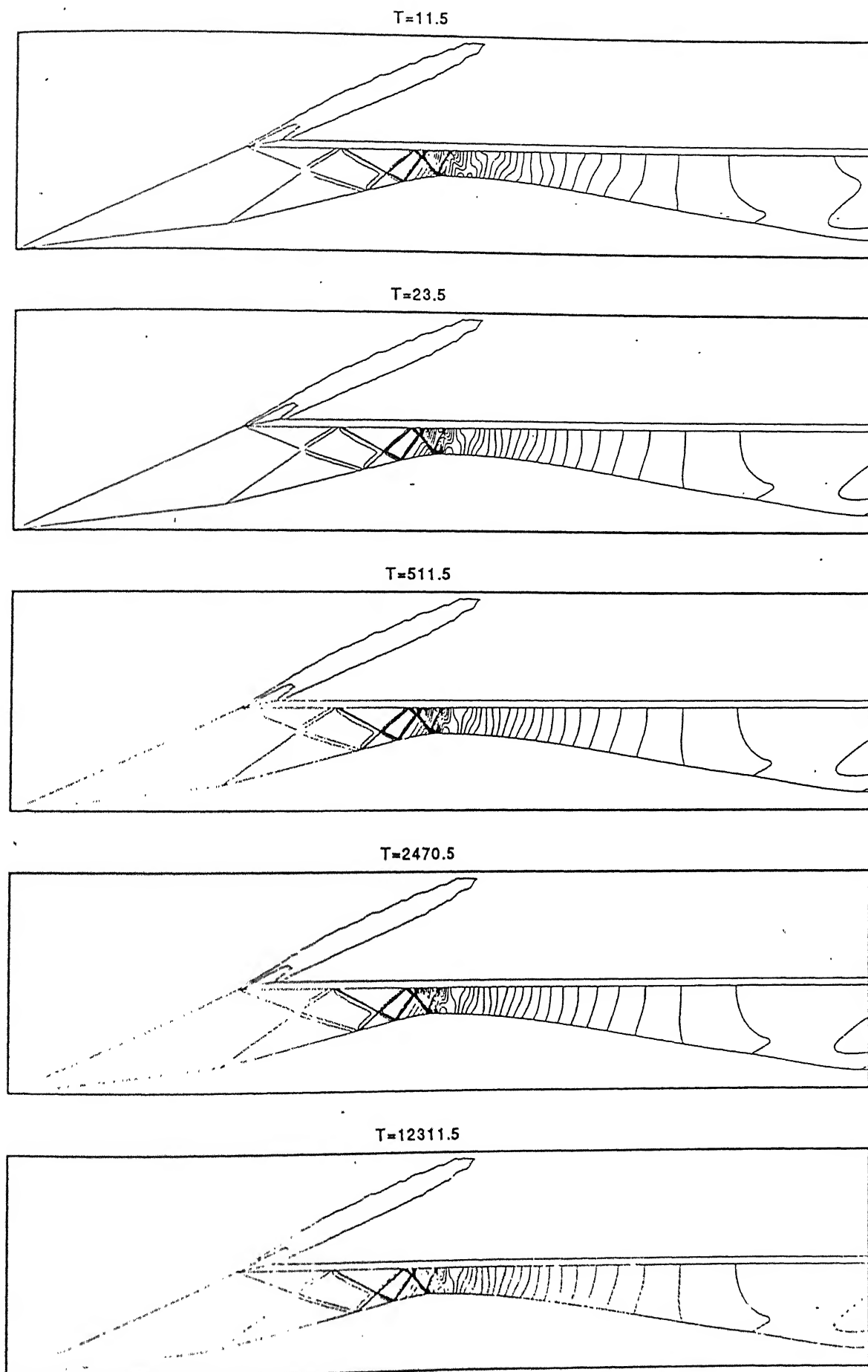
Figure 16.　　　Pressure Contours for the Started Inlet Flow at M=3.0 with Time(T).
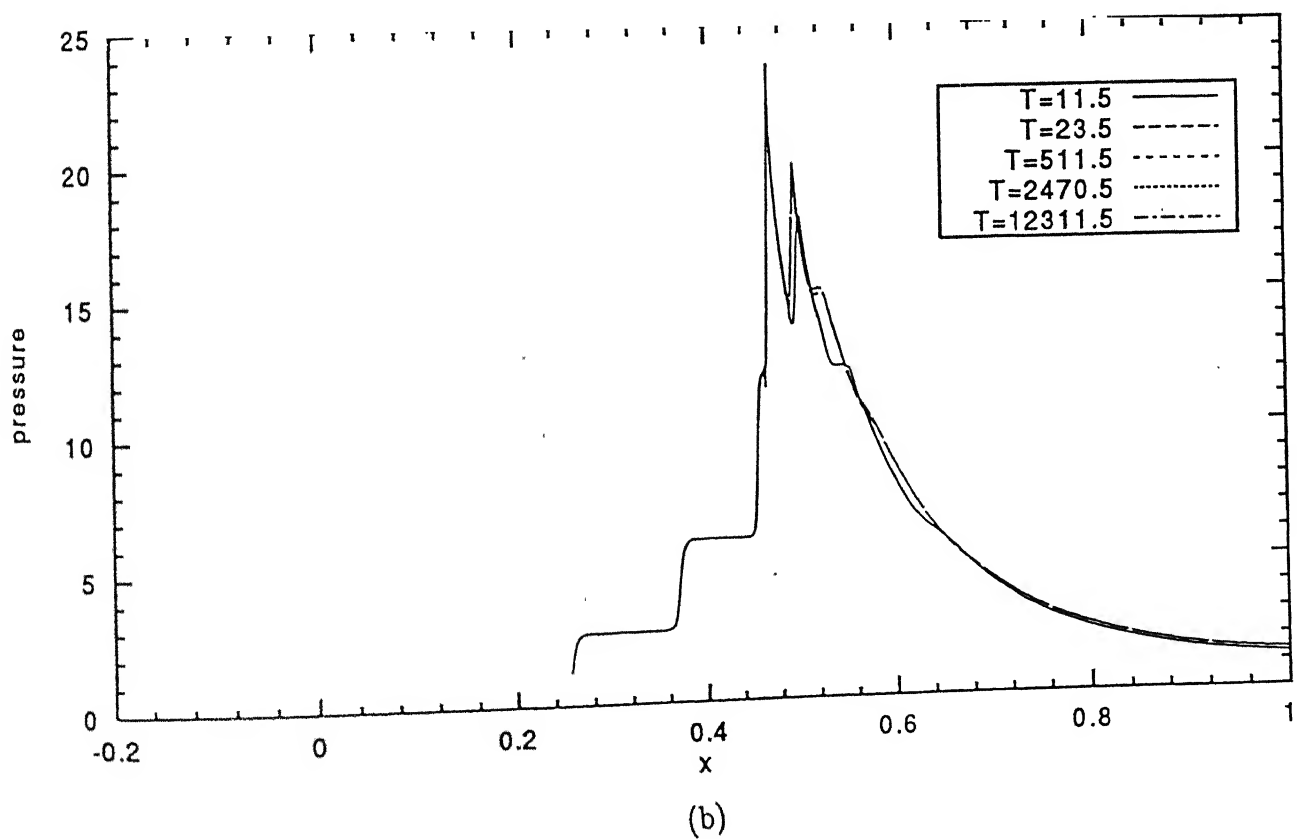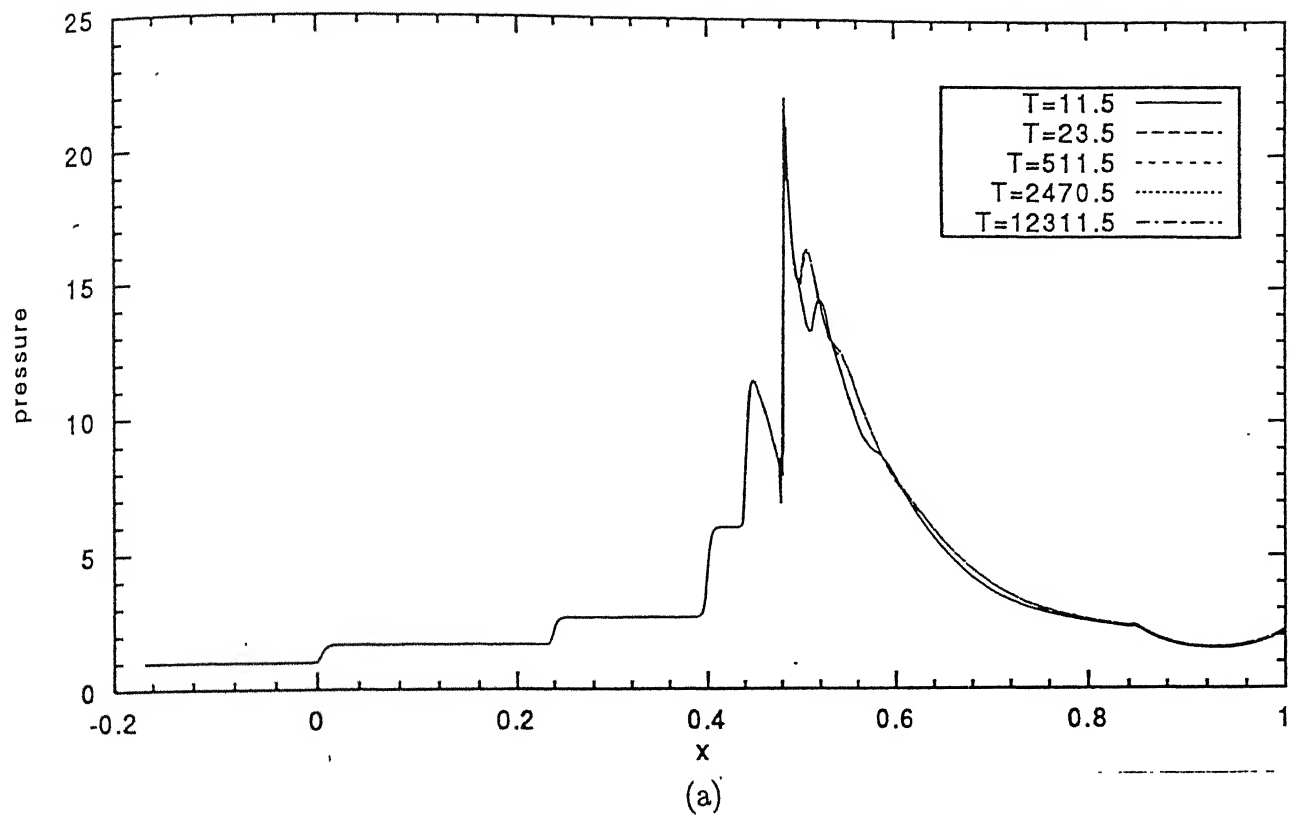
Figure 17.   Effect on Pressure of Started Inlet with Time(T) along
(a) ramp surface, (b) cowl surface.
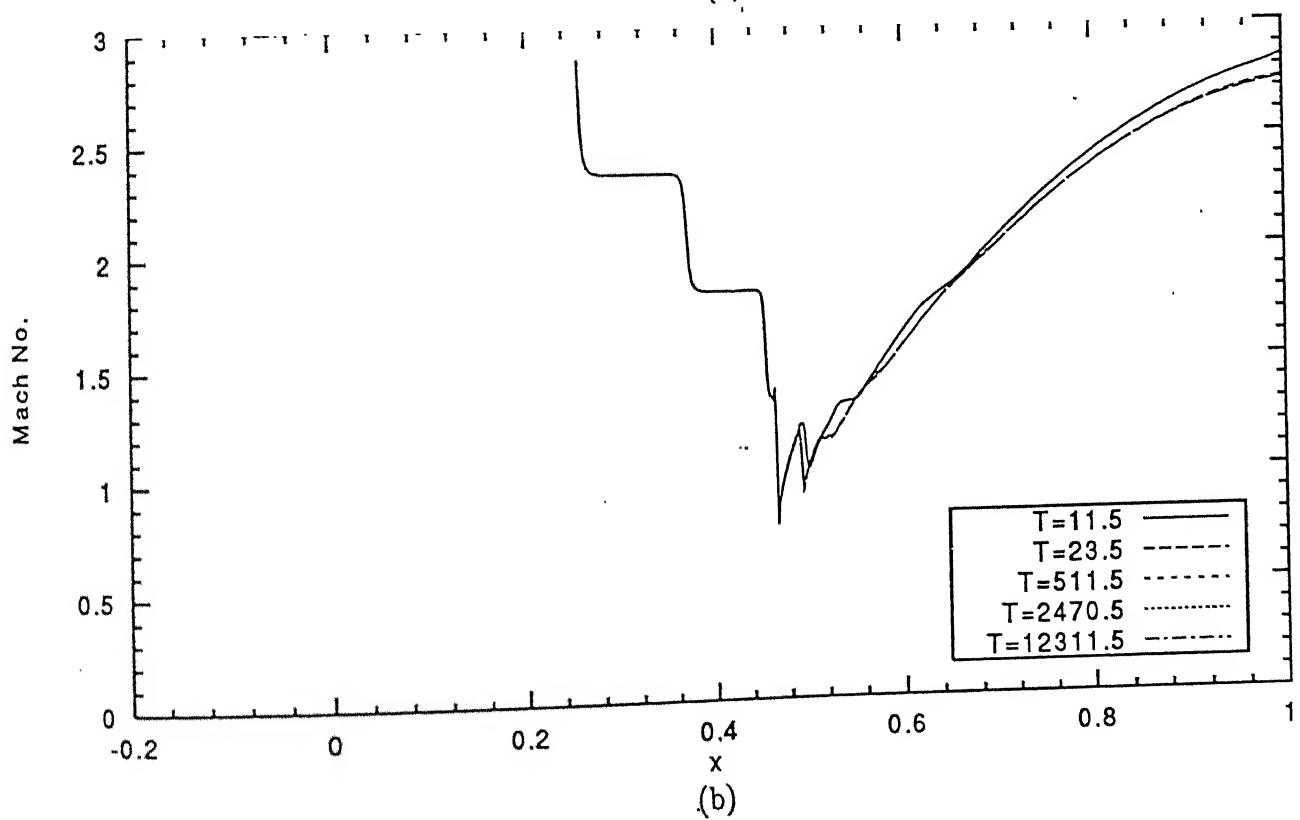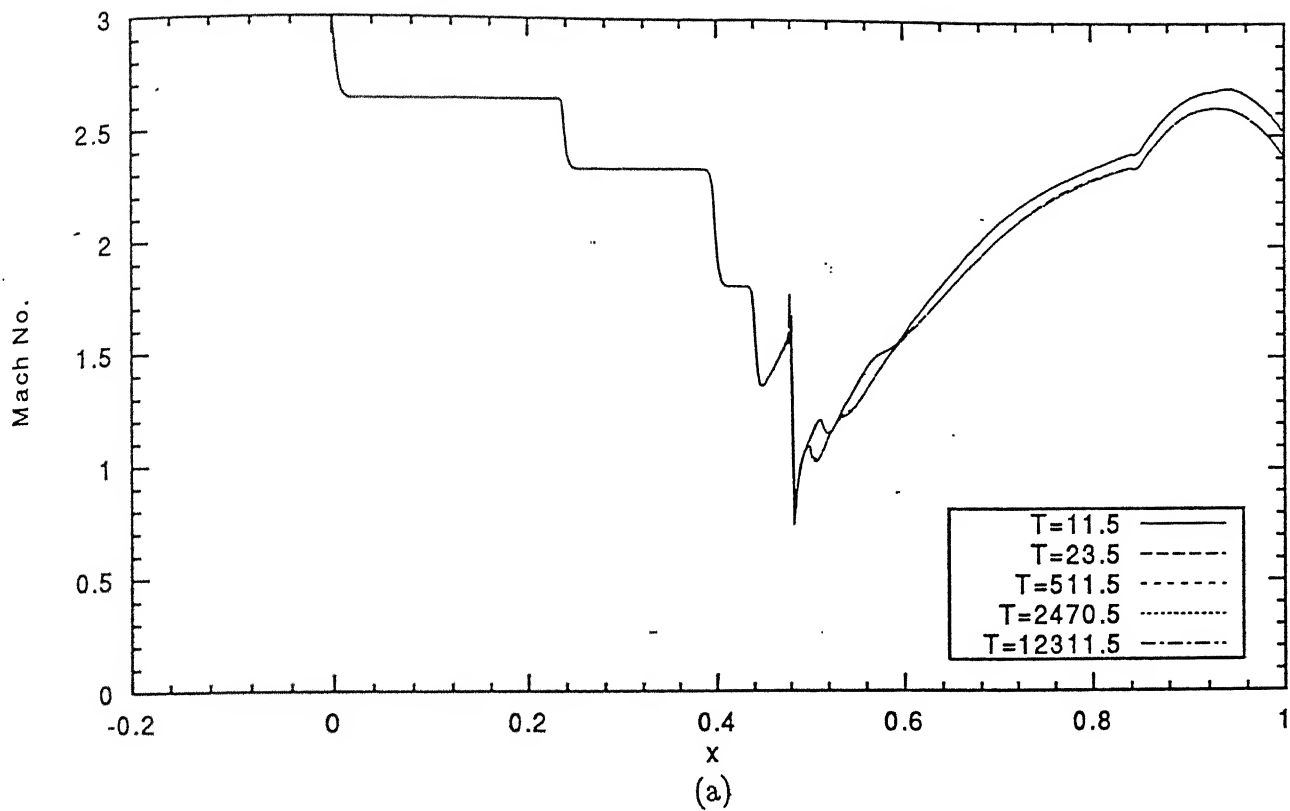
Figure 18.   Effect on Mach No. of Started Inlet with Time(T) along
(a) ramp surface, (b) cowl surface.
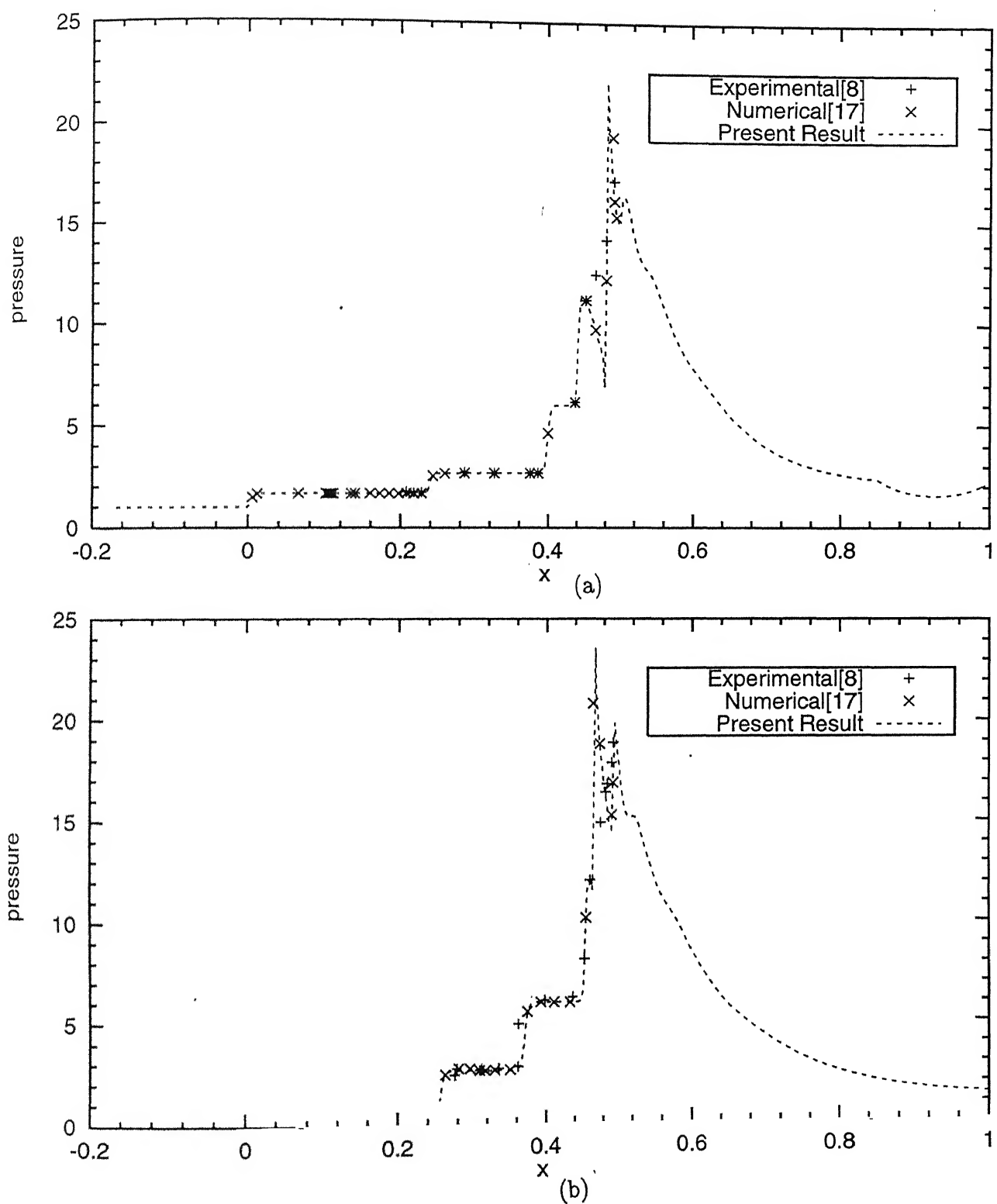
Figure 19.   Comparison of Pressure in Experimental results by Wong [8],
Computational results by Liang [17] and our Calculations
in Supersonic Diffuser along (a) ramp surface, (b) cowl surface.
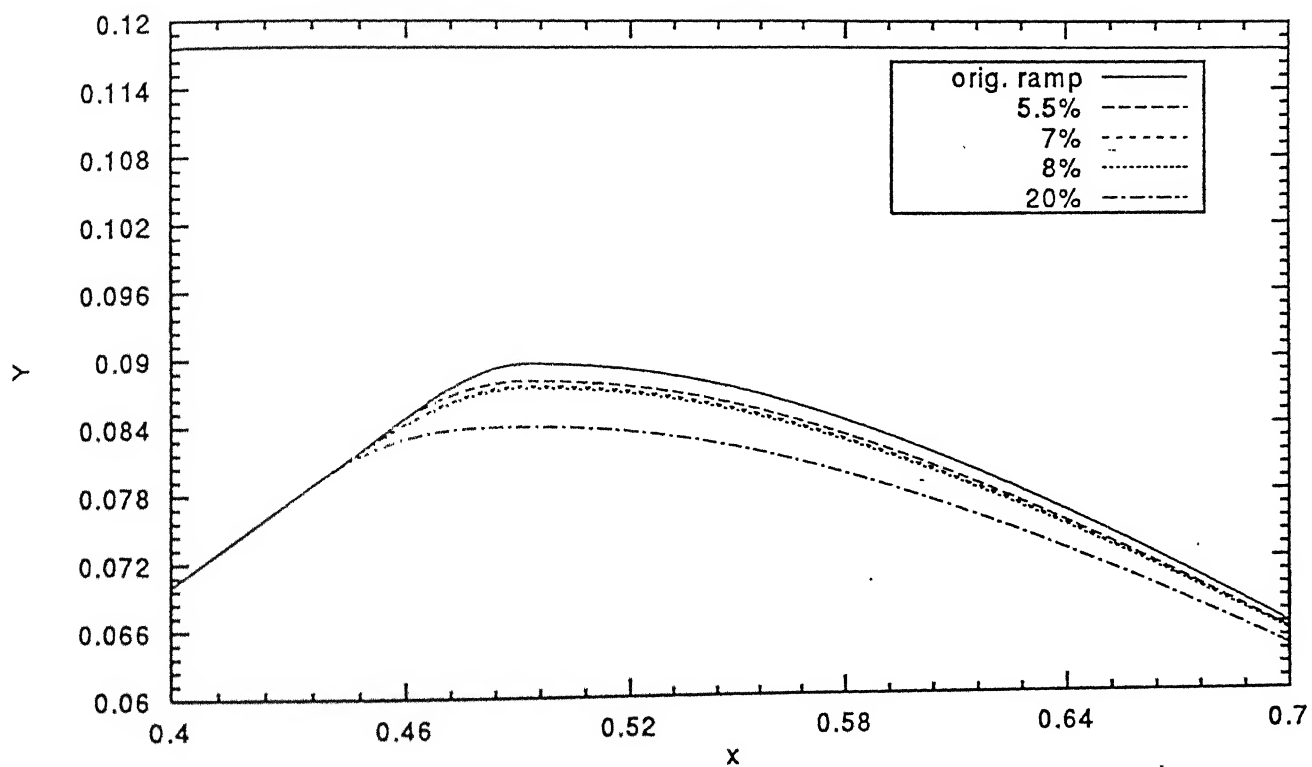
Figure 20.   Modified Geometry at Throat with Throat Area Increase.
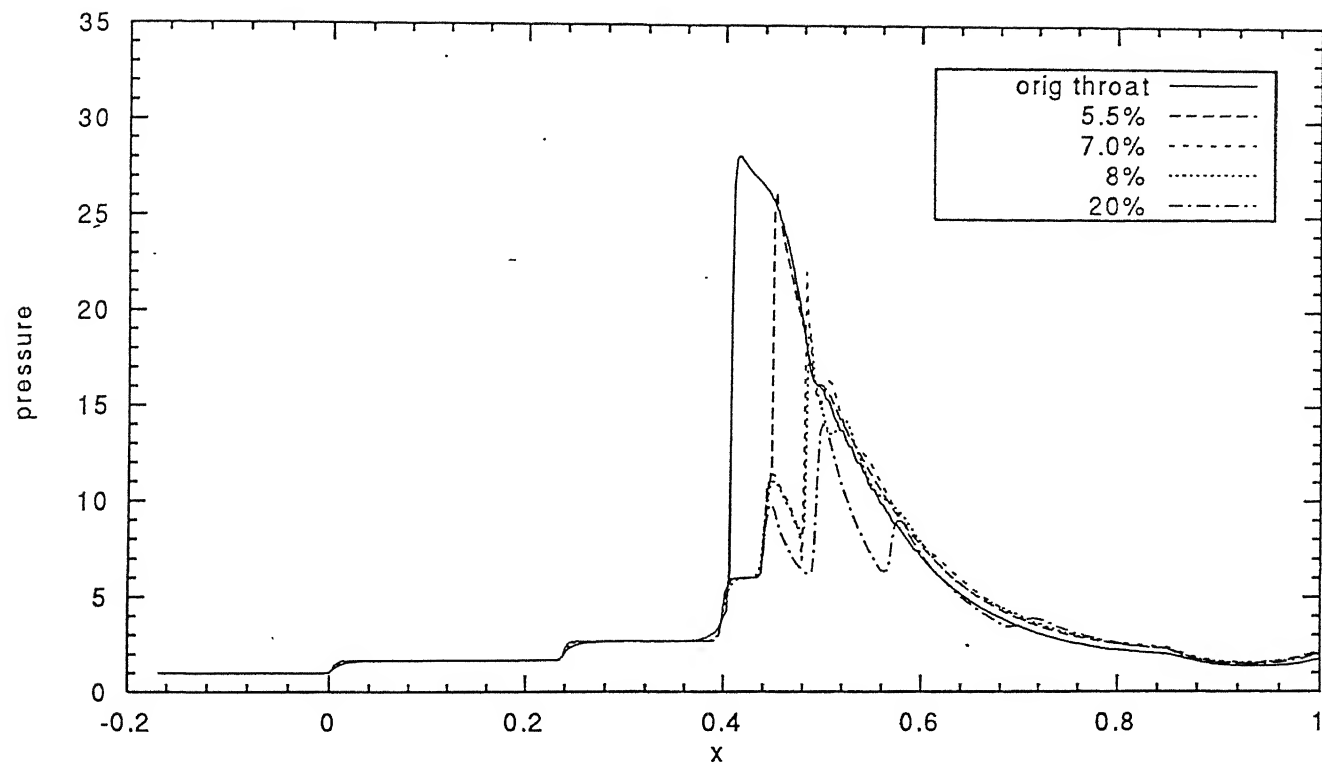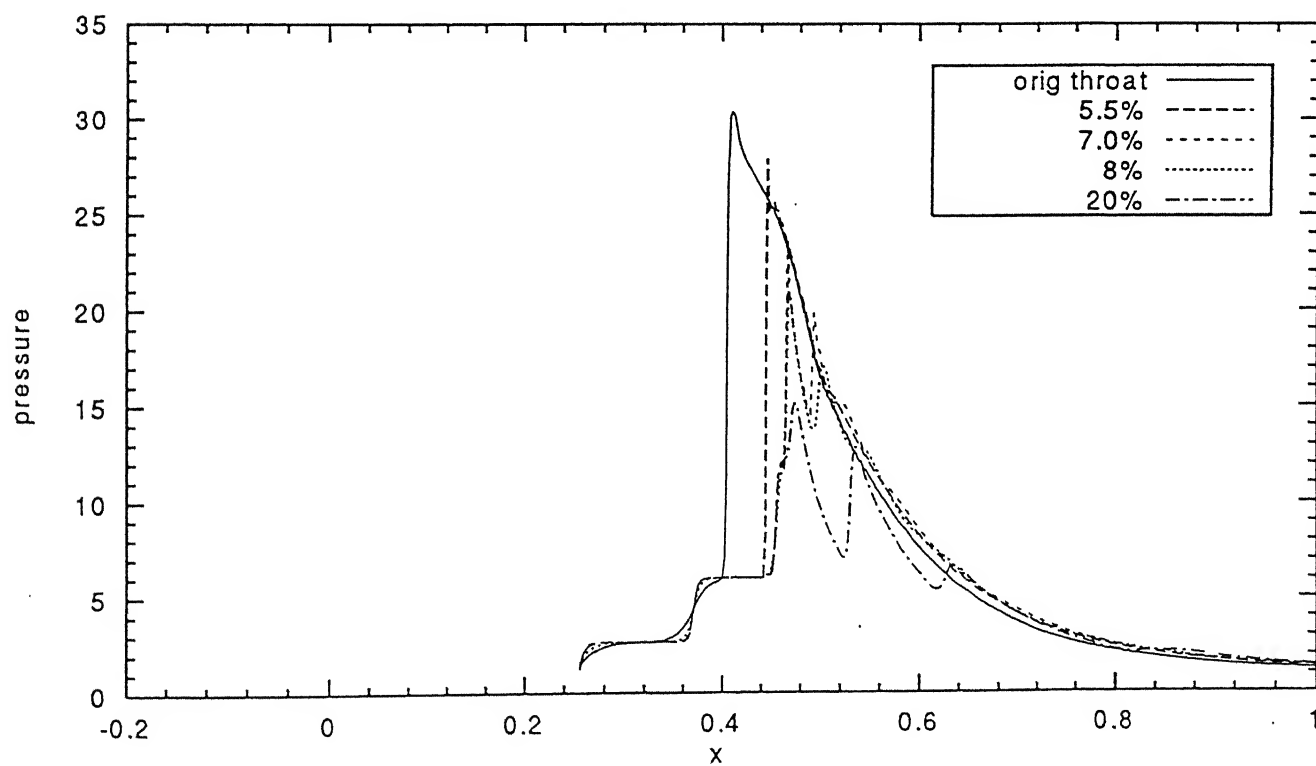
Figure 21.   Effect of Increase of Throat Area on Pressure along
(a) Ramp surface, (b) cowl surface.
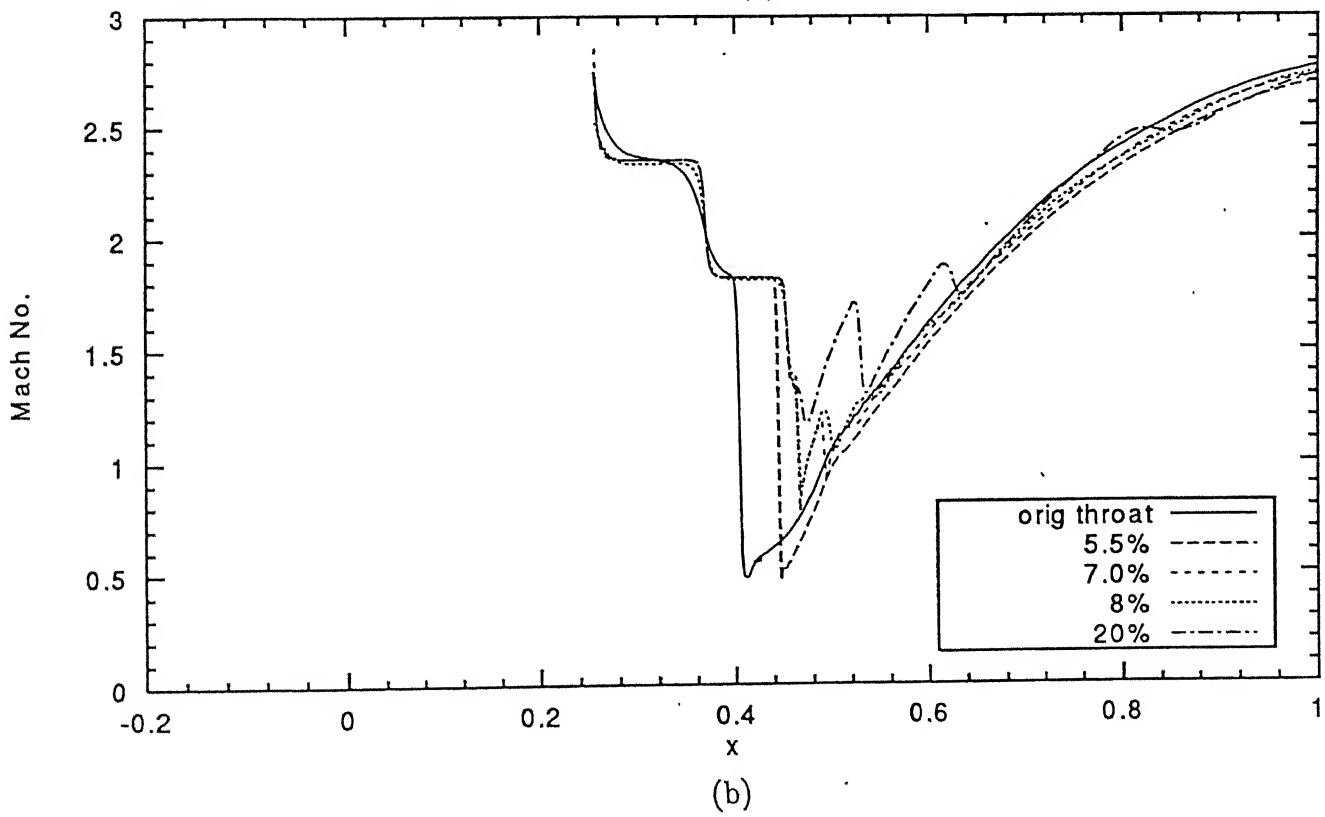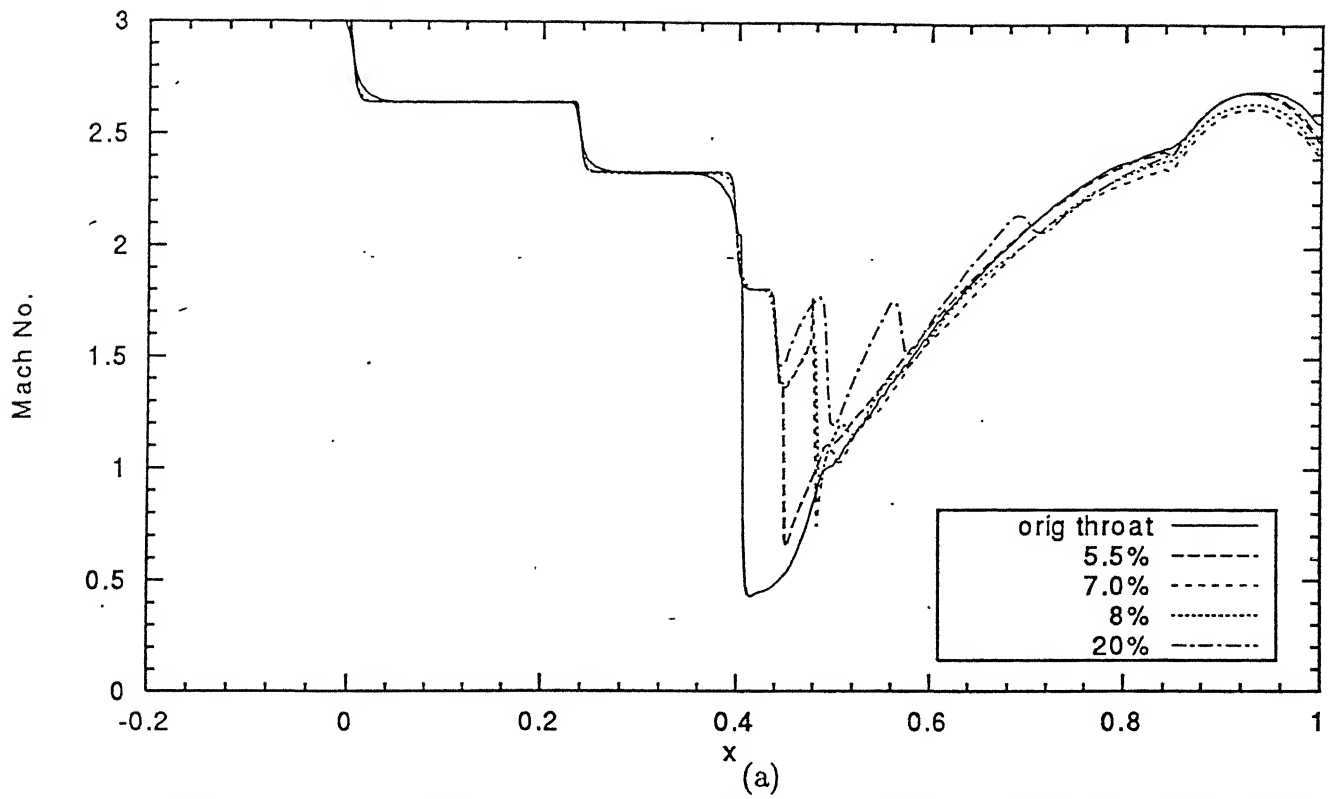
Figure 22.   Effect of Increase of Throat Area on Mach No. along

(a) Ramp surface, (b) cowl surface.
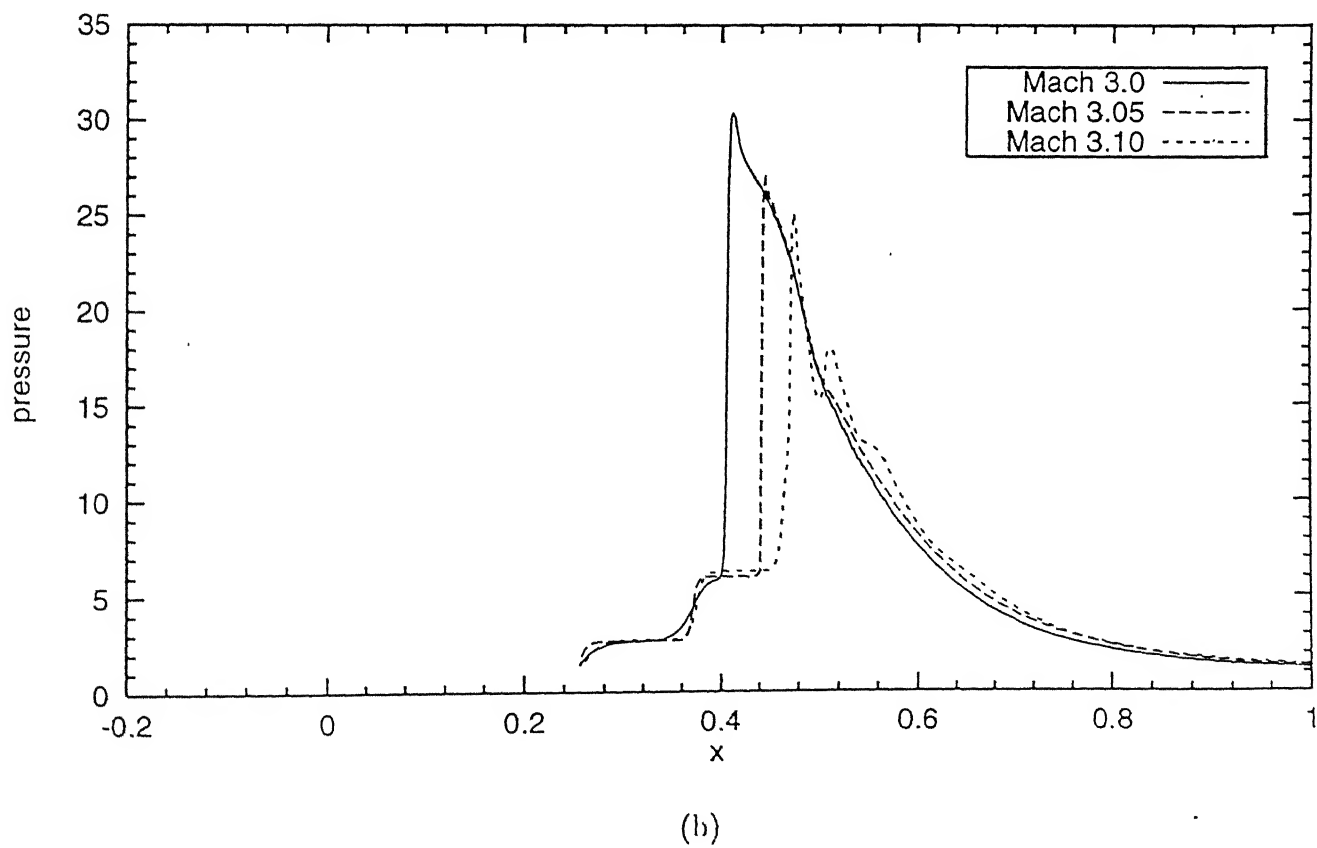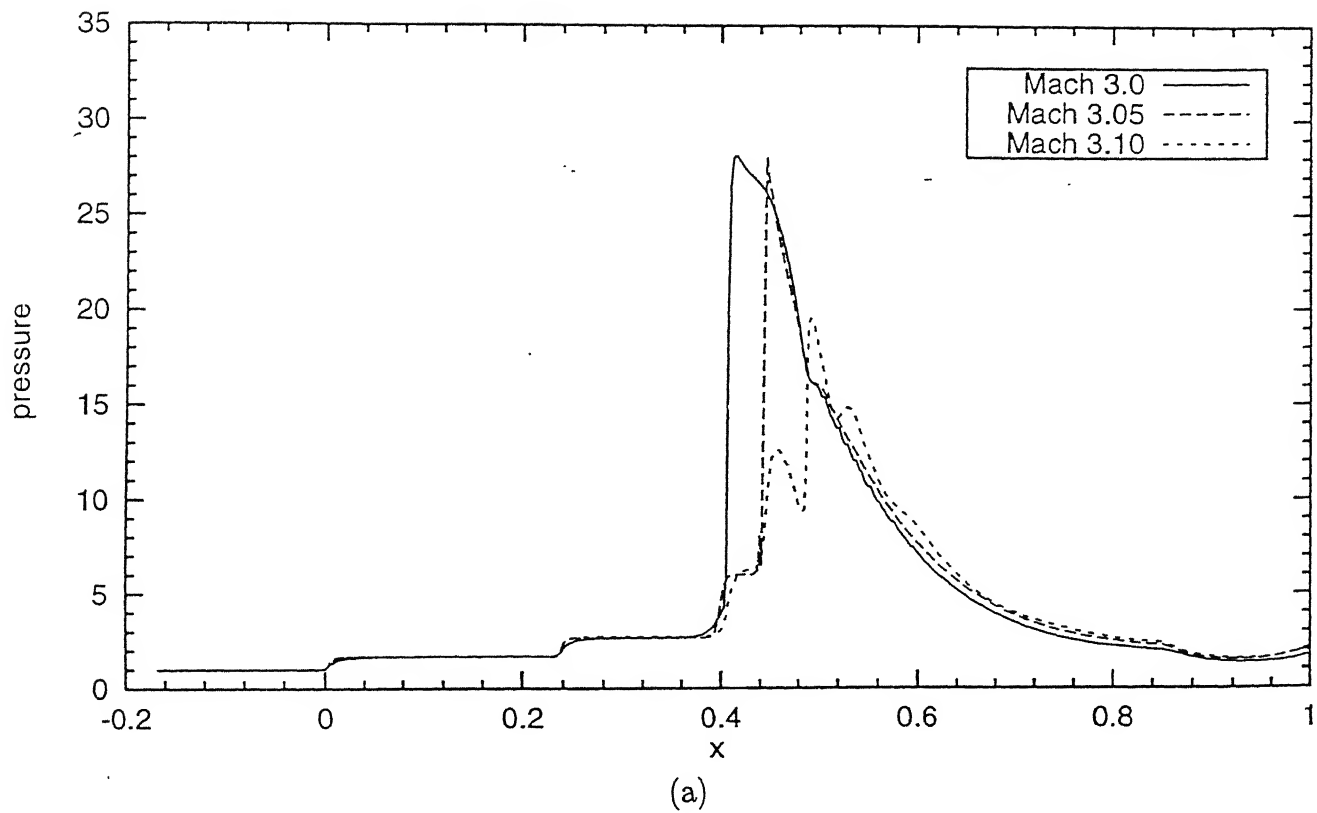
Figure 23.   Effect of Increase of Free Stream Mach No. on Pressure along
(a) Ramp surface, (b) cowl surface.
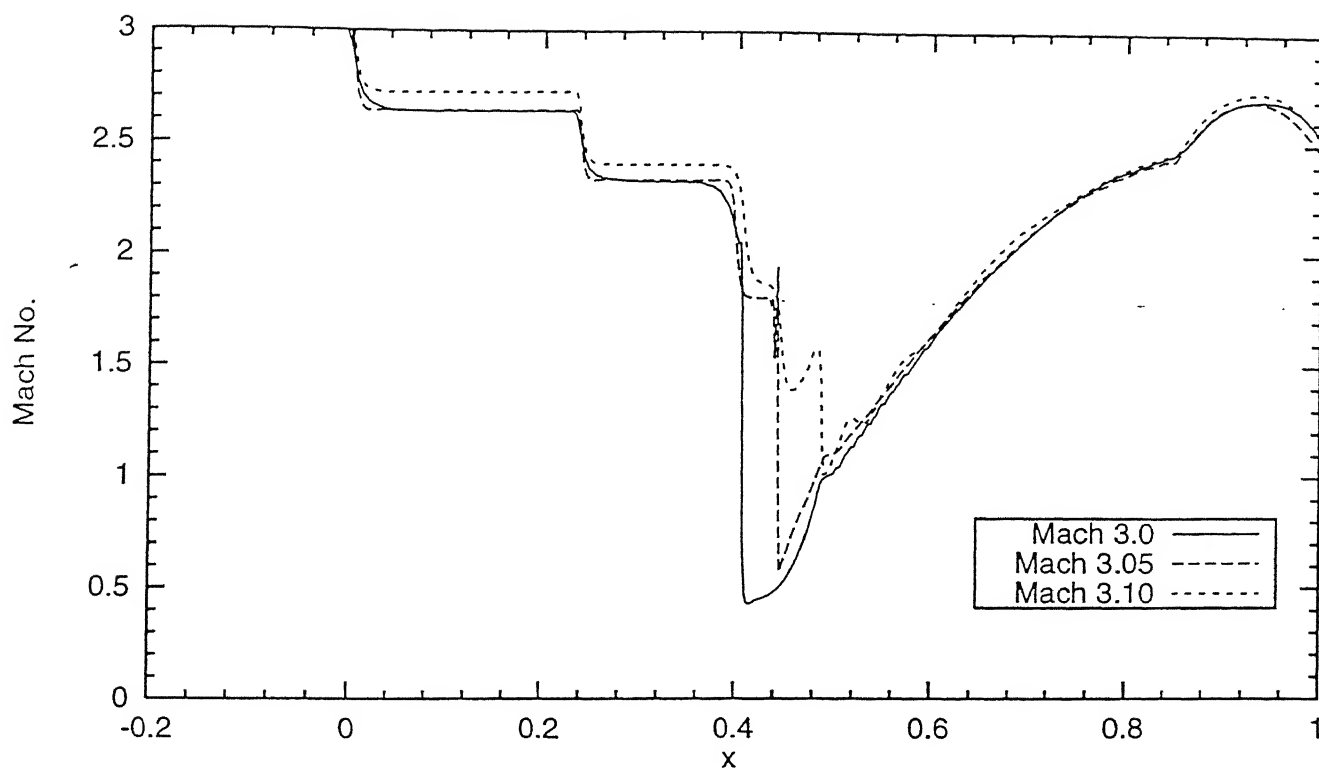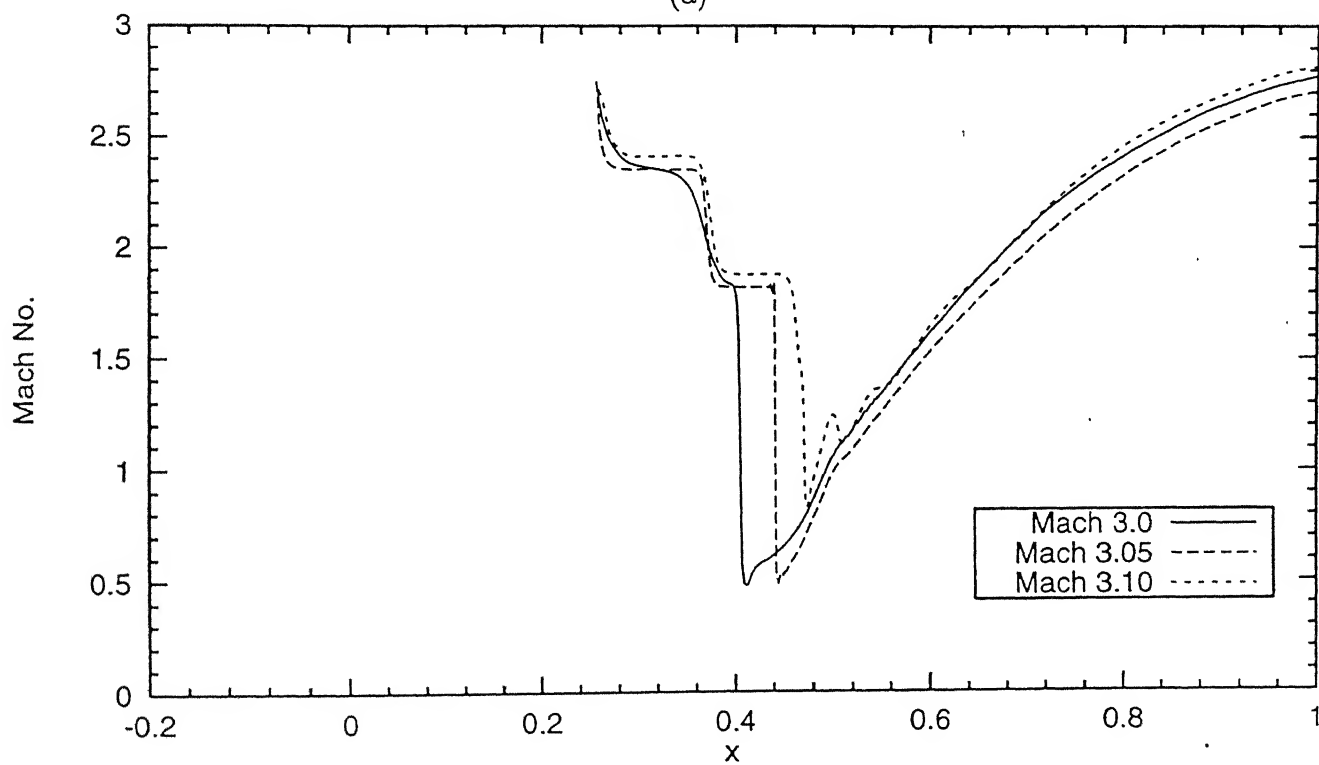
Figure 21.   Effect of Increase of Free Stream Mach No. on Mach No. along
(a) Ramp surface, (b) cowl surface.
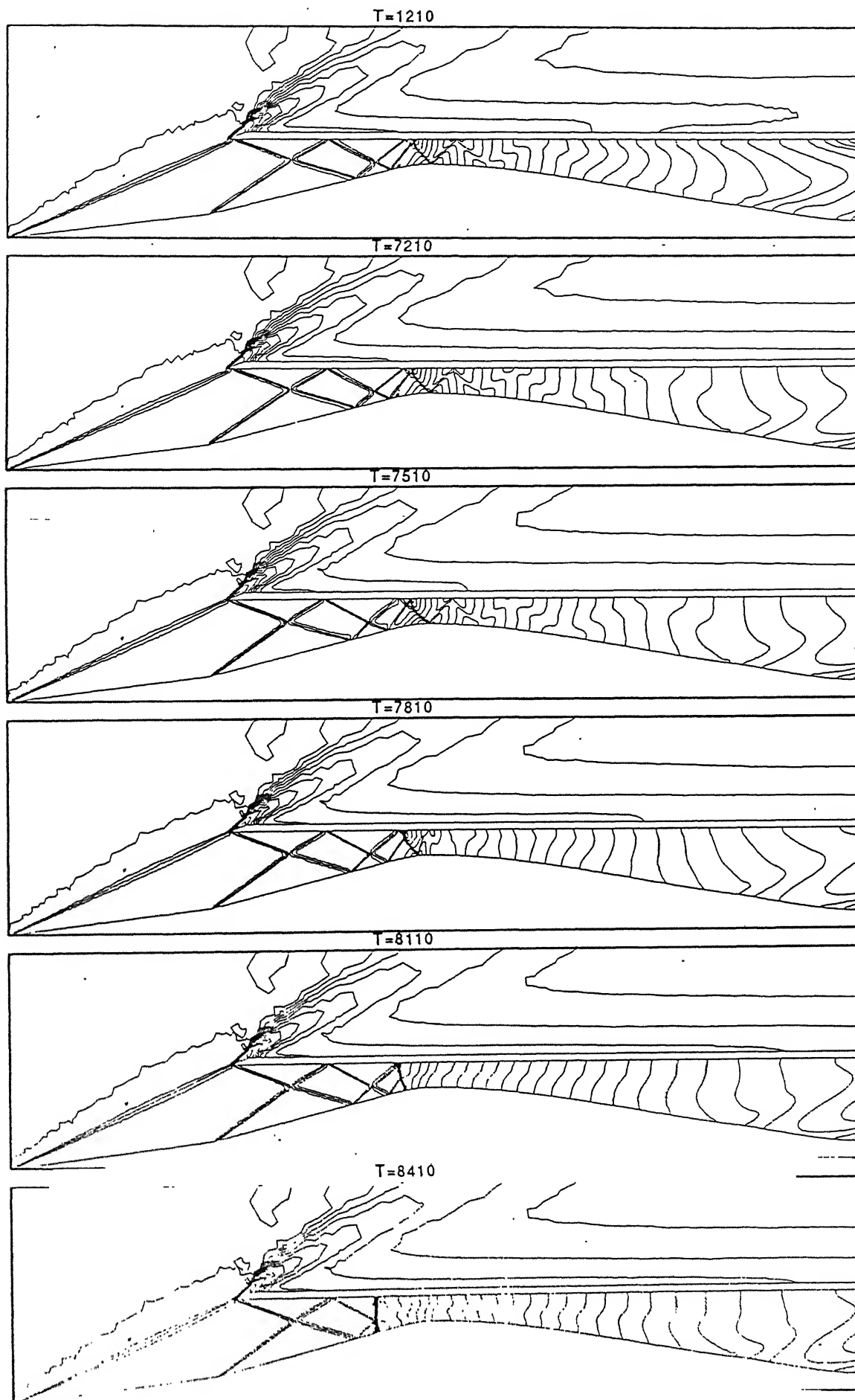
Figure 25.   Mach Contours of Flow reduced from M = 3.1 to M = 3.05.

T=1210

T=7210

T=7510

T=7810

T=8110

T=8410
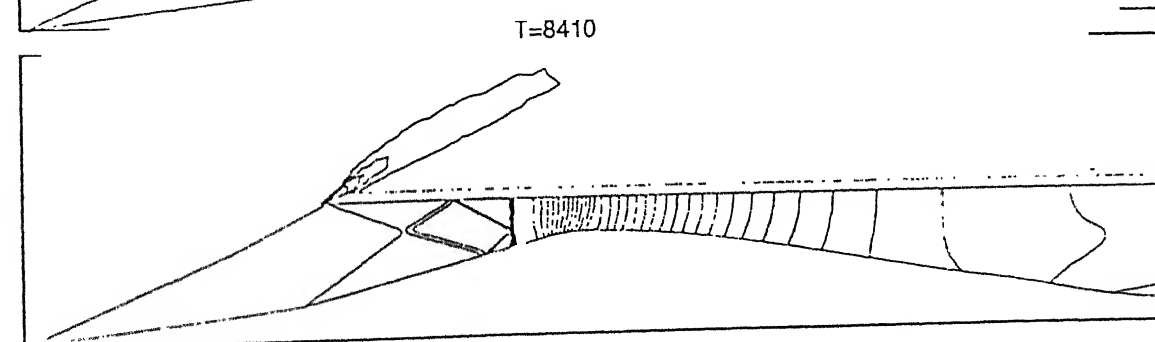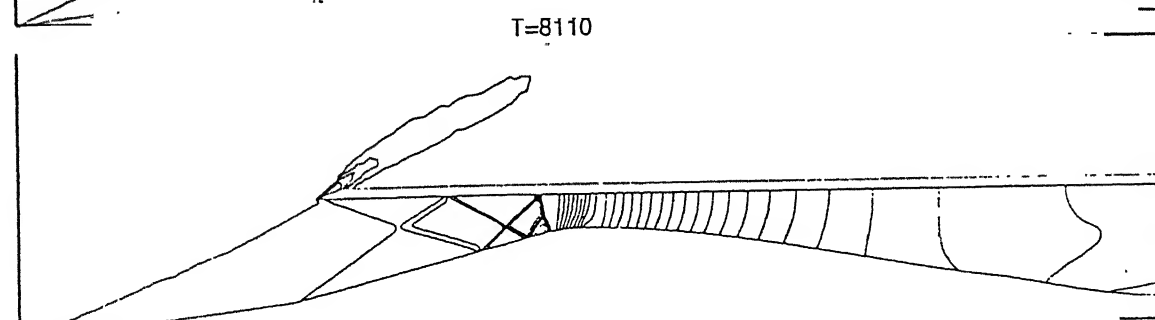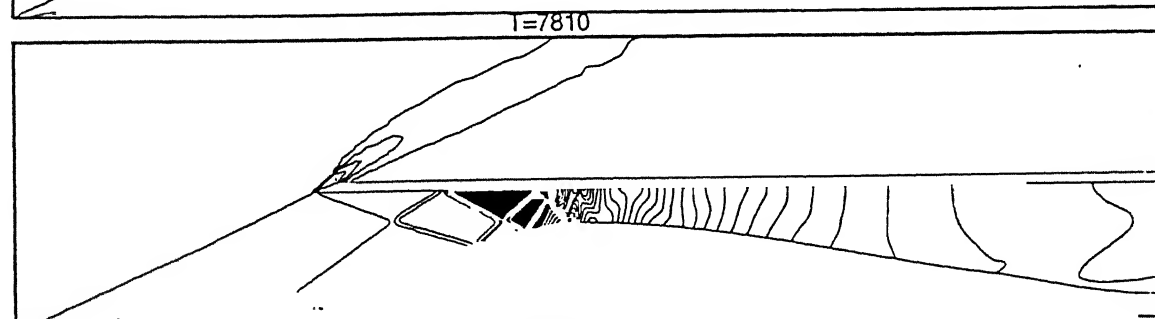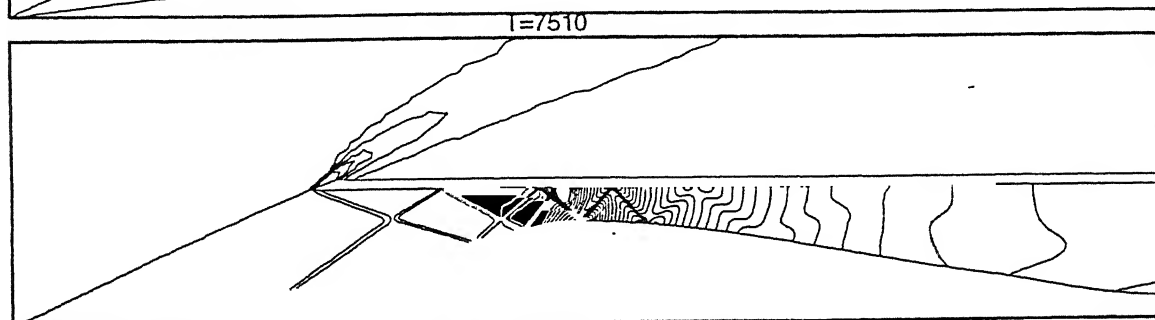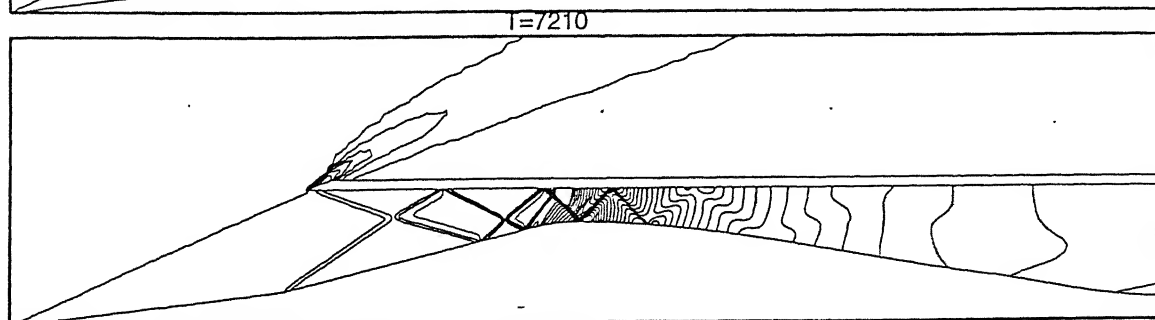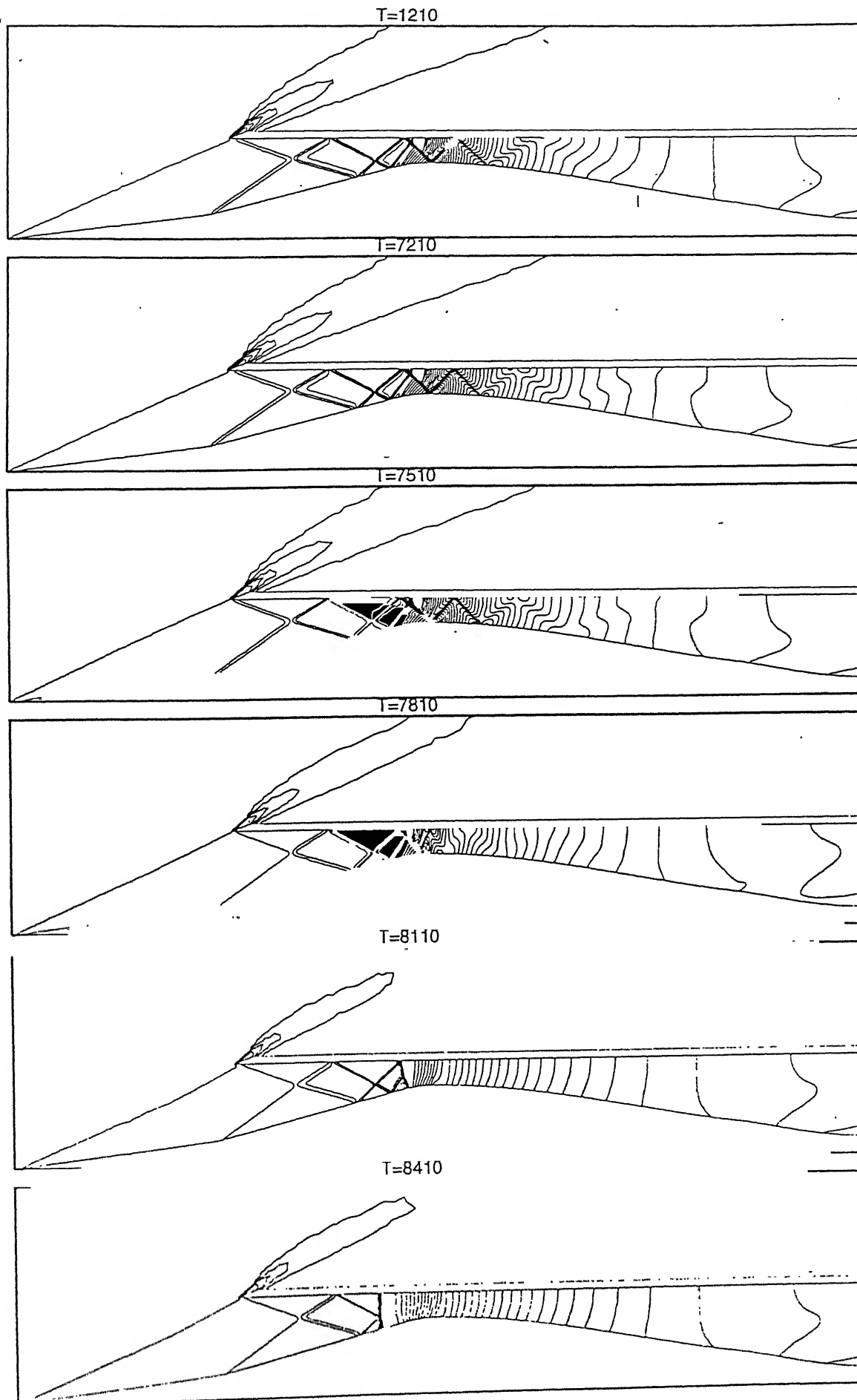
Figure 26. Pressure Contours of Flow reduced from M = 3.1 to M = 3.05.
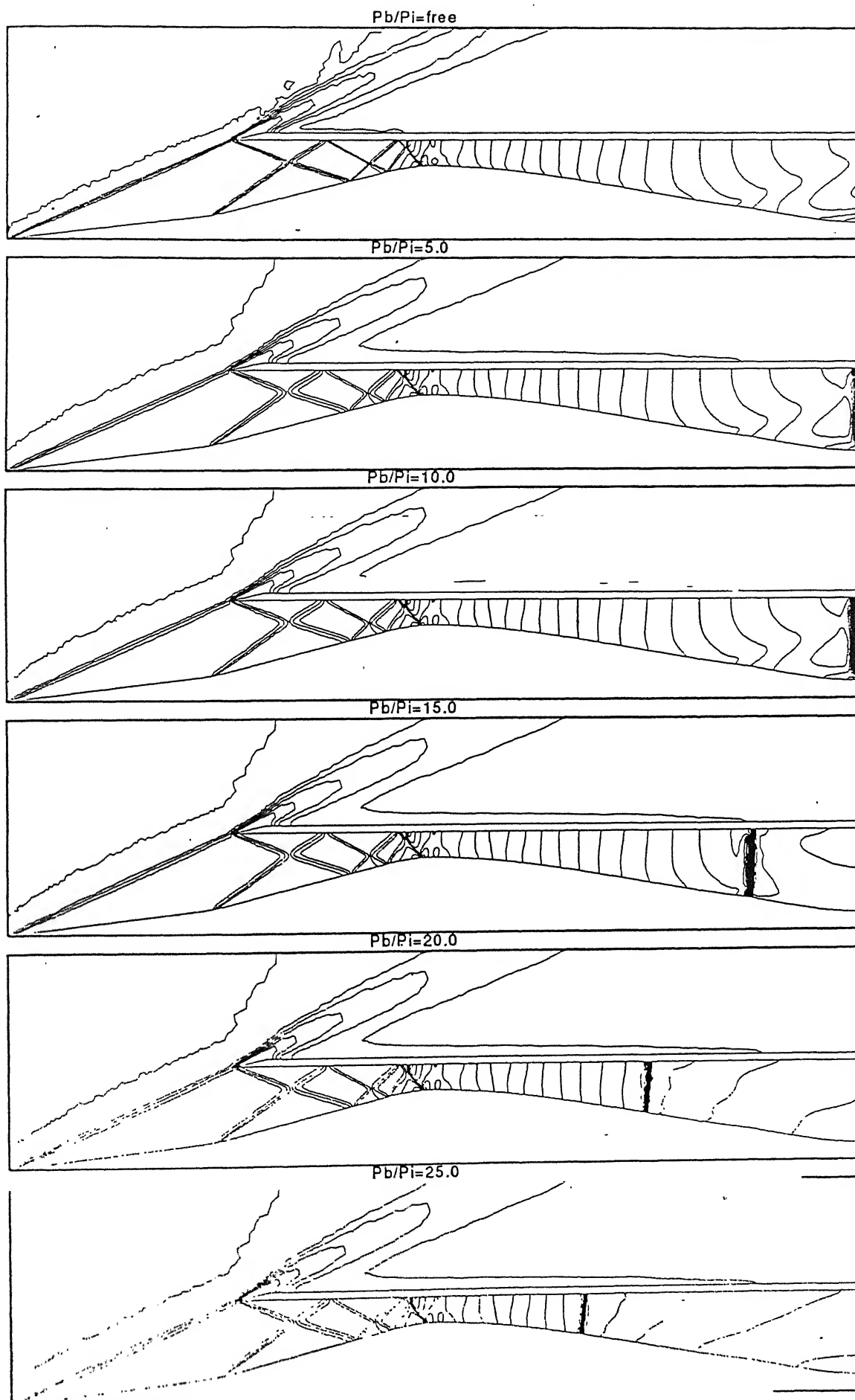
(a)

Figure 27.   Mach Contours of the Movement of Normal Shock of 7%
Throat Area Increase with varying Pb/Pi.

Pb/Pi=30.0

Pb/Pi=32.0

Pb/Pi=33.0

Pb/Pi=33.05

Pb/Pi=33.07

Pb/Pi=33.09

(b)

Figure 27.   Mach Contours of the Movement of Normal Shock of 7%
Throat Area Increase with varying Pb/Pi.

Pb/Pi=free

Pb/Pi=5.0

Pb/Pi=10.0

Pb/Pi=15.0

Pb/Pi=20.0

Pb/Pi=25.0

(a)

Figure 28.   Pressure Contours of the Movement of Normal Shock of 7%
Throat Area Increase with varying Pb/Pi.

Pb/Pi=30.0

Pb/Pi=32.0

Pb/Pi=33.0

Pb/Pi=33.05

Pb/Pi=33.07

Pb/Pi=33.09
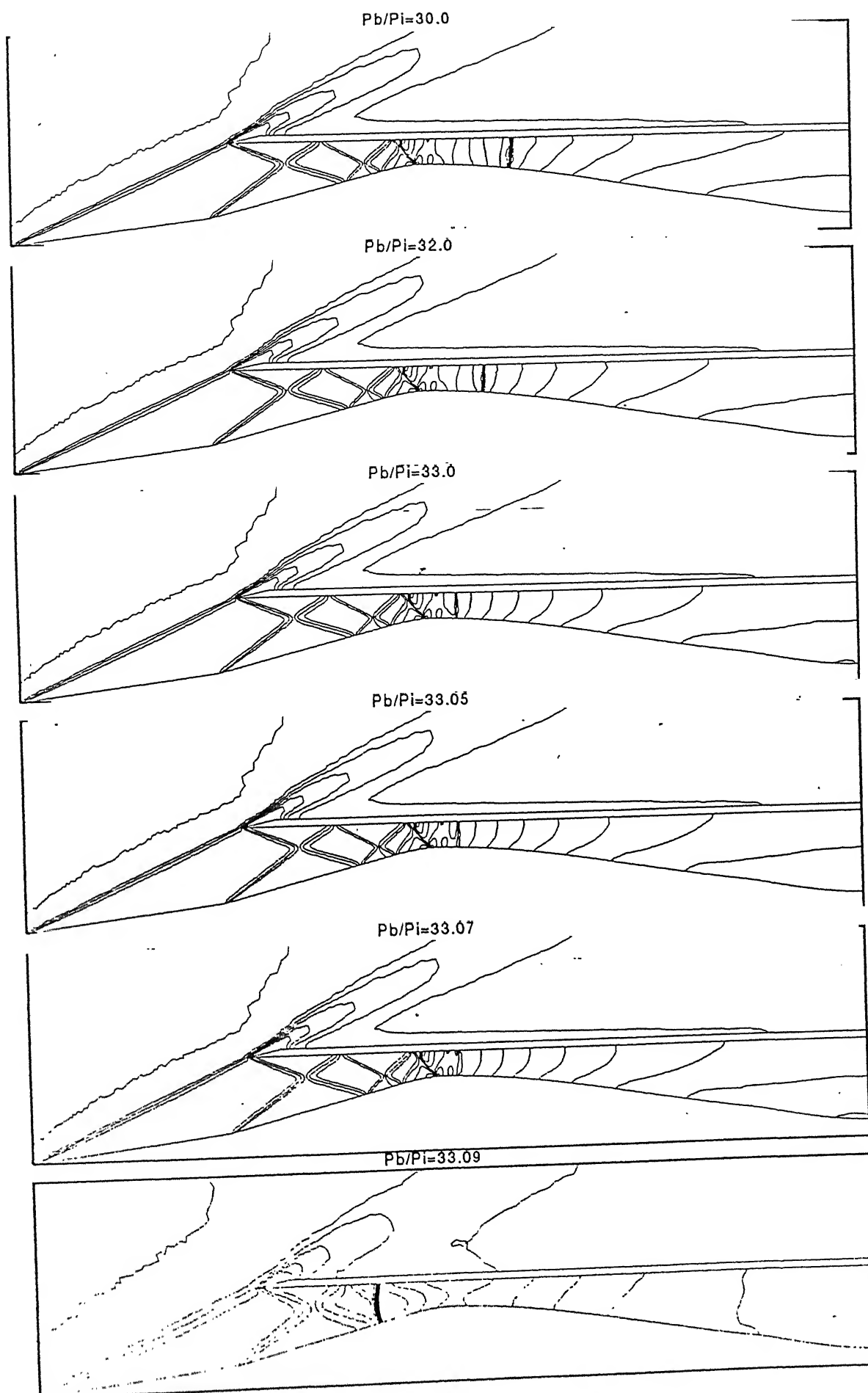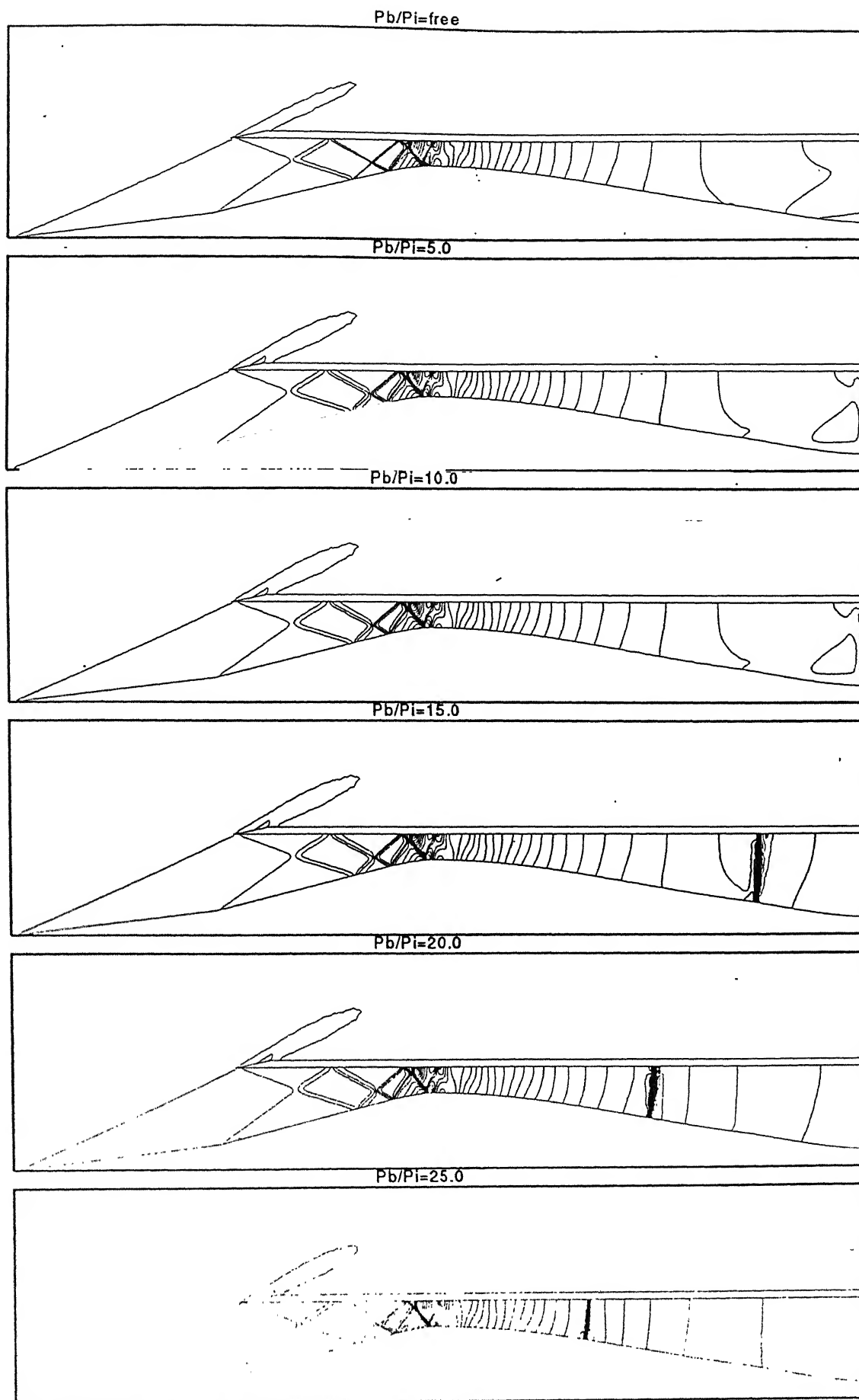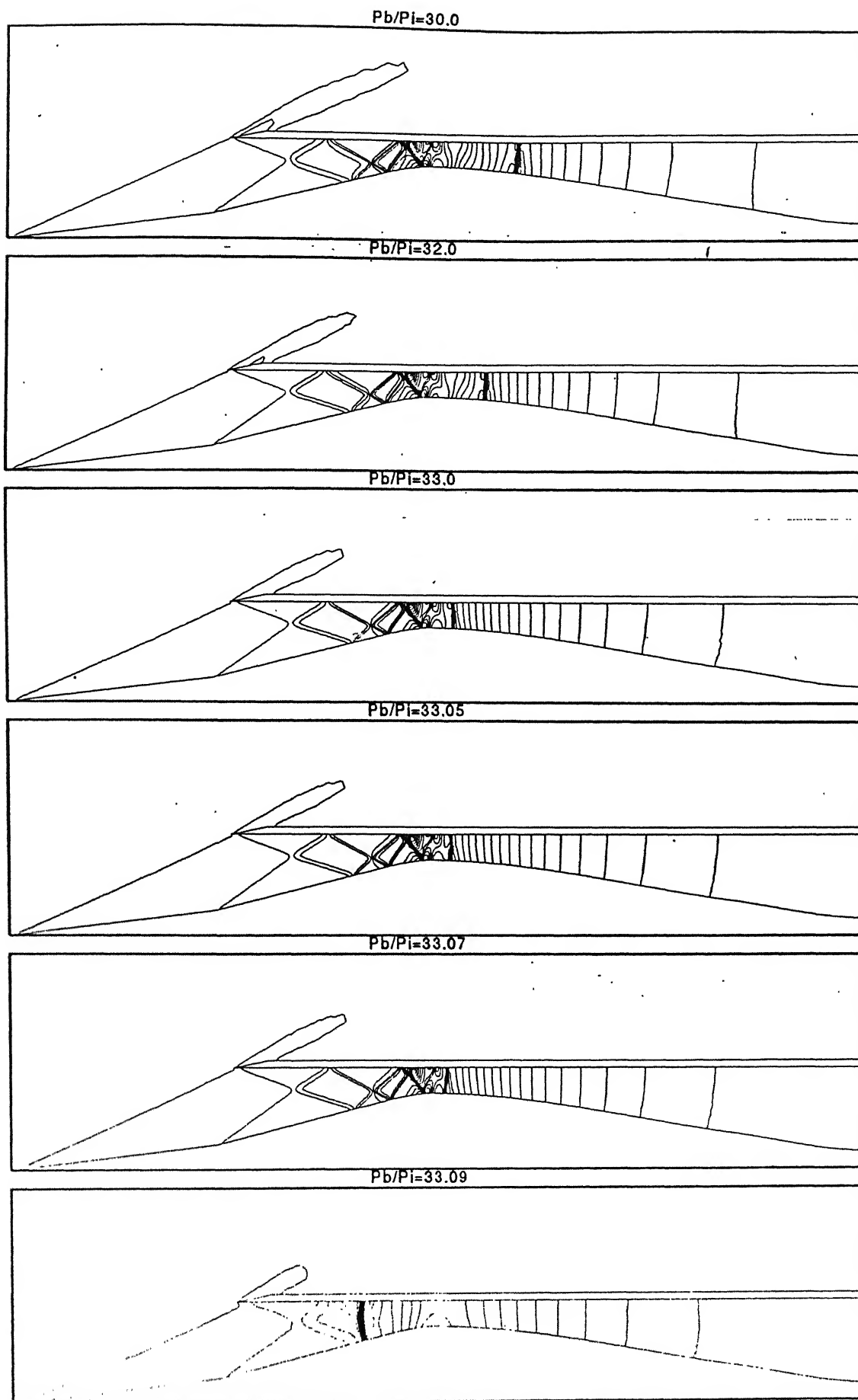
(b)

Figure 28.   Pressure Contours of the Movement of Normal Shock of 7%
Throat Area Increase with varying Pb/Pi.
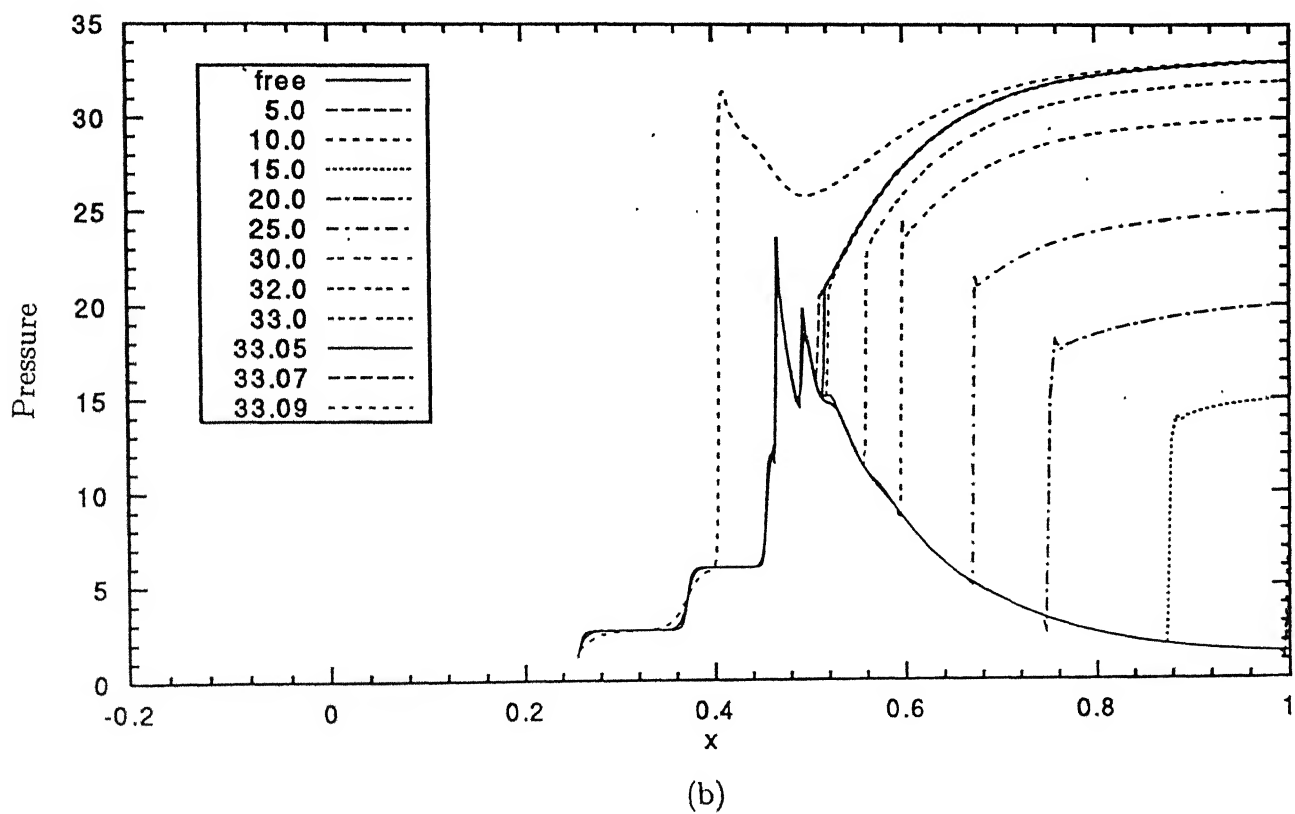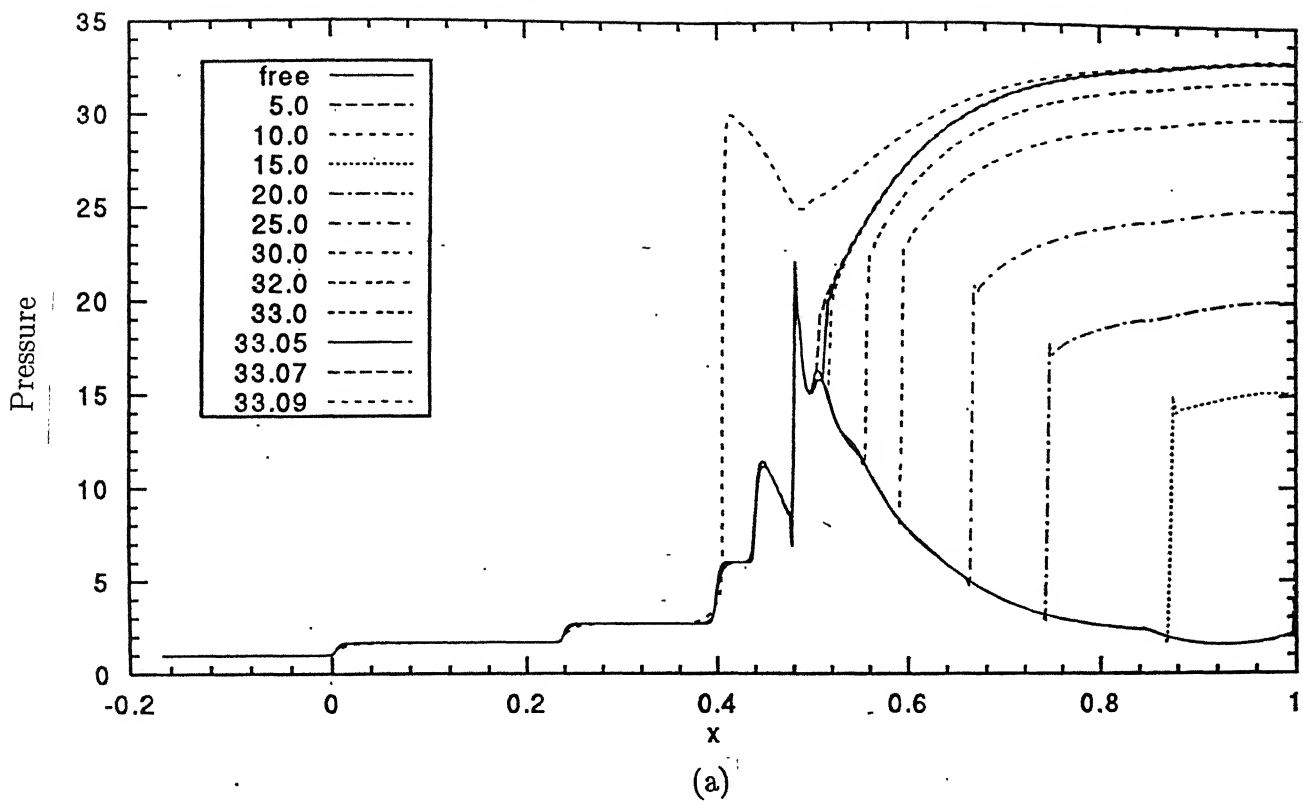
Figure 29.   Effect on Pressure with variation in Pb/Pi at Inlet Exit along
(a) ramp surface, (b) cowl surface, with 7% Throat Area Increase.
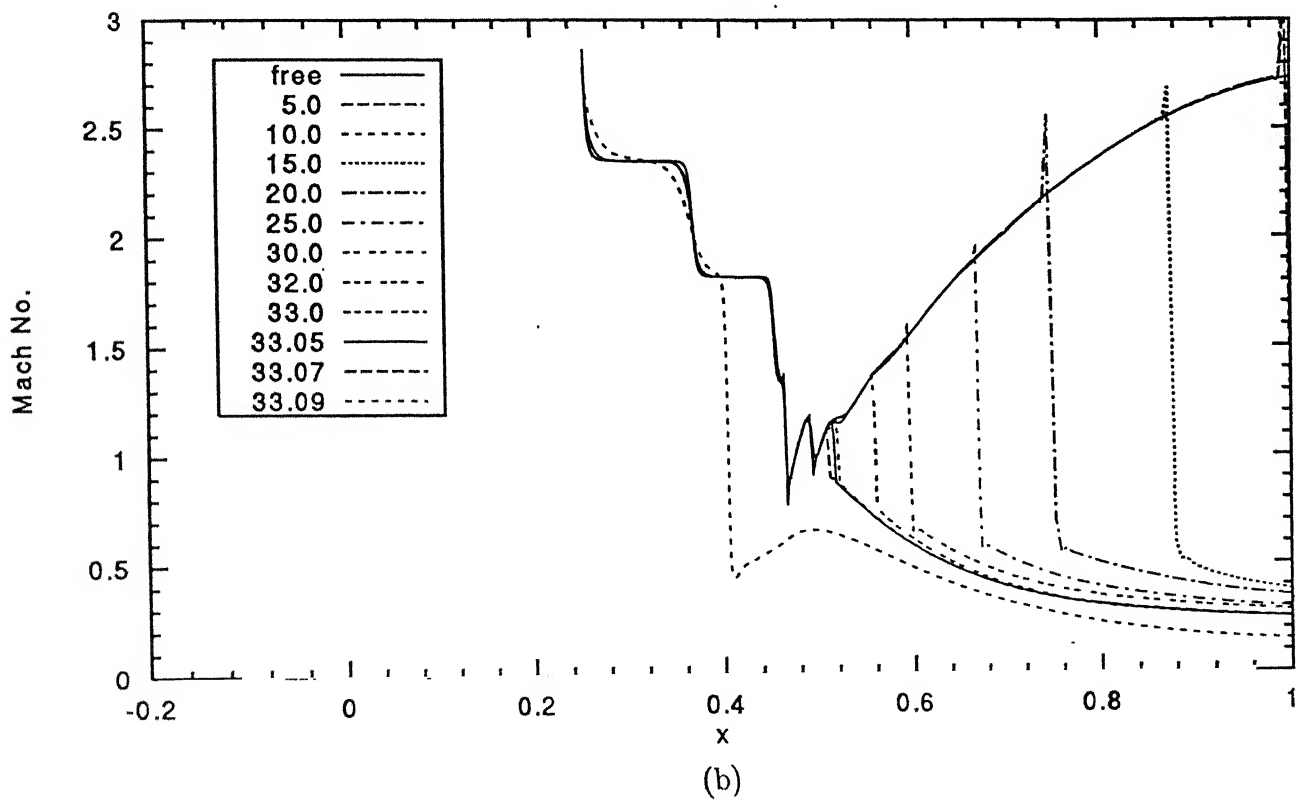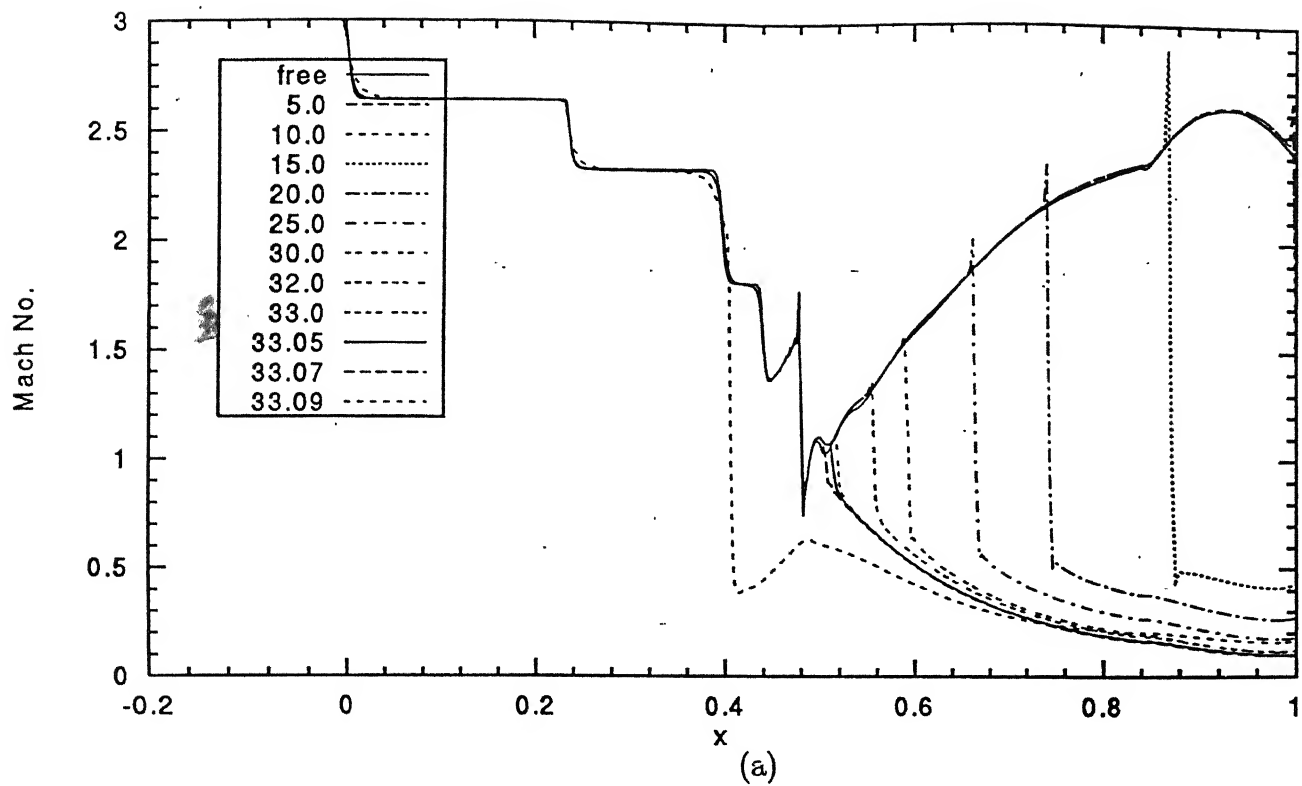
Figure 30. Effect on Mach No. with variation in Pb/Pi at Inlet Exit along (a) ramp surface, (b) cowl surface, with 7% Throat Area Increase.
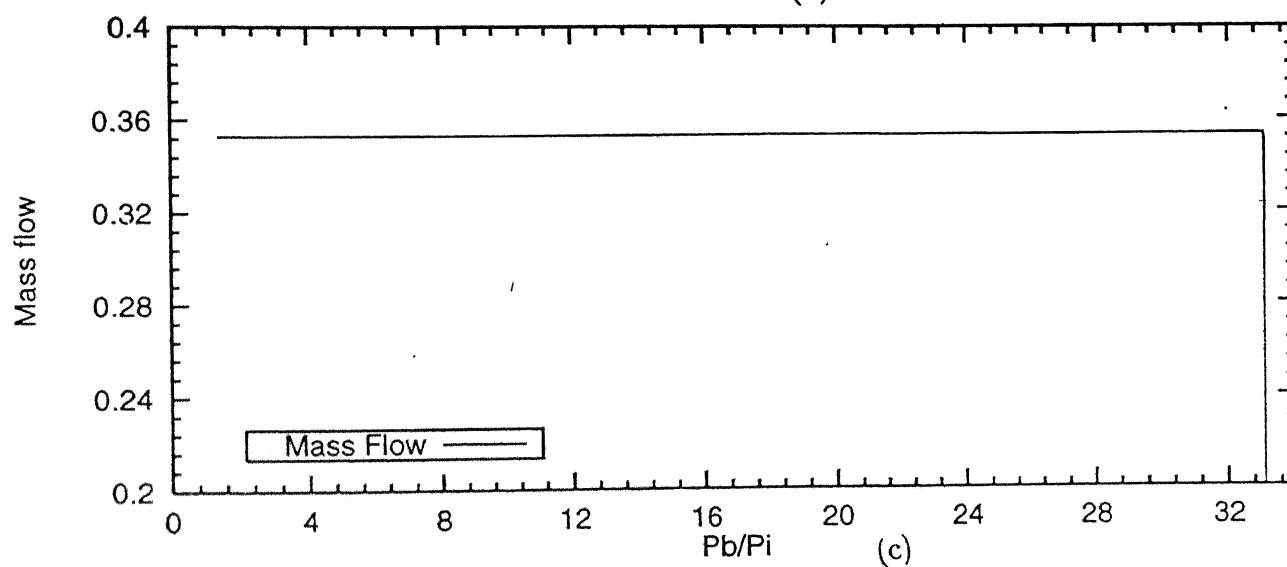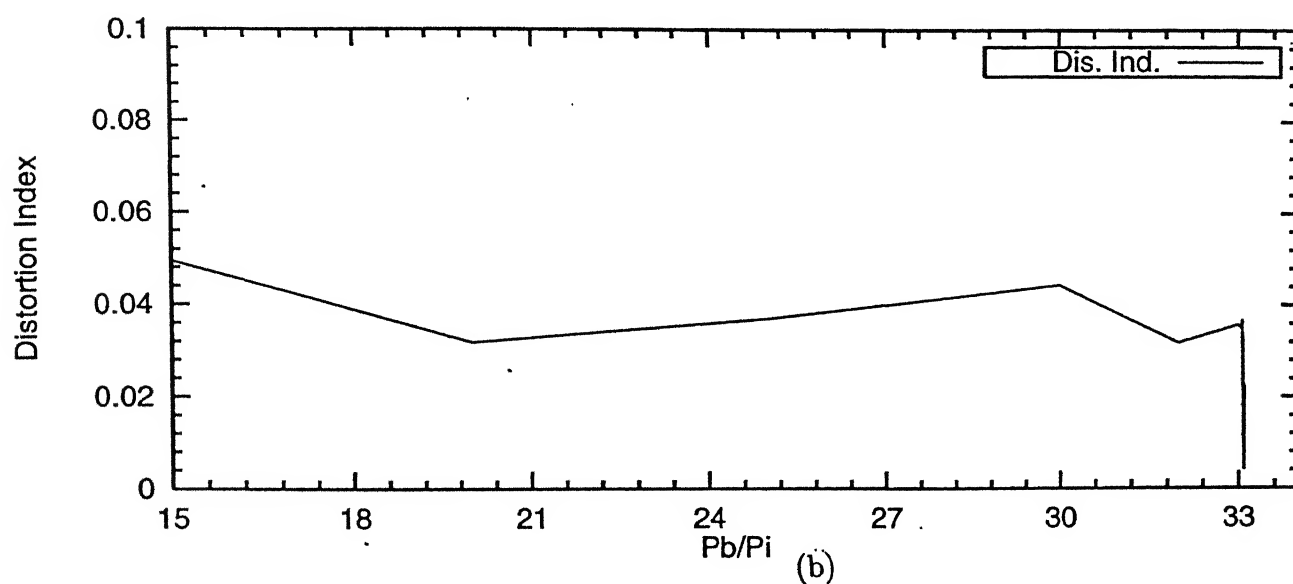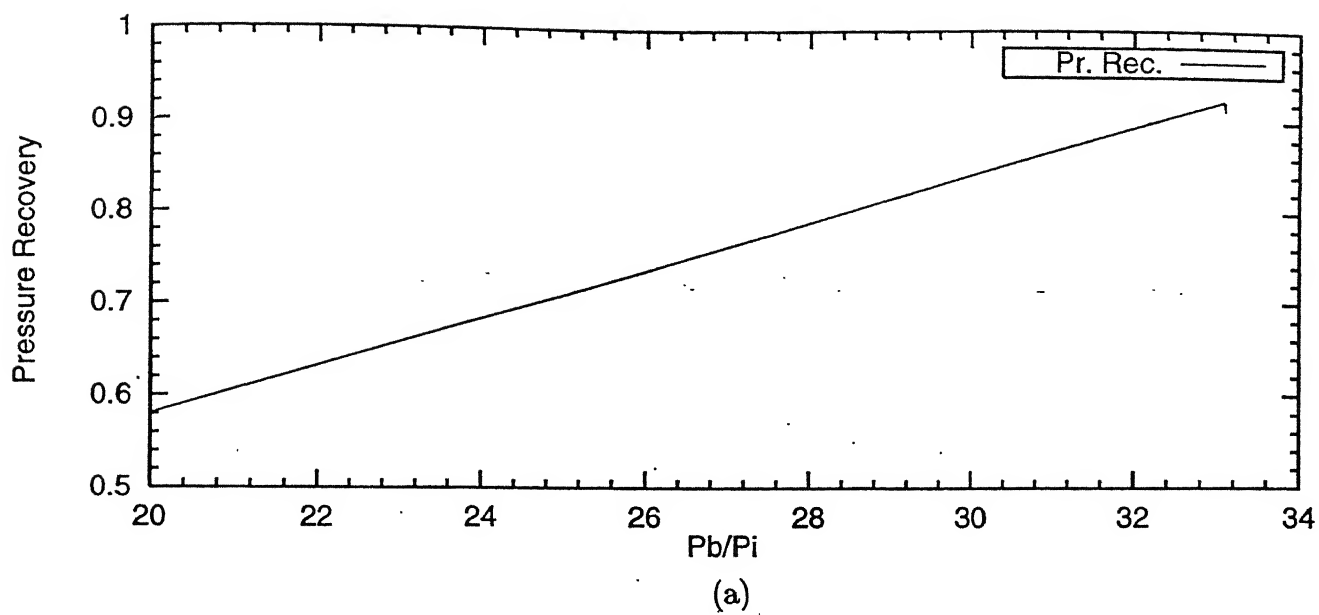
Figure 31. Effect with variation in Pb/Pi at Inlet Exit on
(a) Total Pressure Recovery, (b) Distortion Index, (c) Mass Flow,
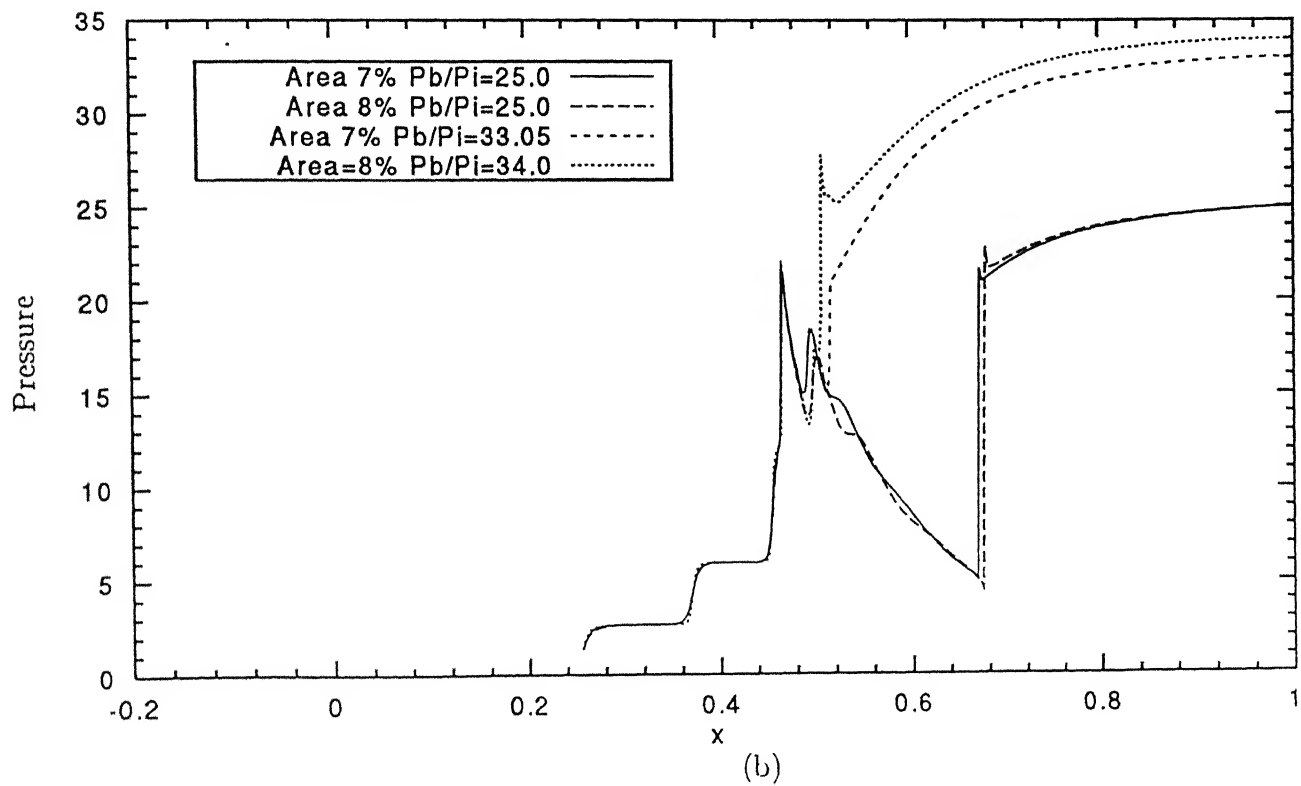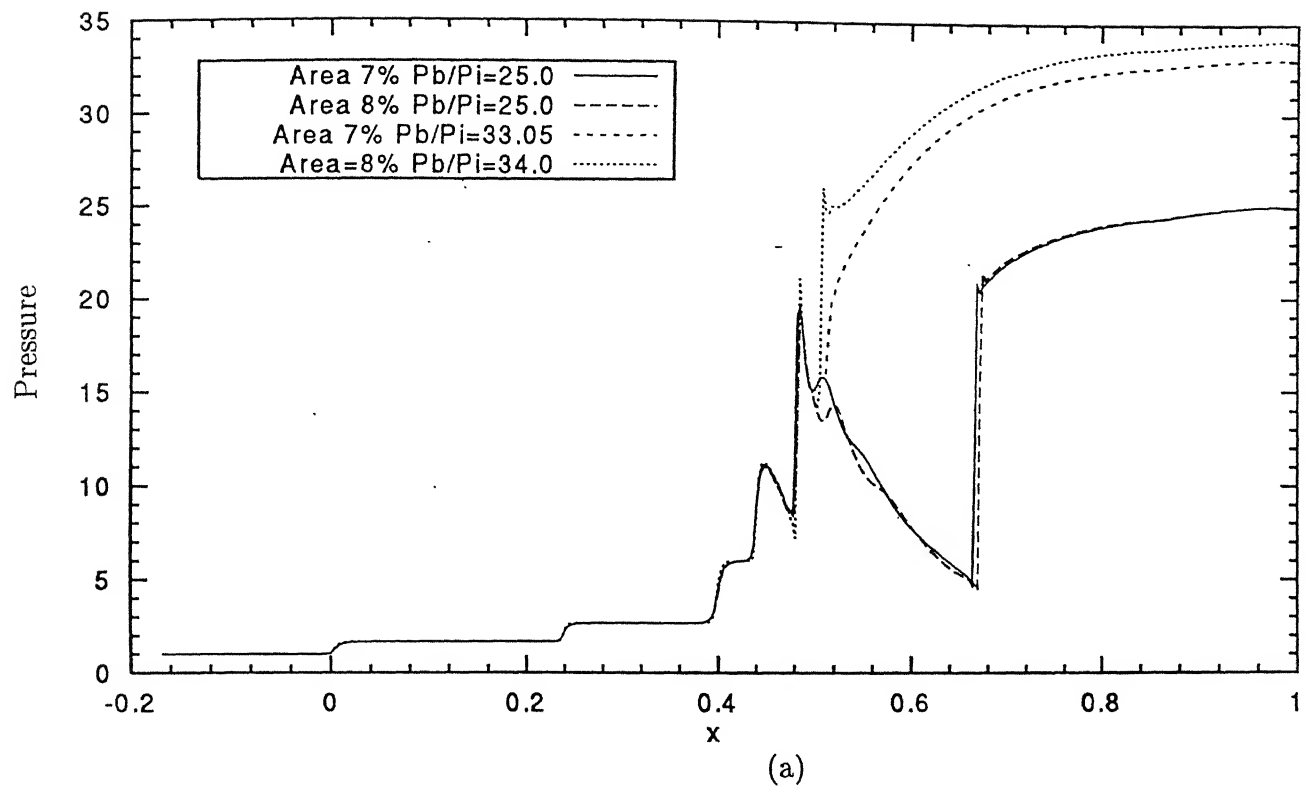with 7% Throat Area Increase.

Pb/Pi=31.0

Pb/Pi=32.0

Pb/Pi=33.0

Pb/Pi=34.0

Pb/Pi=34.5
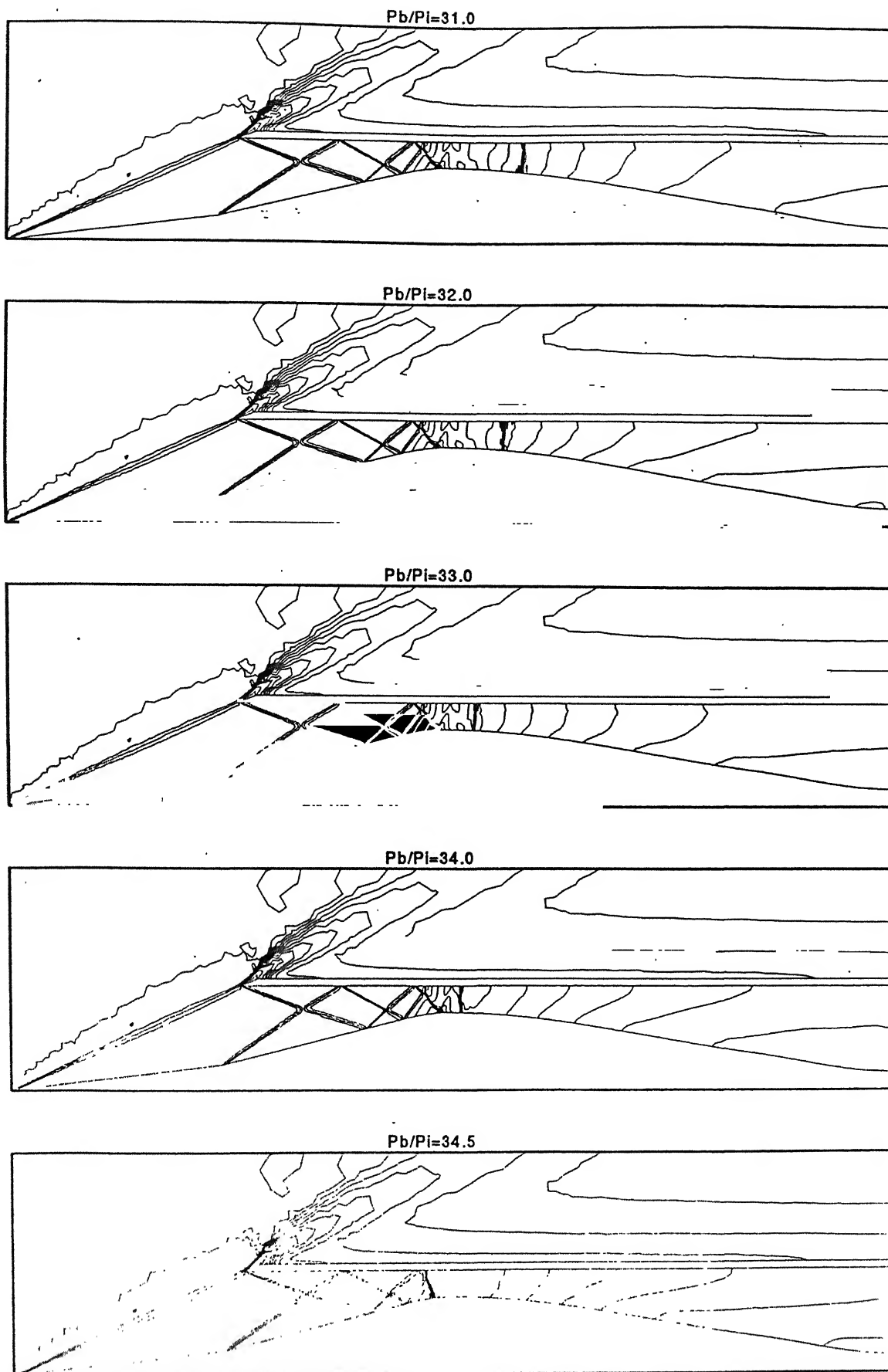
(b)

Figure 32.   Mach Contours of the Movement of Normal Shock of 8%
Throat Area Increase with varying Pb/Pi.
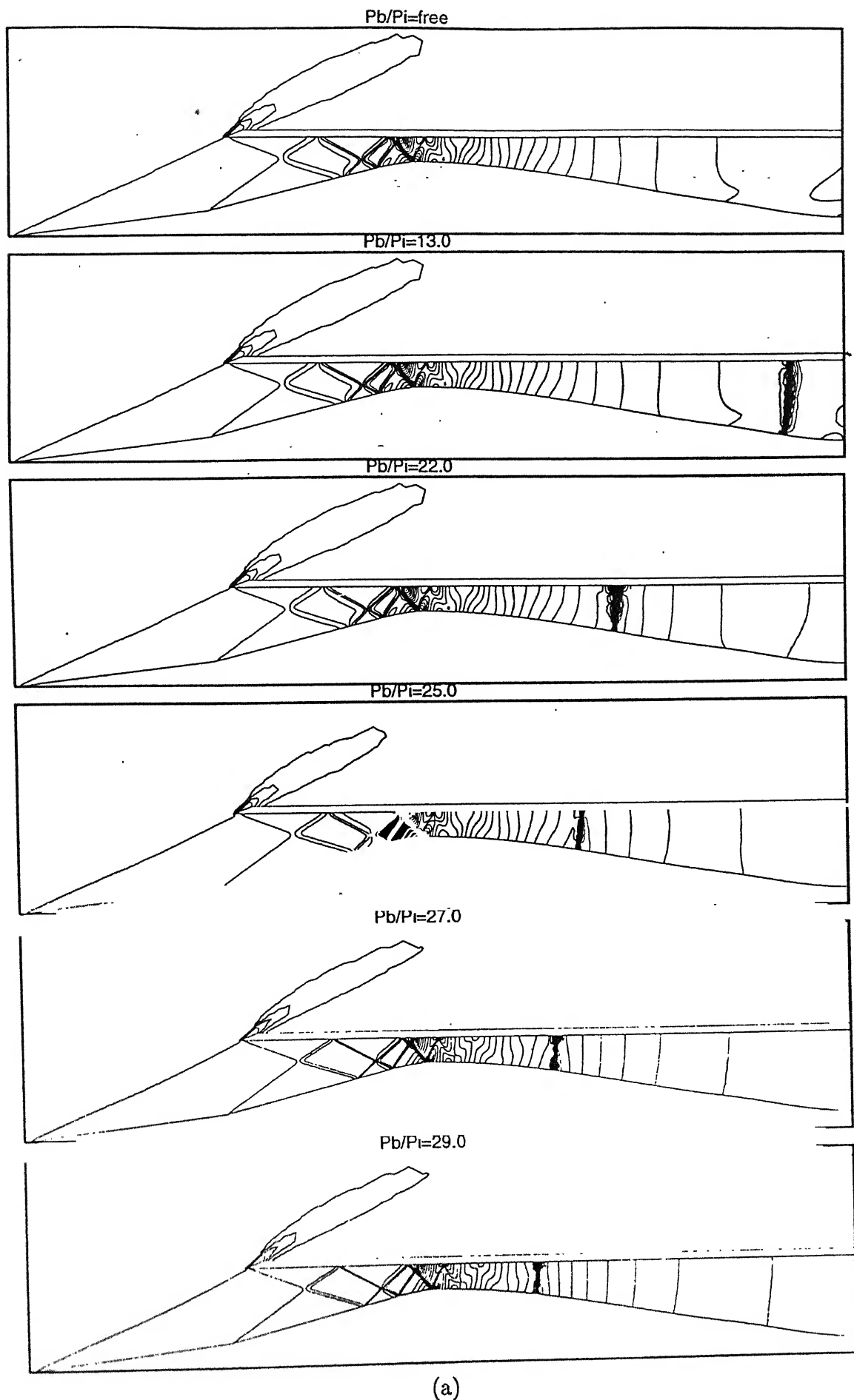
Pb/Pi=free

Pb/Pi=13.0

Pb/Pi=22.0

Pb/Pi=25.0

Pb/Pi=27.0

Pb/Pi=29.0

(a)

Figure 33.   Pressure Contours of the Movement of Normal Shock of 8%
Throat Area Increase with varying Pb/Pi.

Pb/Pi=31.0

Pb/Pi=32.0

Pb/Pi=33.0

Pb/Pi=34.0

Pb/Pi=34.5
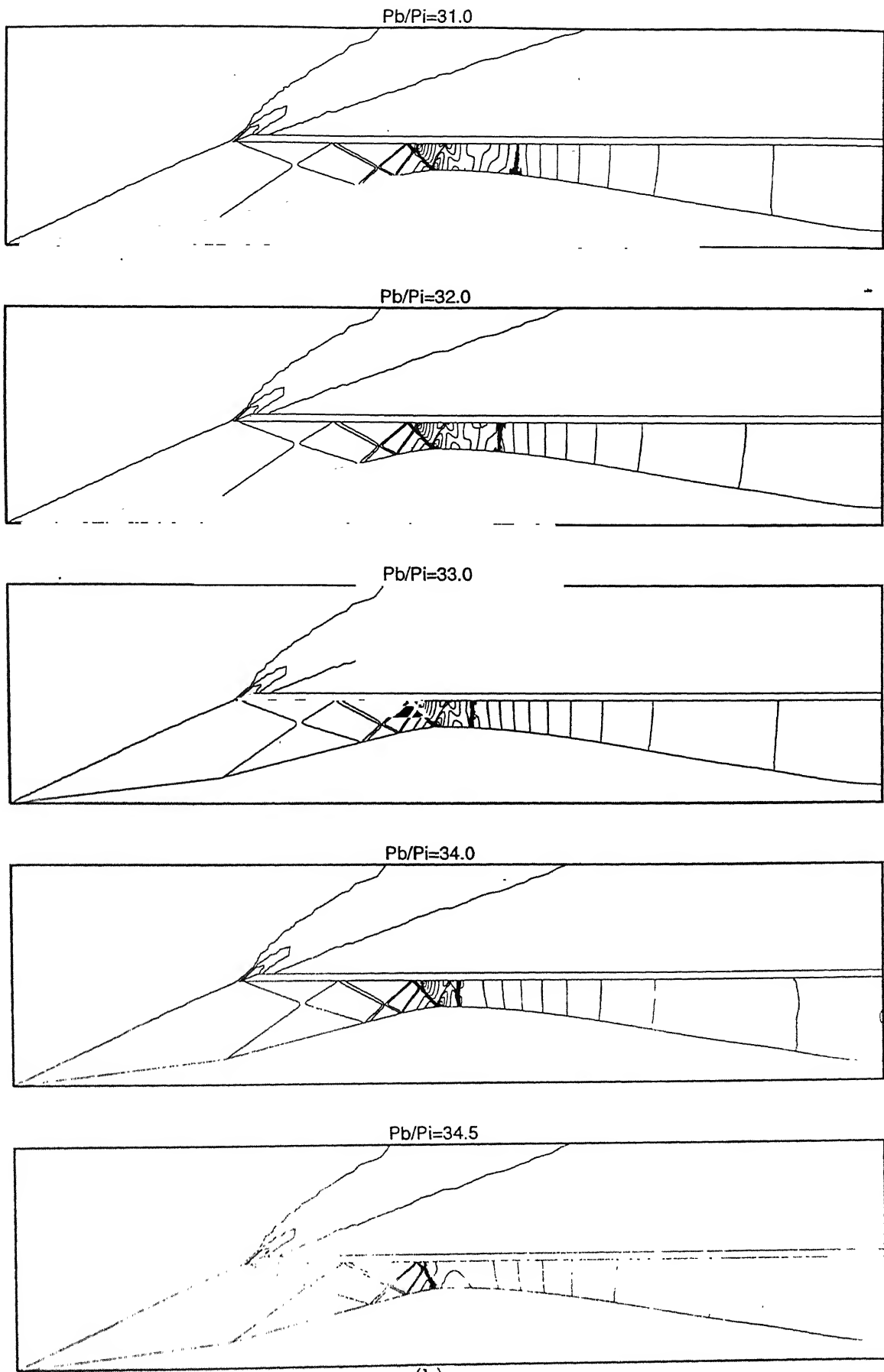
(b)

Figure 33.   Pressure Contours of the Movement of Normal Shock of 8%
Throat Area Increase with varying Pb/Pi.
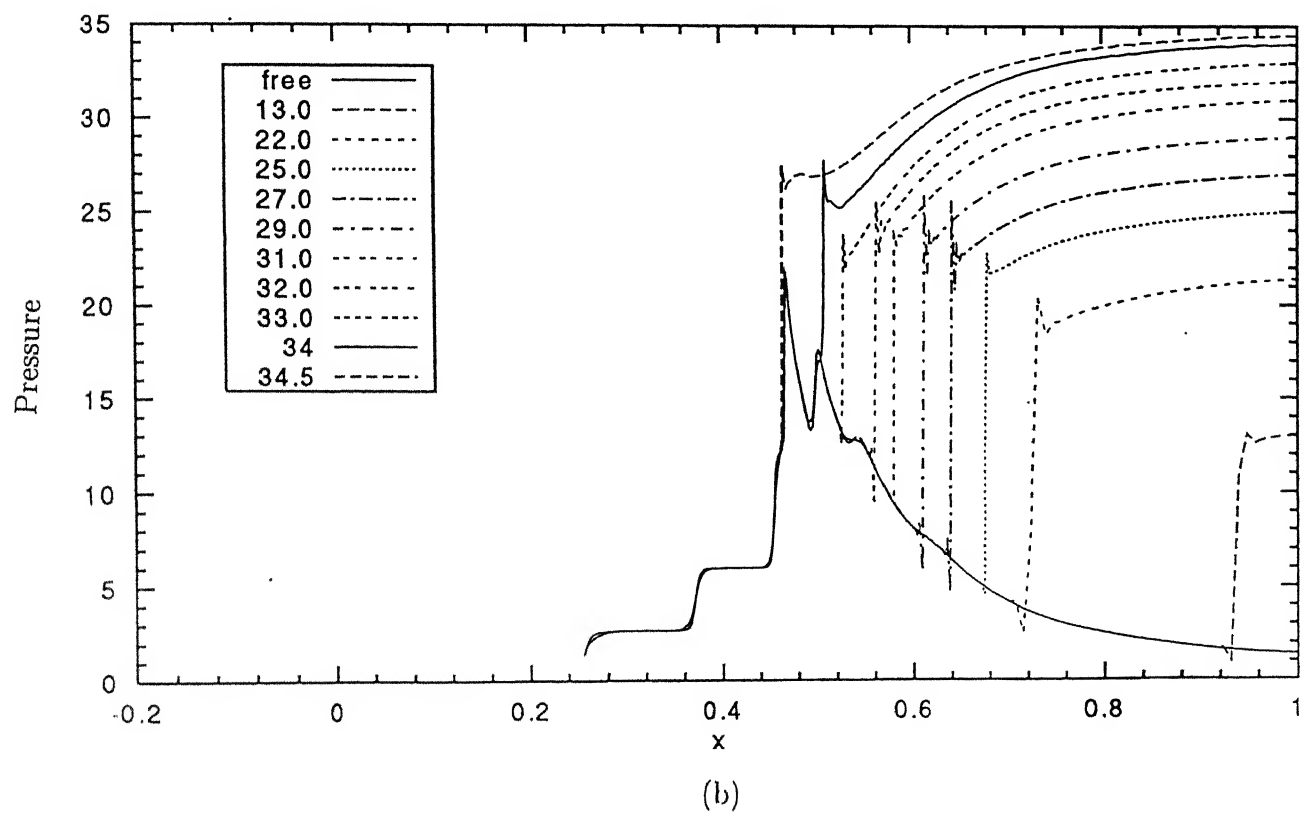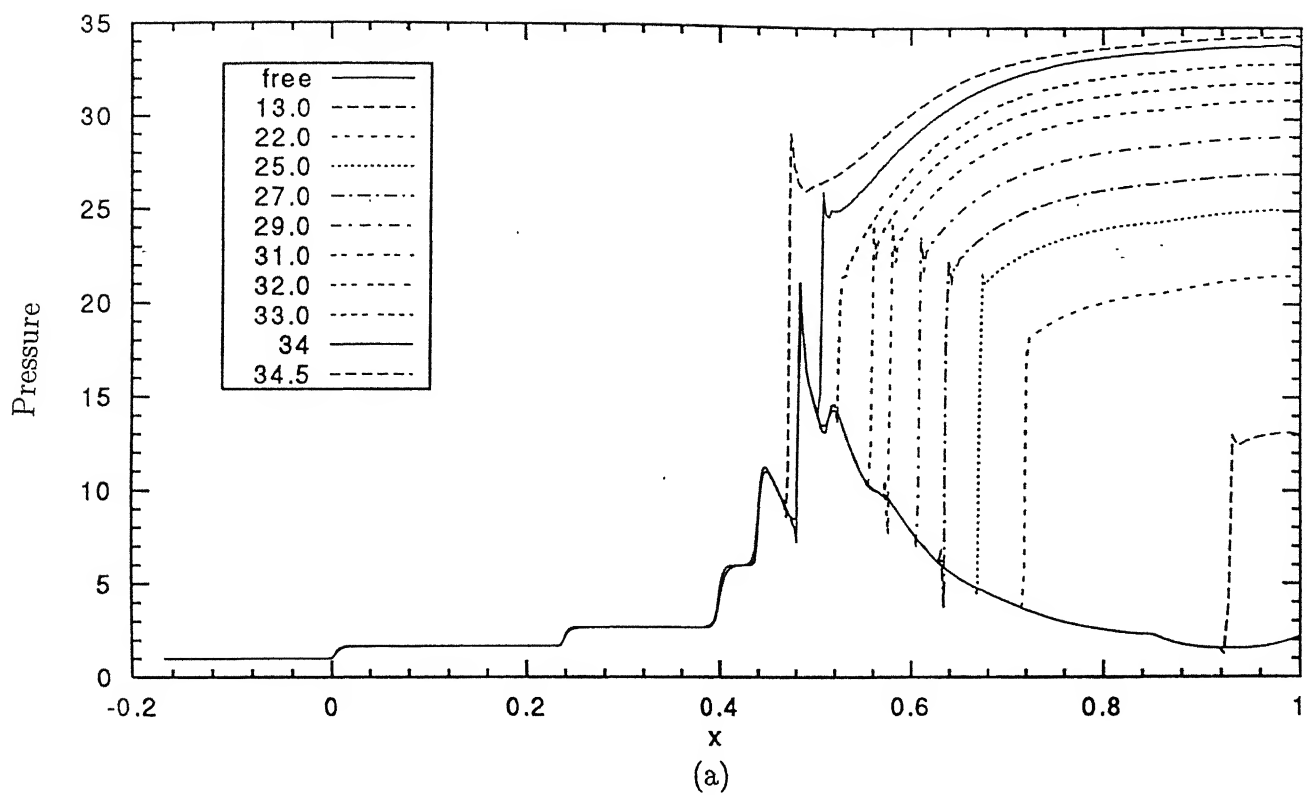
Figure 34.   Effect on Pressure with variation in Pb/Pi at Inlet
Exit along (a) ramp surface, (b) cowl surface,
with 8% Throat Area Increase.
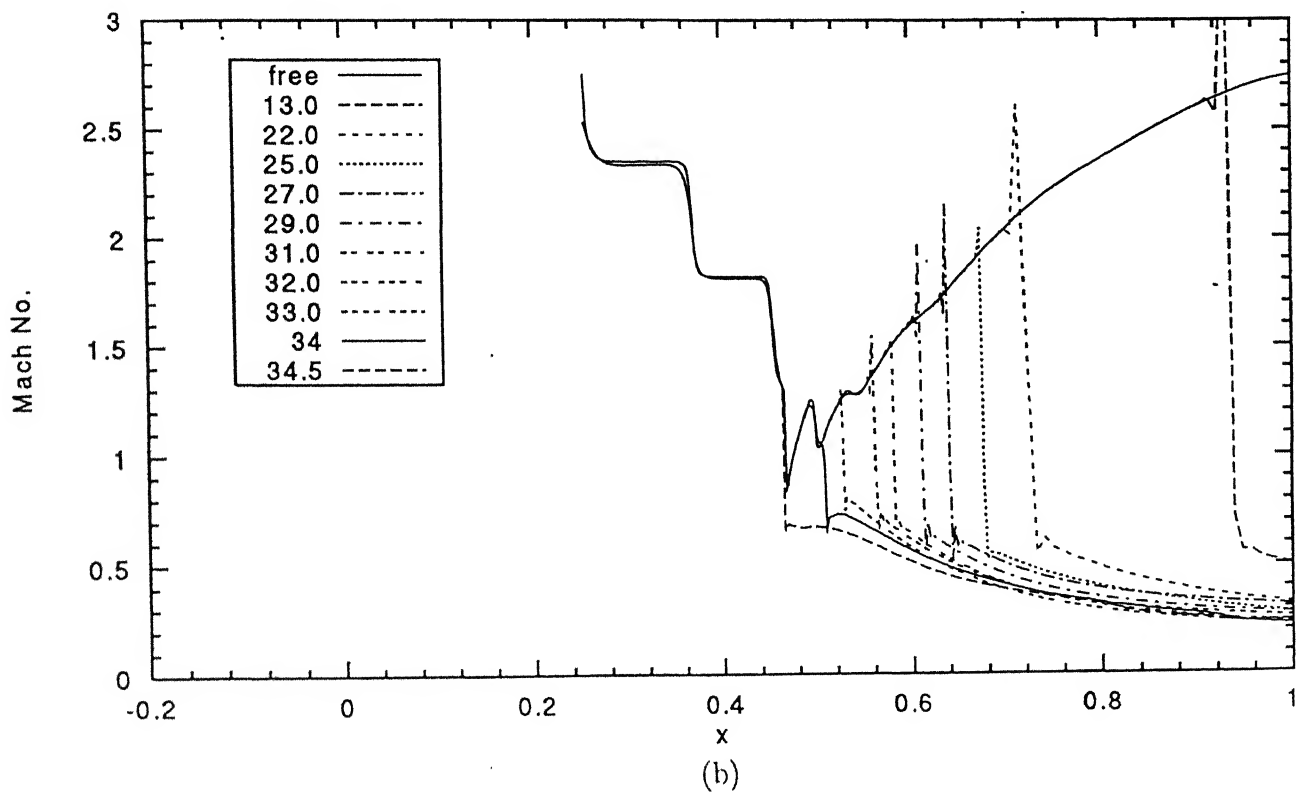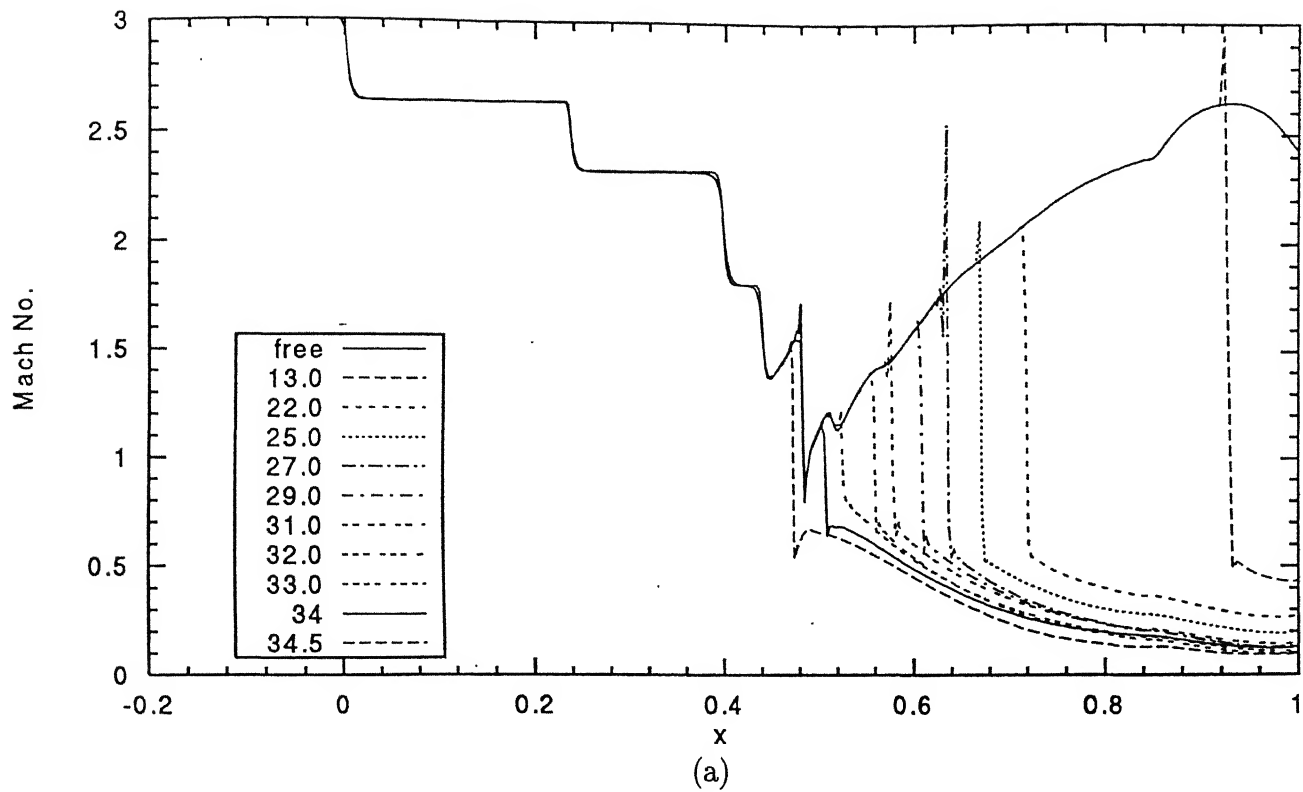
Figure 35.   Effect on Mach No. with variation in Pb/Pi at Inlet Exit along

(a) ramp surface, (b) cowl surface, with 8% Throat Area Increase.
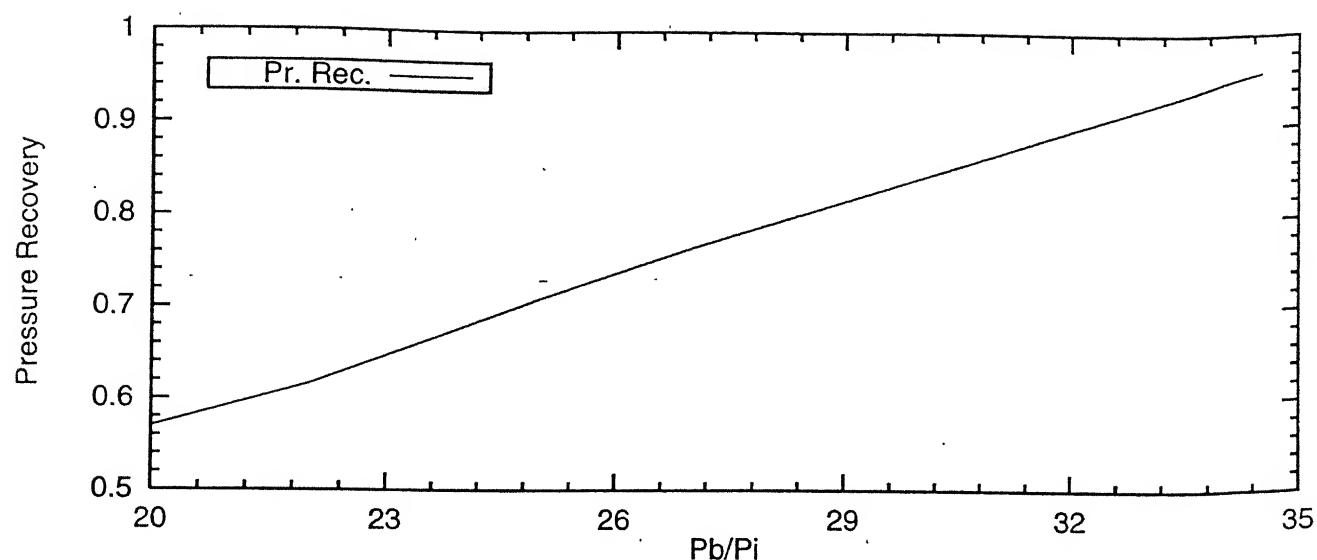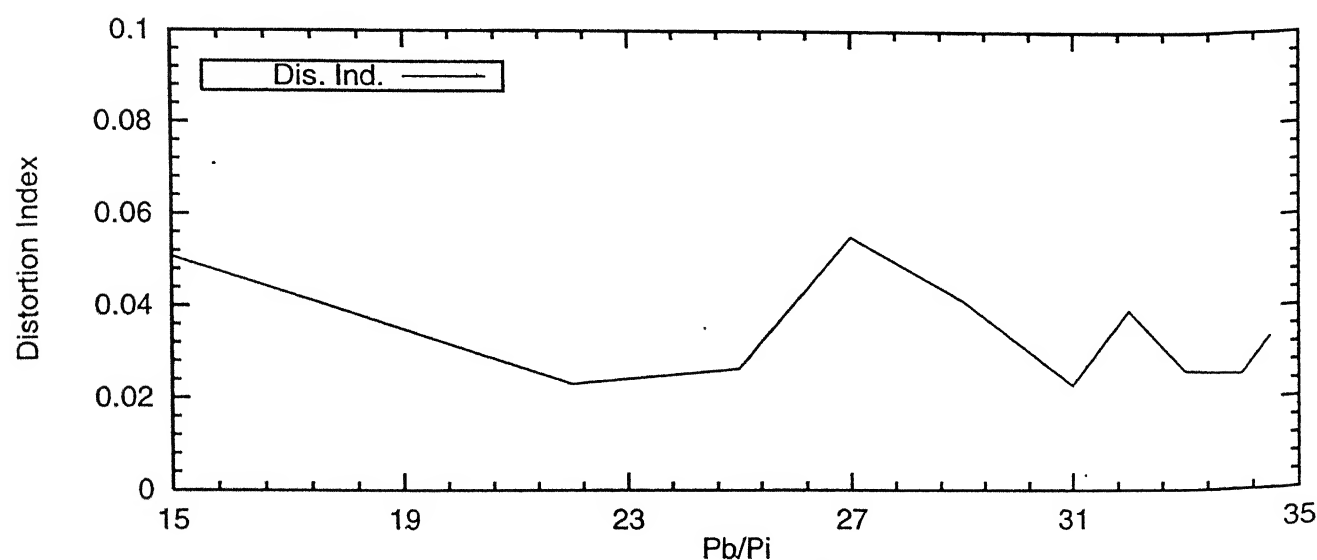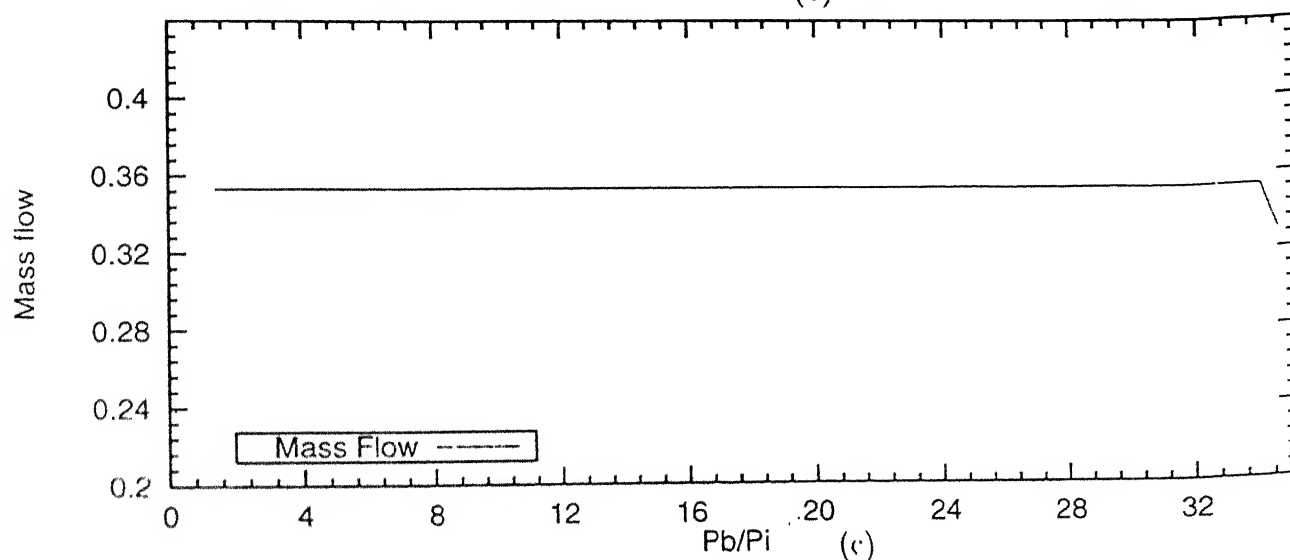
Figure 36.   Effect with variation in Pb/Pi at Inlet Exit on
                  (a) Total Pressure Recovery, (b) Distortion Index, (c) Mass Flow;
                  with 8% Throat Area Increase.

Figure 37.   Comparison of Effect of variation in Pb/Pi at Inlet Exit on
Pressure along (a) ramp surface, (b) cowl surface,
for 7% & 8% Throat Area Increase.
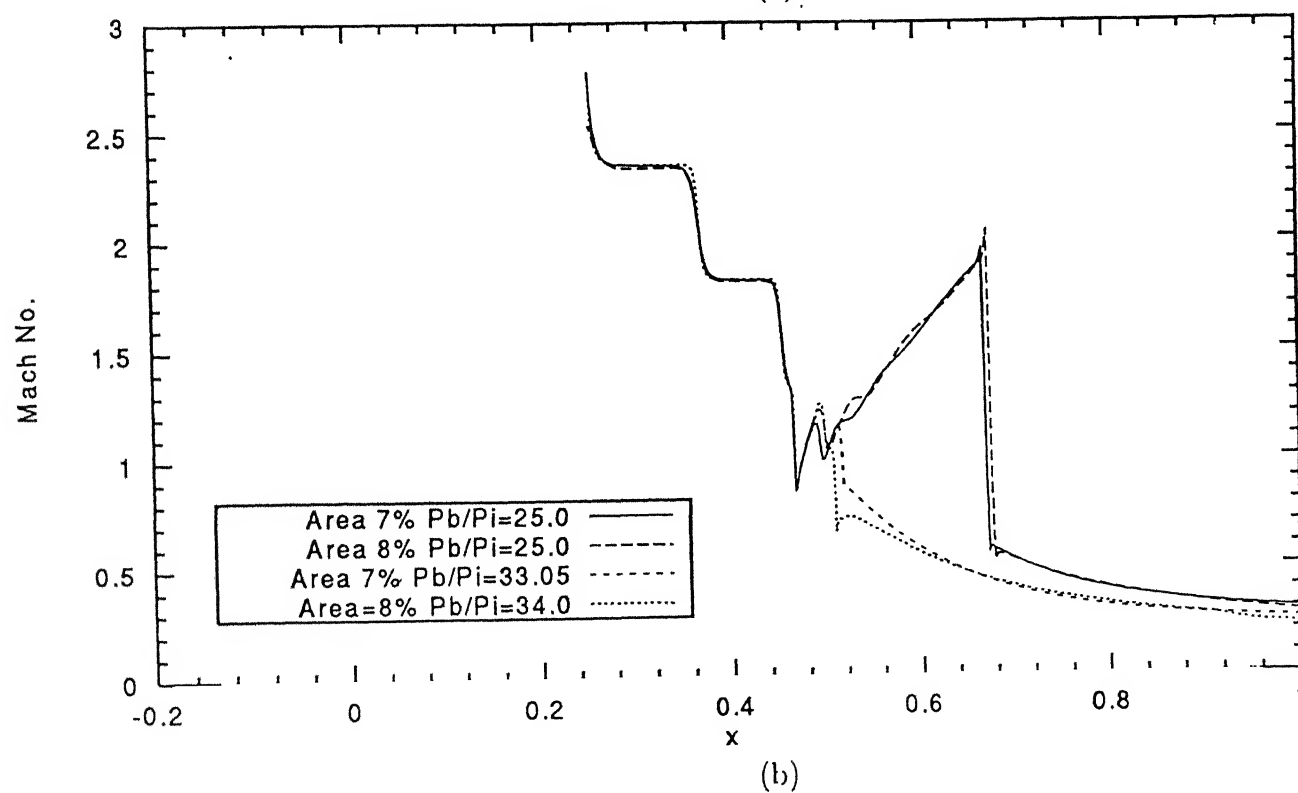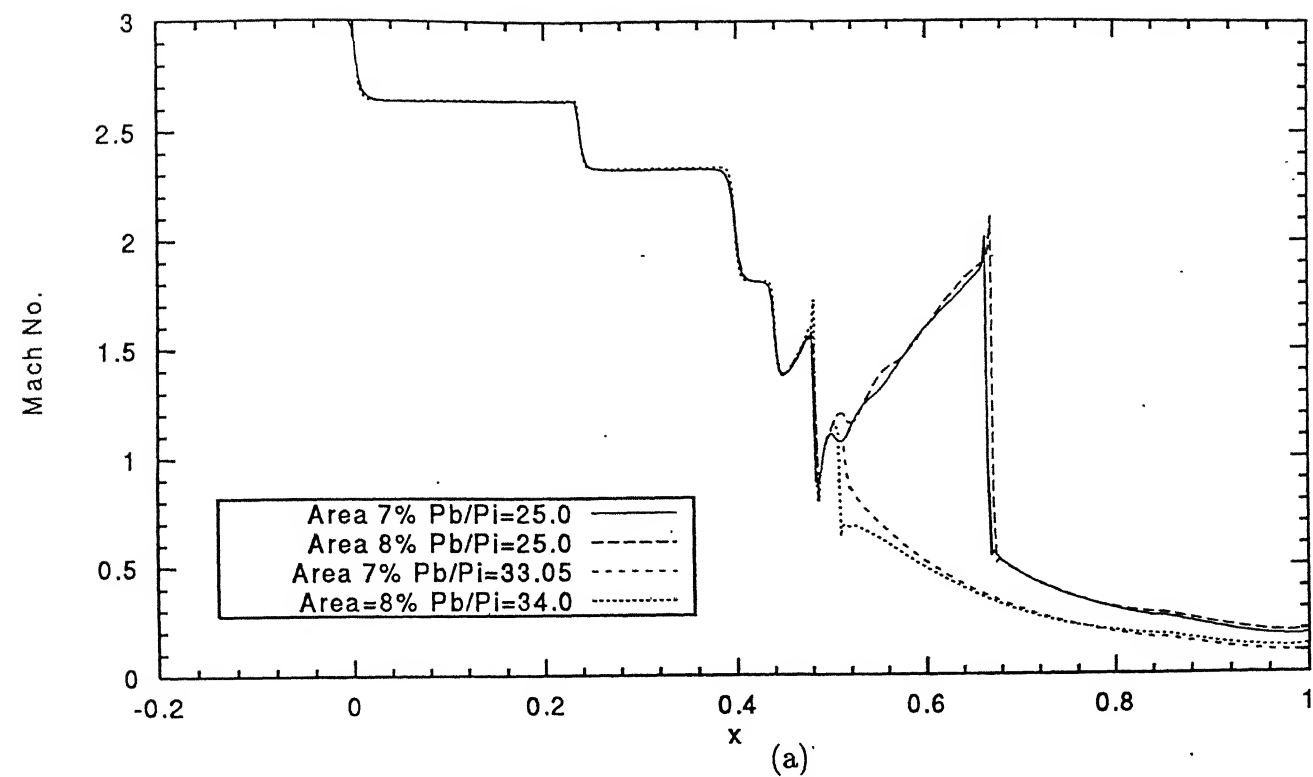
Figure 38.   Comparison of Effect of variation in Pb/Pi at Inlet Exit on
Mach No. along (a) ramp surface, (b) cowl surface,
for 7% & 8% Throat Area Increase.
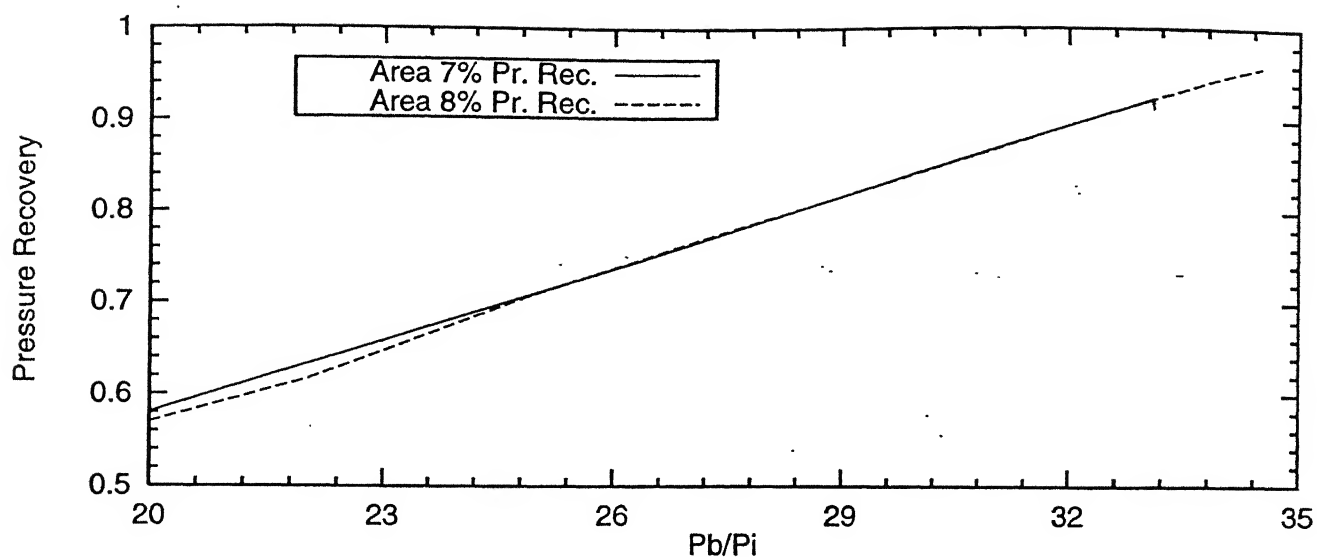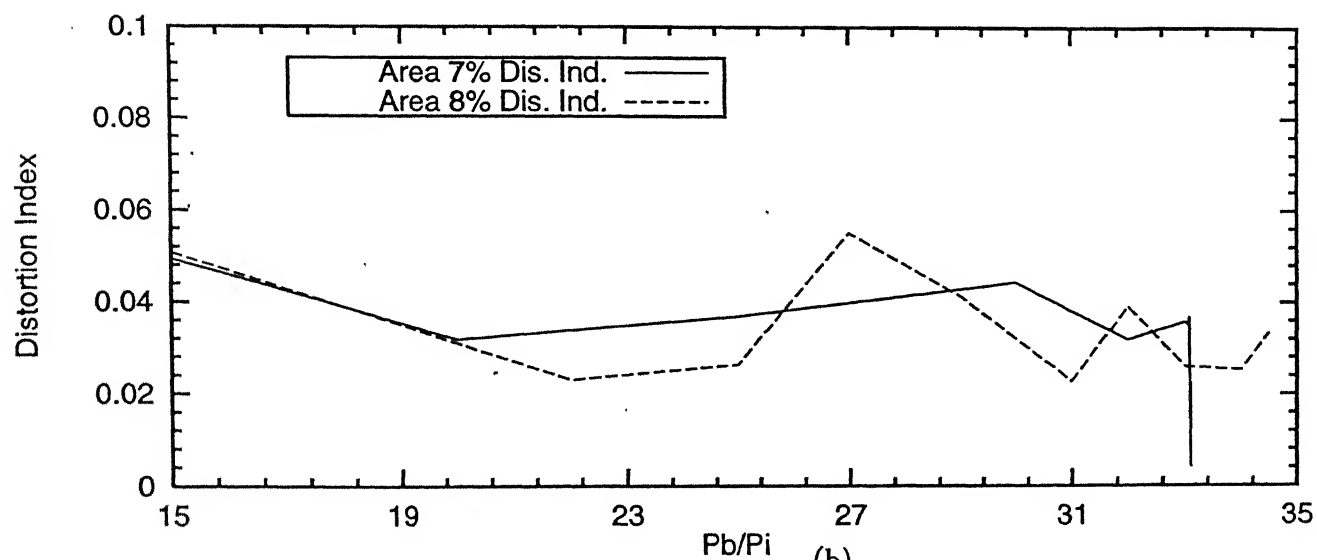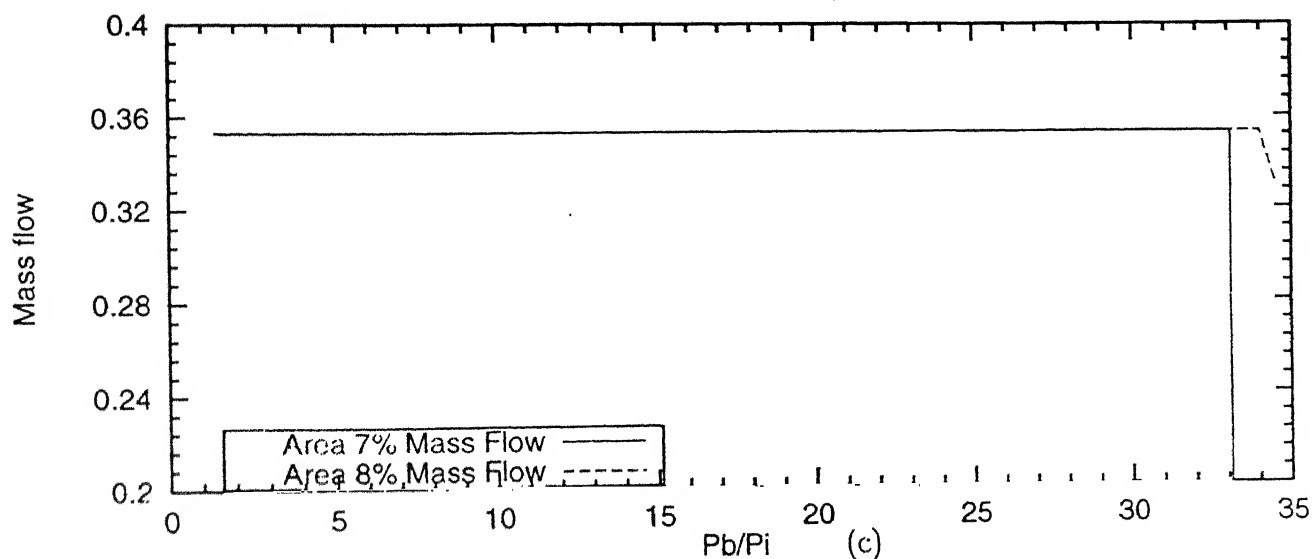
Figure 39.   Comparison of Effect of variation in Pb/Pi at Inlet Exit on

(a) Total Pressure Recovery, (b) Distortion Index, (c) Mass Flow,

for 7% & 8% Throat Area Increase.

T=0.14

T=0.24

T=0.34

T=0.44

T=0.54

T=0.64
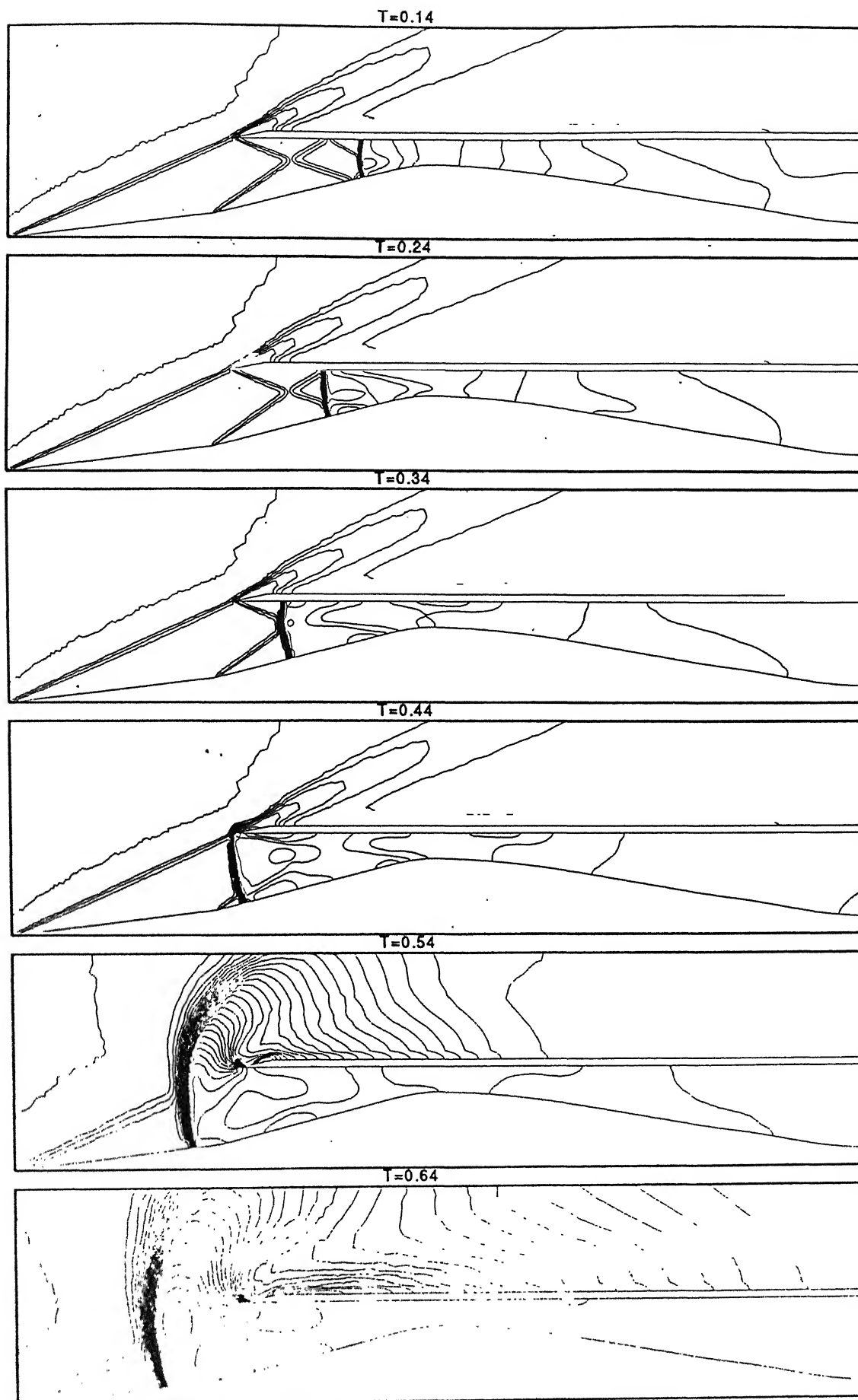
(a)

Figure 40.   Mach Contours of Expelled Flow at Pb/Pi=33.09 for 7% Throat
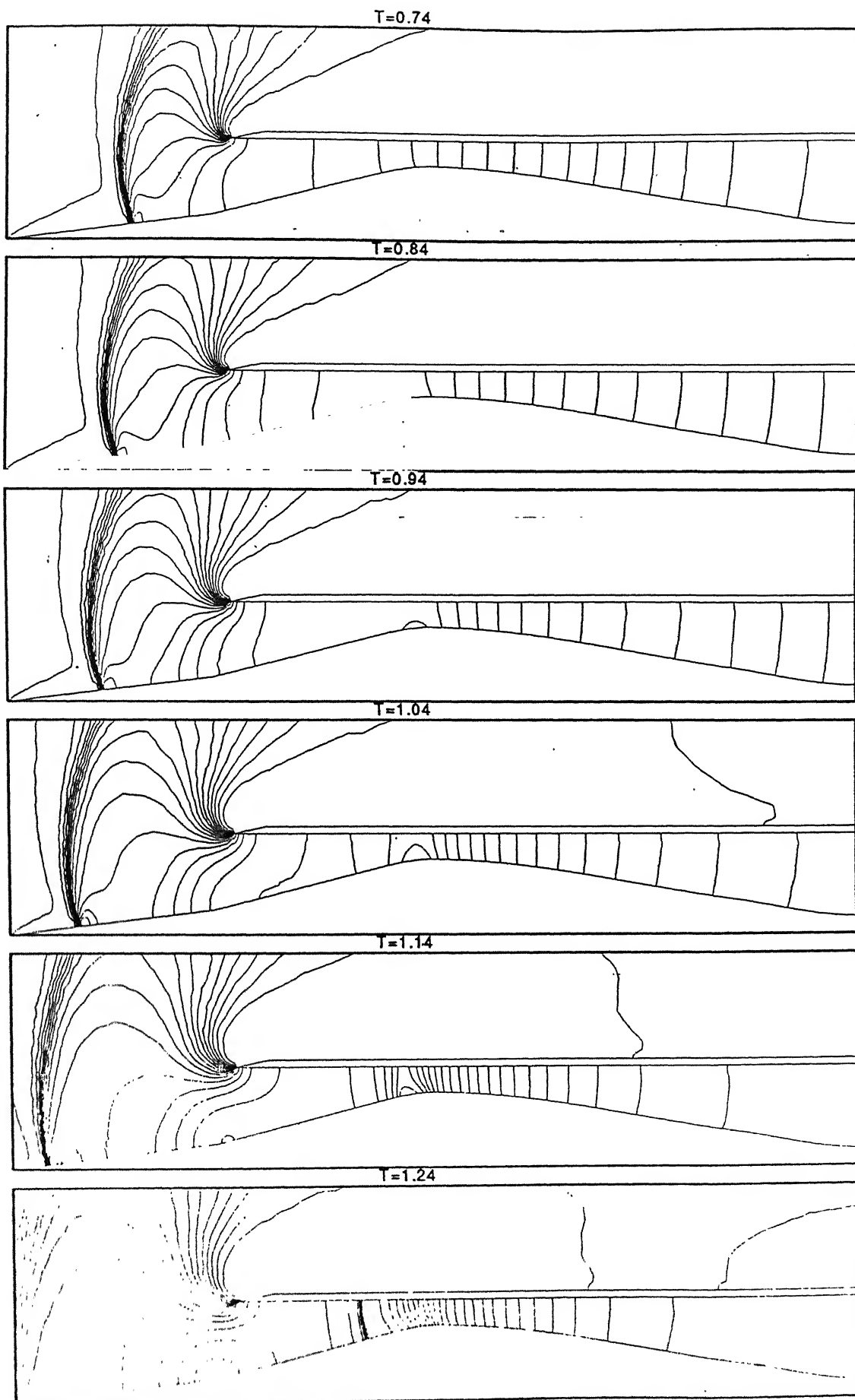Area Increase with Time(T).

Figure 40.   Mach Contours of Expelled Flow at Pb/Pi=33.09 for 7% Throat
               Area Increase with Time(T).
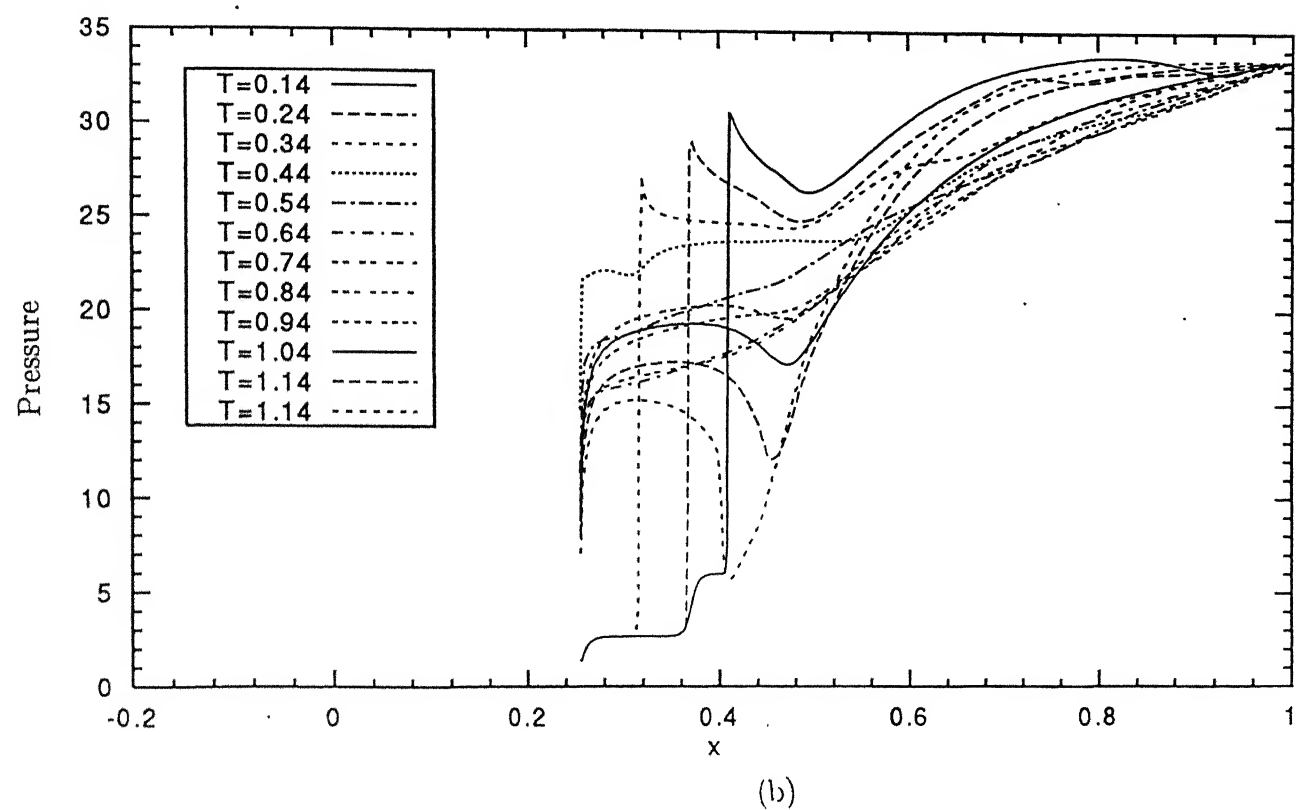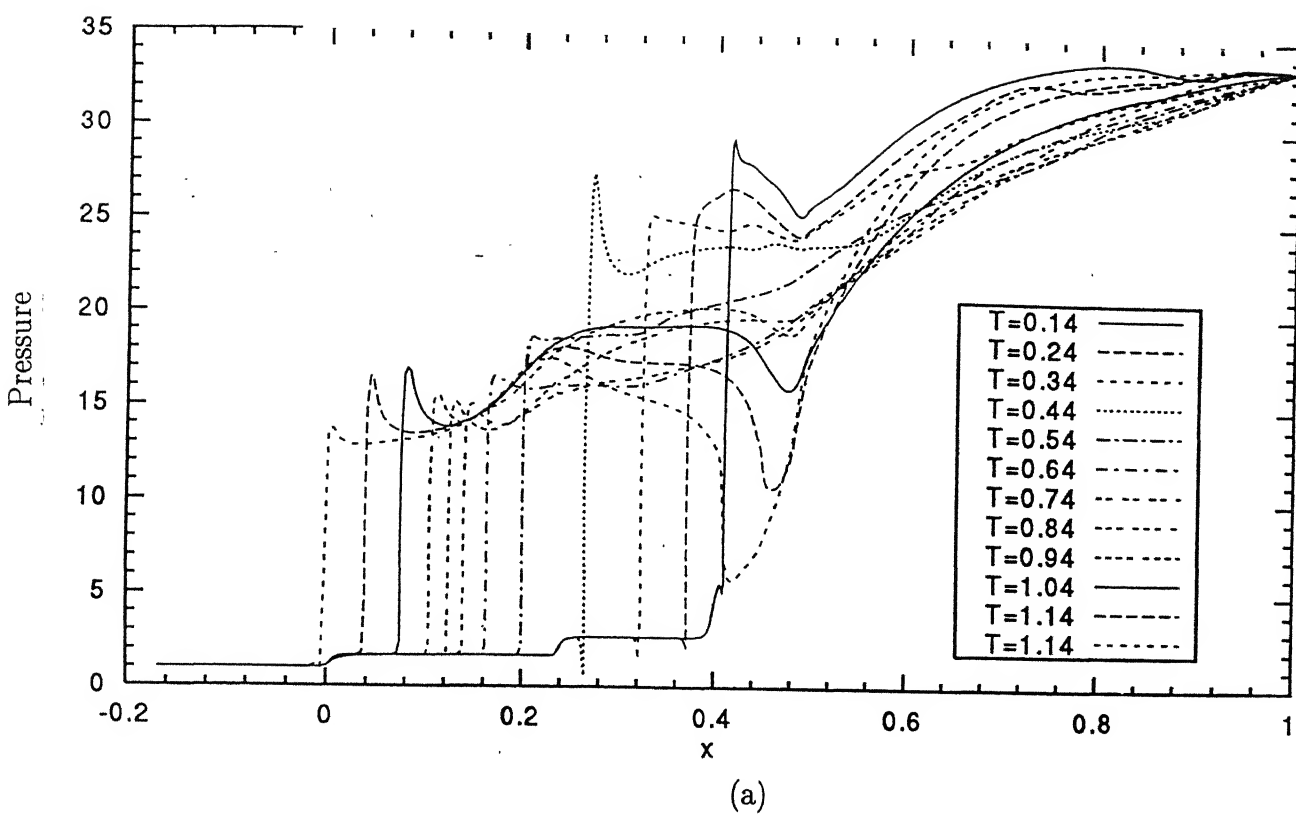
T=0.14

T=0.24

T=0.34

T=0.44

T=0.54

T=0.64
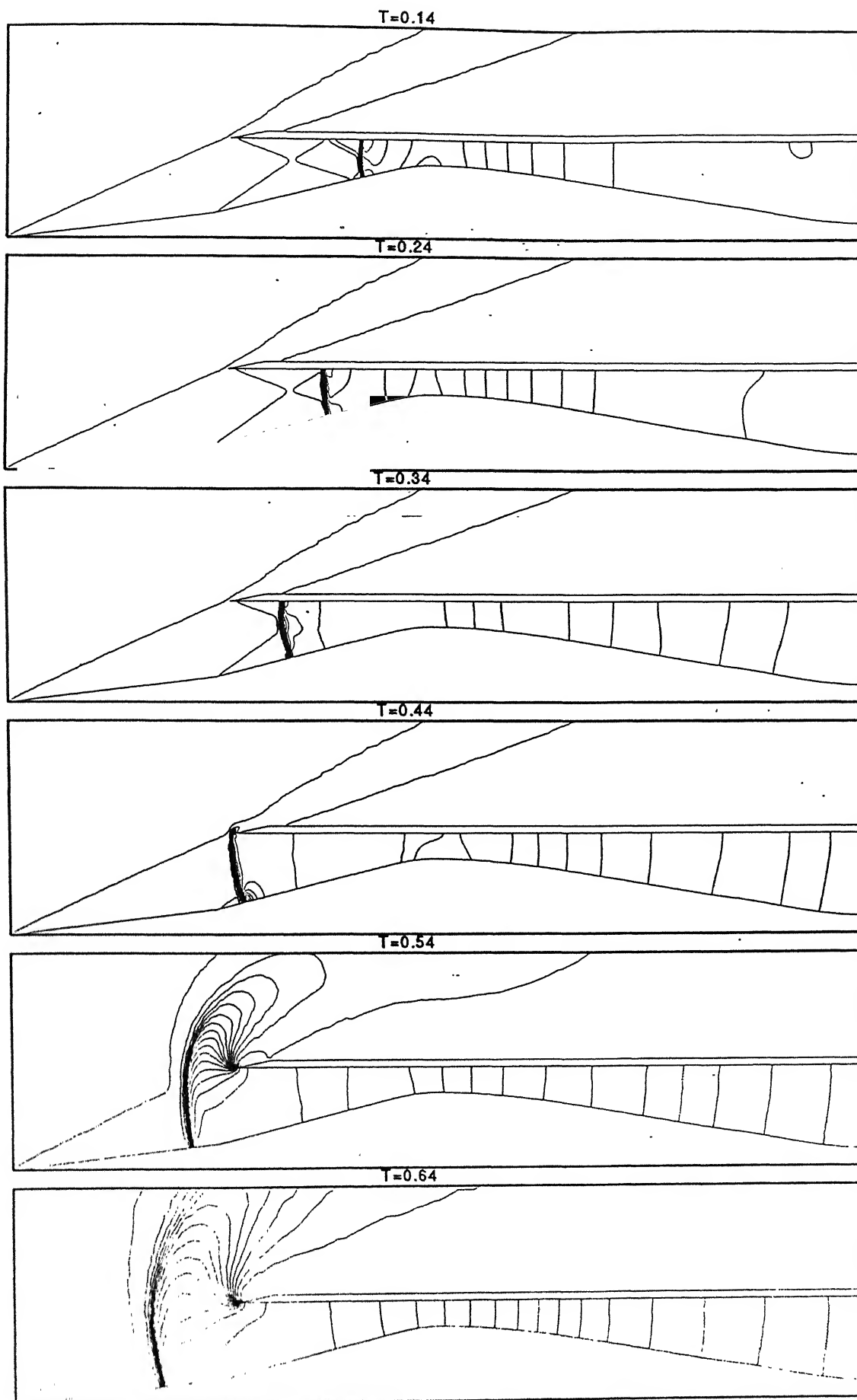
(a)

Figure 41.   Pressure Contours of Expelled Flow at Pb/Pi=33.09 for 7%
Throat Area Increase with Time(T).

T=0.74

T=0.84

T=0.94

T=1.04

T=1.14

T=1.24

(b)

Figure 41. Pressure Contours of Expelled Flow at Pb/Pi=33.09 for 7%
Throat Area Increase with Time(T).

Figure 42.   Effect on Pressure of shock movement of Expelled Flow at
              Pb/Pi=33.09 for 7% Throat Area Increase with Time(T) along
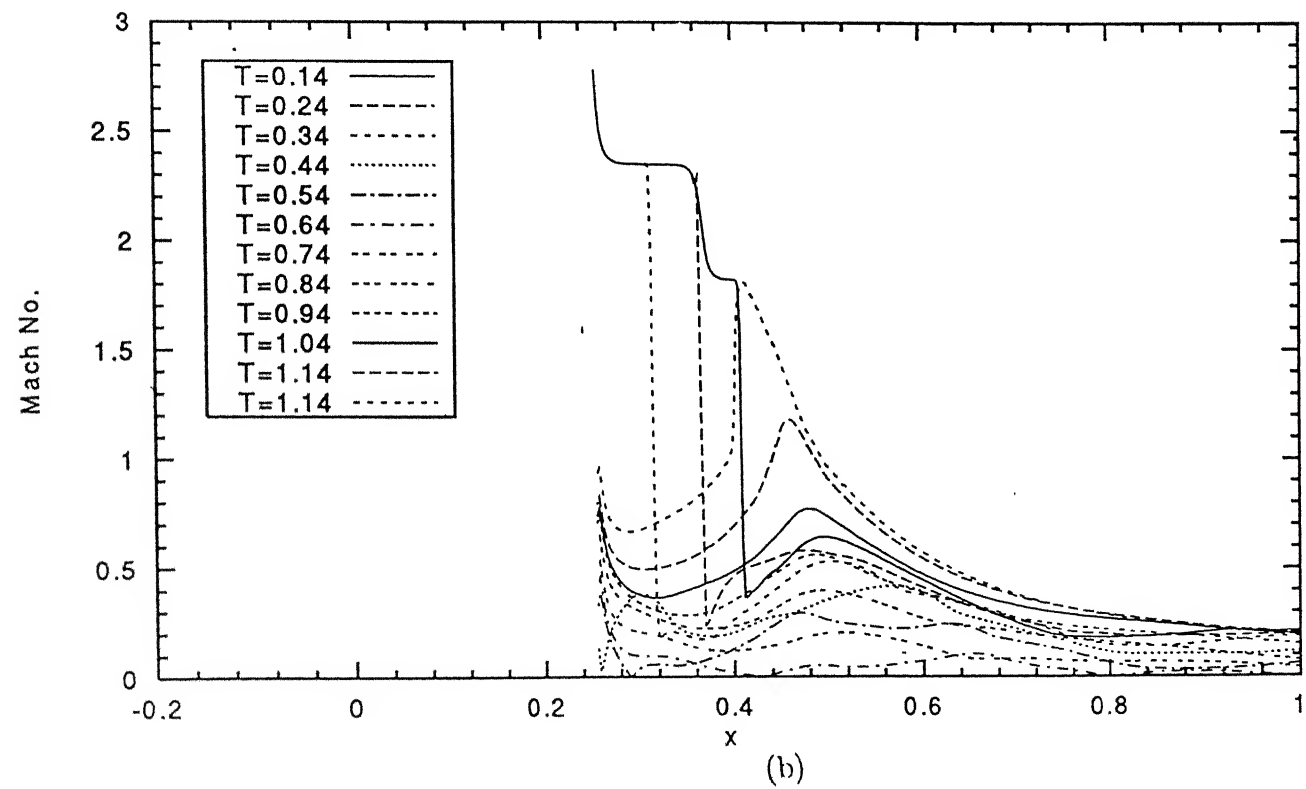   (a) ramp surface, (b) cowl surface.
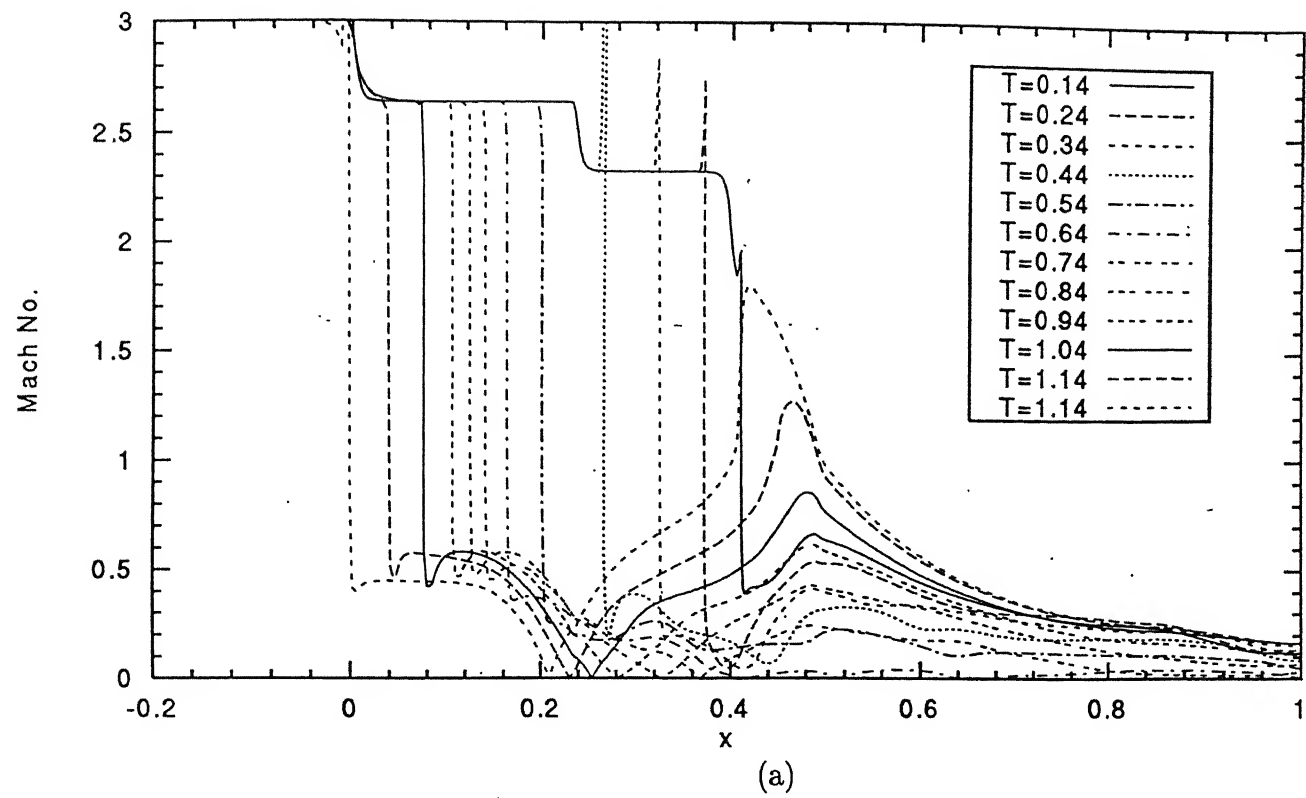
Figure 43. Effect on Mach No. of shock movement of Expelled Flow at
Pb/Pi=33.09 for 7% Throat Area Increase with Time(T) along
(a) ramp surface. (b) cowl surface.

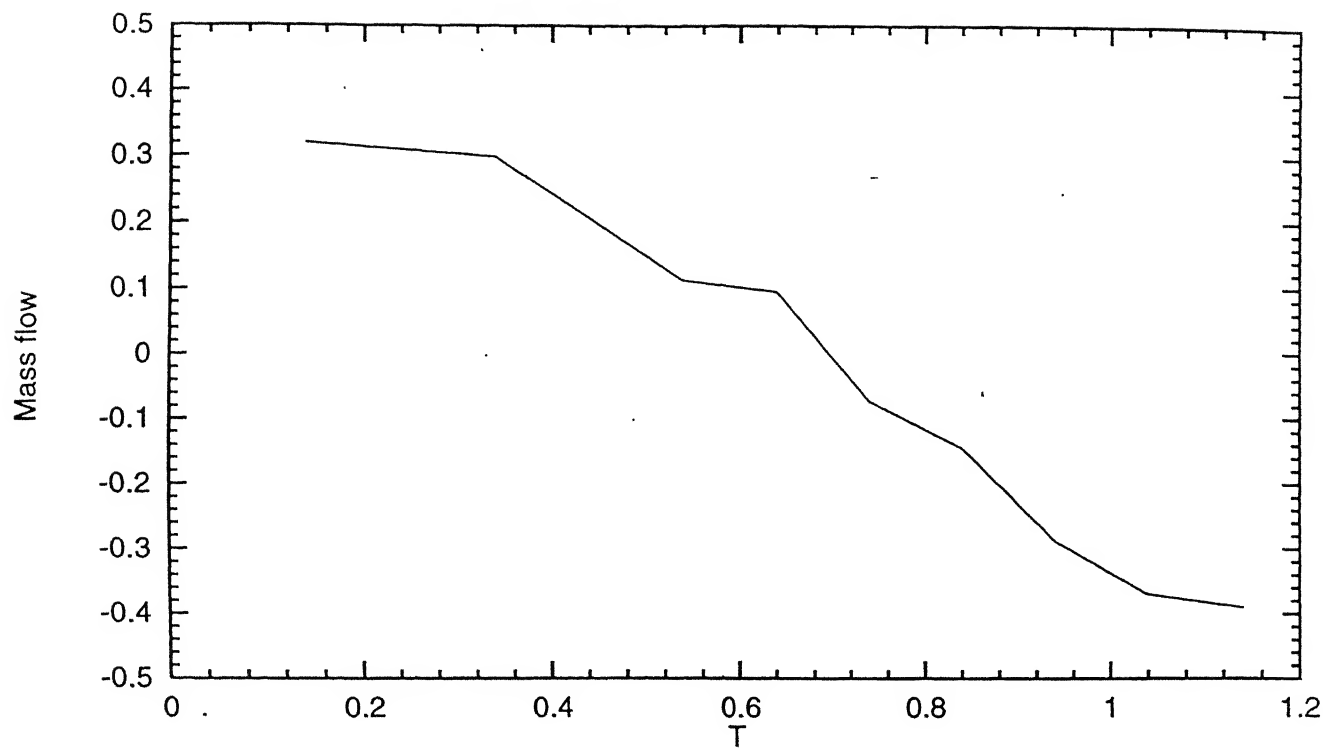Figure 44. Effect on Mass Flow of shock movement of Expelled Flow at
Pb/Pi=33.09 for 7% Throat Area Increase with Time(T).

A 130887

Date Slip

This book is to be returned on the date last stamped.